Light-Emitting Polymers with On-Chain Triplet Emitters

Dissertation

Zur Erlangung des akademischen Grades

Doktor der Naturwissenschaften
(Doktor rerum naturalium)

Eingereicht in der Fakultät 4 - Mathematik und Naturwissenschaften der
Bergischen Universität Wuppertal

von

Eike Heuser

aus Wuppertal

Wuppertal, 2016

Die Dissertation kann wie folgt zitiert werden:

urn:nbn:de:hbz:468-20160614-094258-5
[http://nbn-resolving.de/urn/resolver.pl?urn=urn%3Anbn%3Ade%3Ahbz%3A468-20160614-094258-5]

Die vorliegende Arbeit entstand in der Zeit von Oktober 2010 bis Oktober 2013 in der Arbeitsgruppe Funktionspolymere des Fakultät 4 - Mathematik und Naturwissenschaften der Bergischen Universität Wuppertal unter Anleitung von Jun.-Prof. Dr. Elisabeth Holder.

1. Gutachter: Prof. Dr. Ullrich Scherf

2. Gutachter: Prof. Dr. Michael Tausch

Eingereicht am 16.02.2016

Mündliche Prüfung am 23.05.2016

Meiner Familie in Dankbarkeit

Welch triste Epoche, in der es leichter ist, ein Atom zu zertrümmern als ein Vorurteil.

(Albert Einstein)

Wir müssen unbedingt Raum für Zweifel lassen, sonst gibt es keinen Fortschritt, kein Dazulernen. Man kann nichts Neues herausfinden, wenn man nicht vorher eine Frage stellt. Und um zu fragen, bedarf es des Zweifelns.

(Richard P. Feynman)

Abstract

Organic Light-Emitting Devices (OLEDs) consist of subsequent semiconducting, organic layers and, since this decade, can be found in consumer electronics e.g. in displays, chiefly in mobile phones, or even for lighting. Their main advantages compared to Liquid Crystal Displays (LCDs) are the thinner construction, flexibility and potentially higher efficiency. Iridium(III) complexes are widely used as active emitter species in OLEDs as they are capable of harvesting both, singlet and triplet excitons, thus, enhancing the efficiency of the devices.

In this thesis, the synthesis and characterization of an iridium(III) complex triplet emitter is presented that emits red light due to its 2-phenylisoquinoline cyclometalating ligands. Furthermore, the emitter was furnished with a carbazolyl-functionalized ancillary ligand in order to promote hole trapping at the emitter site. In addition, two series of copolymers based on poly(9,9-dioctylfluorene) as backbone and varying ratios of green fluorescent fluoren-9-one and the iridium(III) complex were synthesized for application in single active layer OLEDs. The first series of copolymers P1-8 revealed color tune ability from green to red and efficient energy transfer from the polymer backbone to the guest moieties. To improve hole injection into the single active layer, two comonomers, fluorene-based 4,4'-(2,7-dibromo-9*H*-fluorene-9,9-diyl)bis(*N*,*N*-diphenylaniline) and carbazole-based 3,6-dibromo-9-(2-ethylhexyl)-9*H*-carbazole, were synthesized. Subsequently, optimized copolymers PW1-5 were prepared and tested in white light-emitting OLEDs (WOLEDs).

Moreover, a second iridium(III) complex with 6-fluoro-2-phenylbenzo[*d*]thiazole as cyclometallating ligands and carbazolyl-functionalized ancillary ligand (Z)-6-(9*H*-carbazol-9-yl)-5-hydroxy-2,2-dimethylhex-4-en-3-one was prepared as orange emitter and tested in an OLED.

During the fabrication of polymer OLEDs (POLEDs), either inkjet printing or spin coating of polymer solutions on underlying organic functional layers is usually applied. Spin coating suffers from material of the underlying layer(s) being dissolved in the polymer solution and washed away during the process. Thus, either orthogonal solvents or cross-linking of the underlying layer(s) is needed. Both techniques require the introduction of functional groups, either for cross-linking or for controlling the polarity, thus increasing the synthetic and technical effort. As a possible solution, aqueous suspensions of a copolymer were prepared with concentrations of up to $50\ \mathrm{mg} \cdot \mathrm{L}^{-1}$. In first attempts, the suspensions could be successfully printed on glass substrates.

Table of Contents

1. Introduction

In the last decades, organic light-emitting diodes (OLEDs) have received high attention in the advancing field of display technology and solid state lighting. Since the discovery of electroluminescence (EL) in organic materials by A. Bernanose in the early 1950s[1] and of electric conductivity in polymers with alternating double and single bonds as polyacetylene (PA) by Shirakawa *et al.*, OLEDs have been developed to market maturity.[2] Today, they are used in a wide variety of consumer electronics, such as mobile phones, while bigger full color displays, e.g., for televisions, are still not available at reasonable prices. At the beginning of 2010, HTC fabricated the first mobile phone with an OLED display (manufactured by Samsung) that was successfully established on the market at a reasonable price. Since then, especially Samsung has developed various smartphones with full-color OLED screens with sales as high as 50 million devices, e.g., for the Samsung Galaxy S3.[3] In 2014, LG Electronics announced the first curved, flexible smartphone, equipped with an OLED display.[4] In this emerging market, as well as in potential new markets as TV flat panel displays and solid state lighting, the development of high efficient OLEDs is of great interest for the industry. Still, major problems need to be solved: the lower efficiency and long term stability of blue emitters compared to their red and green counterparts,[5] encapsulation of flexible devices and cost efficient manufacturing.

1.1 OLEDs – devices and materials

In this paragraph, a simplified device structure of an OLED is presented along with a short description of commonly used materials.

OLEDs are fabricated by adding several (semi)conductive layers on top of a transparent substrate. The individual layer thickness is usually in the range of a few nanometers (nm) up to a few hundred nm. A simplified device structure is shown in Figure 1. The functional principle of an OLED is based on the movement of charges. Positive charges (holes) migrate from the anode towards optional transport layers to a layer containing an emitter material. Simultaneously, negative charges (electrons) are injected from the cathode and move towards the emitter layer where the positive and negative charges combine to form an exciton. An

exciton can be seen as a bound state of an electron and an electron hole that are attracted through electrostatic Coulomb force.[6] The subsequent recombination of the charges leads to an excited state of the molecule at that the exciton was formed. Subsequent relaxation of the excited states takes place until the lowest excited state is reached which then relaxes to the ground state by emitting electromagnetic waves or by concurrent relaxation modes.

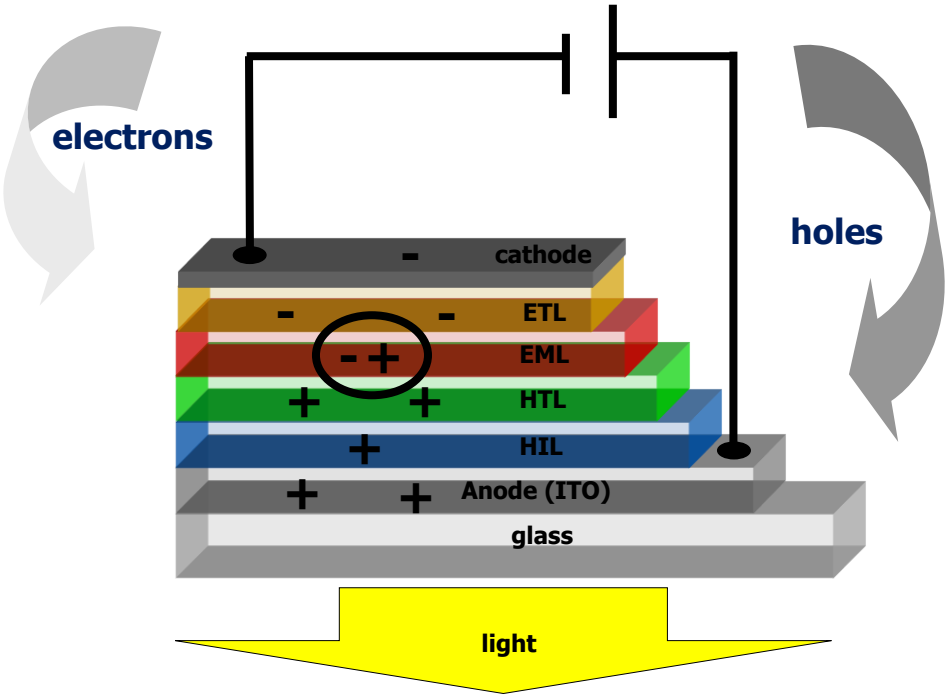

Figure 1. Schematic representation of a multi-layer device architecture.

While glass is usually used as a transparent substrate because it is cheap and impermeable for oxygen and moisture, transparent plastic foils allow the production of flexible OLEDs. However, up to now, there is no foil available that is adequately impermeable for oxygen which has an impact on the long term stability of OLEDs as well as on the performance due to efficient quenching of the excited states.[7]

Indium tin oxide (ITO) is widely used as an anode material because of its high transparency in the visible range of the electromagnetic spectrum and low electrical resistivity of $2 - 4 \cdot 10^{-4}\ \Omega \cdot cm^{-1}$.[8-9] Due to the fact that indium is a rare element and therefore expensive, alternative metal oxides[10] as well as carbon nanotubes[11] and graphene[12] are currently being investigated as anode materials.

Hole injection layers (HIL) are used to facilitate the injection of positive charges (holes) into a hole transport layer (HTL) by replacing the high barrier for charge injection with a cascade of lower barriers.[13-14] Common materials are PEDOT:PSS, an ionomer of poly(3,4-ethylenedioxythiophene) and poly(styrenesulfonate) as well as triphenyl-diamine (TPD) and naphthyl-phenyl-diamine (NPD) and other triarylamines with 'bi-phenyl' substructures (Scheme 1).[15]

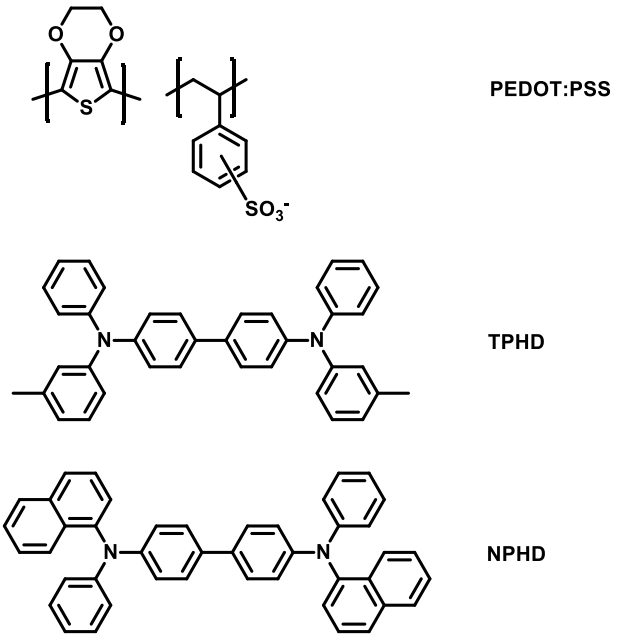

Scheme 1. Chemical structures of common hole injection materials.

Depending on the architecture of an OLED, the hole transport layer allows for the migration of positive charges towards the emitting layer, or, in some cases, is also utilized as the host material for an emitter. The first efficient OLED fabricated by Tang and VanSlyke[16] consisted of only two layers between the electrodes: namely a TPD derivate[17] as HTL and 8-hydroxyquinline aluminum, a fluorescent metal chelate complex, as luminescent material that is also capable of electron transport.[18-19] It was the first device to operate at voltages below several hundred volts (turn-on voltage of about 3V) and proved that, in this two-layer architecture, recombination of positive and negative charges and electroluminescence occur in the middle of the layers[16]. It was the starting point of OLED development as we know it today.[20] Since then, other HTL materials have been developed for optimized device architecture. Among these are polymers such as poly(*N*-vinyl carbazole) (PVK)[21], various star-shaped materials derived from 1,3,5-tris(diphenylamino)benzene (TDAB)[22],

triphenylamine derivates (TPD) type molecules like *N*,*N*'-bis(3-methylphenyl)-*N*,*N*'-diphenylbenzidine, spiro-linked molecules such as 'Spiro-2'[23] and carbazole-based materials like 5,11-di(naphthalen-1-yl)-5,11-dihydroindolo[3,2-*b*]carbazole (Scheme 2).[15]

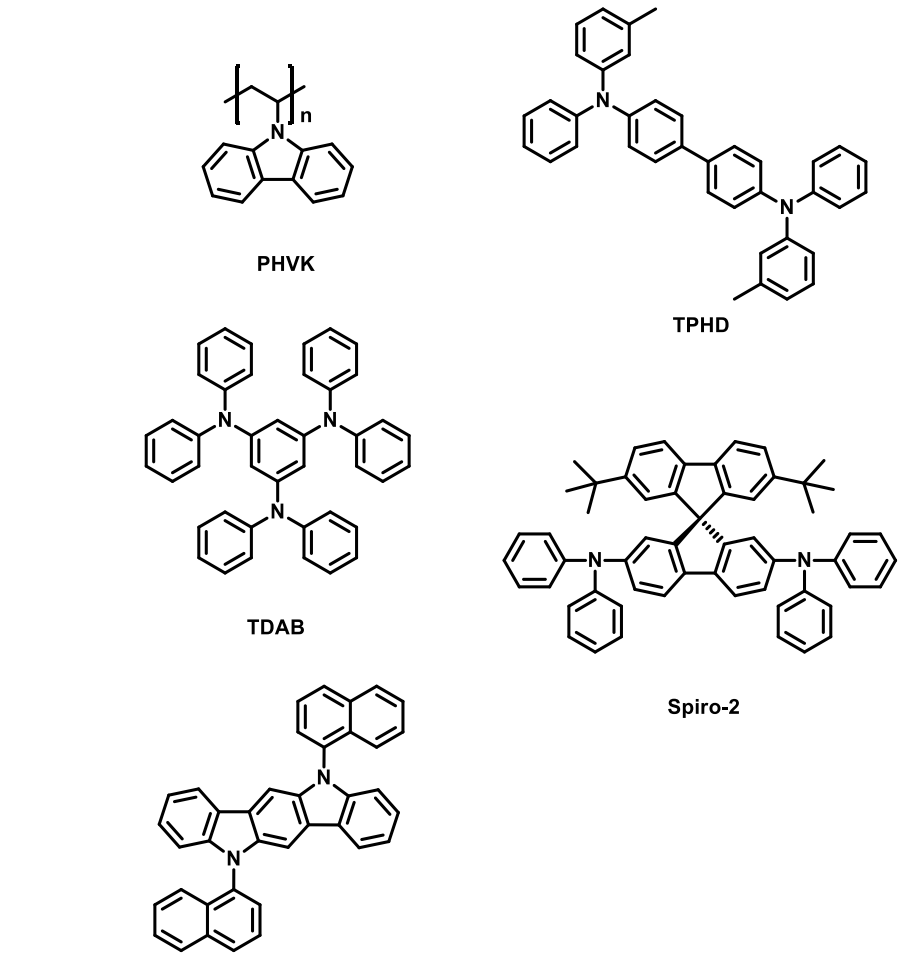

Scheme 2. Chemical structures of common hole transport materials.

Materials for the emitting layer (EML) can be divided into two classes, fluorescent and phosphorescent substances. In both cases, the materials are usually doped into a matrix to form a host-guest doped emitter system. With optimized transport and luminescent properties, the host material may be used with various fluorescent or phosphorescent guest materials leading to electroluminescence of high efficiency. The operational stability may also be improved by transferring the exciton to a highly stable and emissive guest, thus minimizing the possibility of non-radiative decay.[15, 24] Various matrices have been developed, most of them being derivates of hole and/or electron transport materials.

Among others, fluorescent emitters were derived from coumarin, e.g., 10-(2-benzothiazolyl)-1,1,7,7-tetramethyl-2,3,6,7-tetrahydro-1*H*,5*H*,11*H*-[*l*]benzo-pyrano[6,7,8-*ij*]quinolizin-11-one, known as C-545T,[15] which emits in the green region of the electromagnetic spectrum, just like *N*,*N*'-diethylquinacridone (DEQ)[25]. One example of a red emitter is given by 4-(dicyanomethylene)-2-*t*-butyl-6-(1,1,7,7-tetramethyljulolidyl-9-enyl)-4*H*-pyran (DCJTB)[26-28].

Phosphorescence in common organic molecules is known to be weak.[29] Even though new approaches like bypassing Kasha's rule of internal conversion in order to enhance the yield of the triplet and singlet excitons for light out-coupling have been recently developed,[30] harvesting of the excited triplet states is usually achieved by incorporating heavy transition metal complexes as guests. These allow intersystem crossing (ISC) due to their strong spin-orbit coupling.[31] Especially by using platinum(II) and iridium(III) complexes, it is possible to achieve nearly 100% internal quantum efficiency.[32-33]

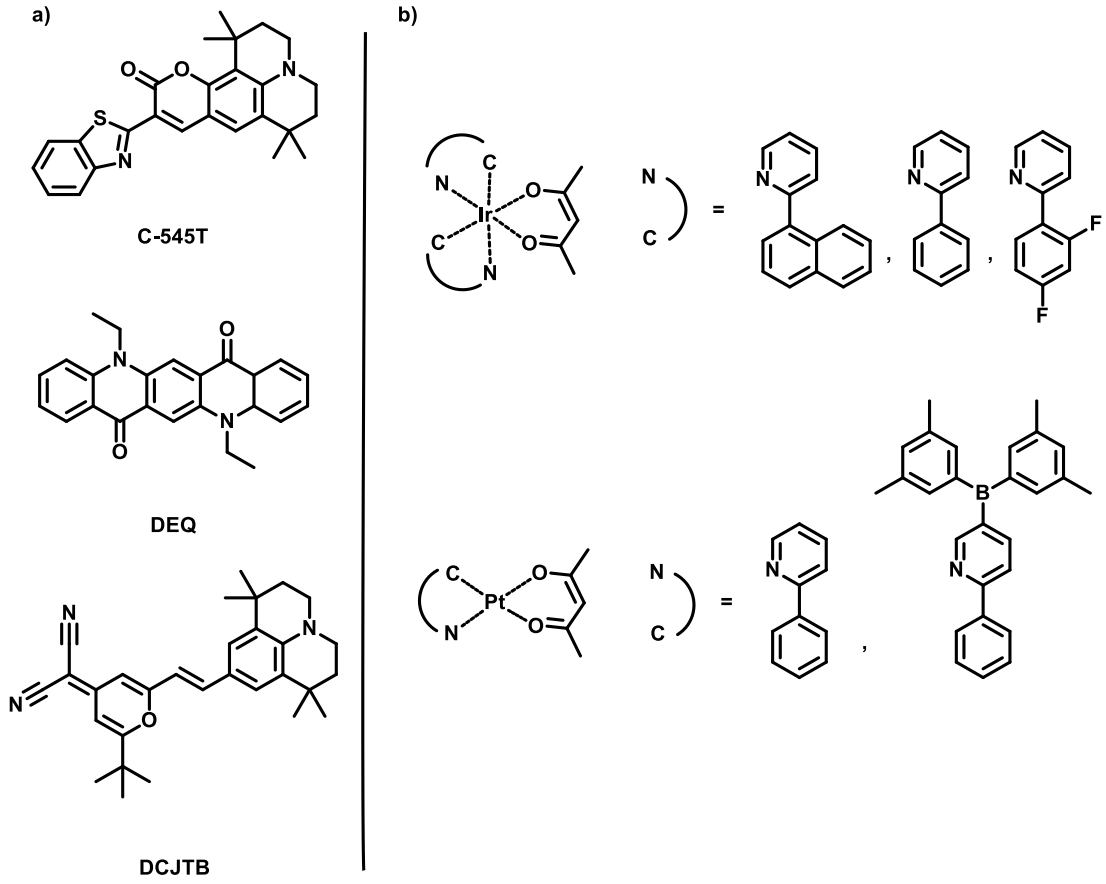

Scheme 3. Chemical structures of examples for a) fluorescent organic molecules. b) phosphorescent iridium(III) and platinum(II) complexes.

Therefore, a wide variety of cyclometallating and ancillary ligands have been developed allowing for emission wavelength tuning from ultra violet (UV) to the infrared. Scheme 3 a) illustrates some fluorescent organic materials that have been applied in OLEDs. Scheme 3 b) presents a selection of phosphorescent iridium(III)[32, 34] and platinum(II)[33, 35] complexes with acetylacetonate (acac) ancillary ligands.

In the electron transporting layer (ETL), electrons are injected from the cathode to migrate to the emitting layer. Depending on the workfunction of cathode material and EML, various different materials have been developed. Two commonly used ETL-materials are outlined in Scheme 4, 2-([1,1'-biphenyl]-4-yl)-5-(4-(*tert*-butyl)phenyl)-1,3,4-oxadiazole (*t*-Bu-PBD) and 1,3,5-tris(2-*N*-phenylbenzimidazolyl) benzene (TPBI).[36-37] Lately, conjugated polyelectrolytes have been developed allowing the use of high work function metals as cathodes, such as gold.[38]

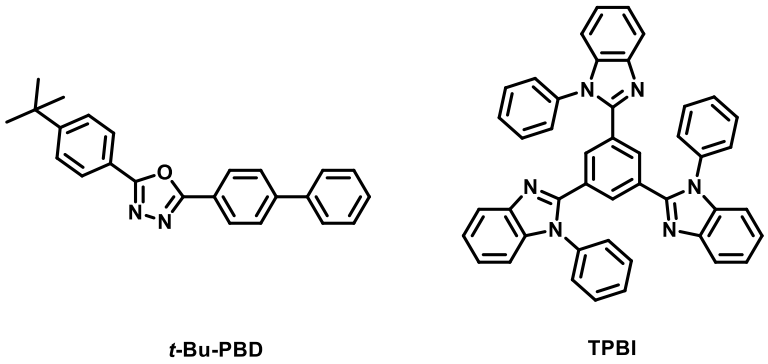

t-Bu-PBD TPBI

Scheme 4. Chemical structures of two examples of widely used electron transport materials.[36]

1.2 Device fabrication

Depending on the desired device architecture and the applied active materials, different techniques for the fabrication of OLEDs are used in order to form thin films.

Small molecules can be deposited on surfaces by vapor phase deposition.[39-40] The material is vaporized at raised temperature in a hot-walled chamber where it condenses on the cooled substrate. By repeating this step again with a different material, subsequent thin layers can be achieved. The main drawbacks are the high costs when it comes to mass production and the limitation to small molecules that are evaporable and stable at raised temperature.

Another technique is spin coating where a material is dissolved in a solvent and the solution is slowly dropped onto the middle of a substrate which is rotating around its central axis.[41-42] Due to the centrifugal force, the solution is quickly spread while the solvent evaporates, leaving a thin film of the material. The thickness of the films depends on the concentration of the solution, the solvent's properties like viscosity and volatility, and the angular speed applied. The advantage of this technique is the fast and cost-effective production. It allows the processing of materials that are not stable enough for vapor deposition or those having higher molecular weights, e.g., (co)polymers. However, fabrication of multiple layers *via* spin coating can cause problems due to the fact that the solvent of the new layer can remove parts of the material of the underlying layer if these are soluble in the used solvent. Therefore, orthogonal solvents are needed, requiring the development of, e.g., water-soluble materials. Much research effort has been spent to circumvent the need of orthogonal solvents, e.g. by applying spray[43] and inkjet-printing[44] techniques as well as by cross-linking a layer to the underlying layer by either thermal annealing[45-46] or irradiation of allyl-functionalized compounds.[47]

1.3 Processes during device operation

Figure 2 depicts a simplified schematic illustration of a multilayer OLED during operation.[48]

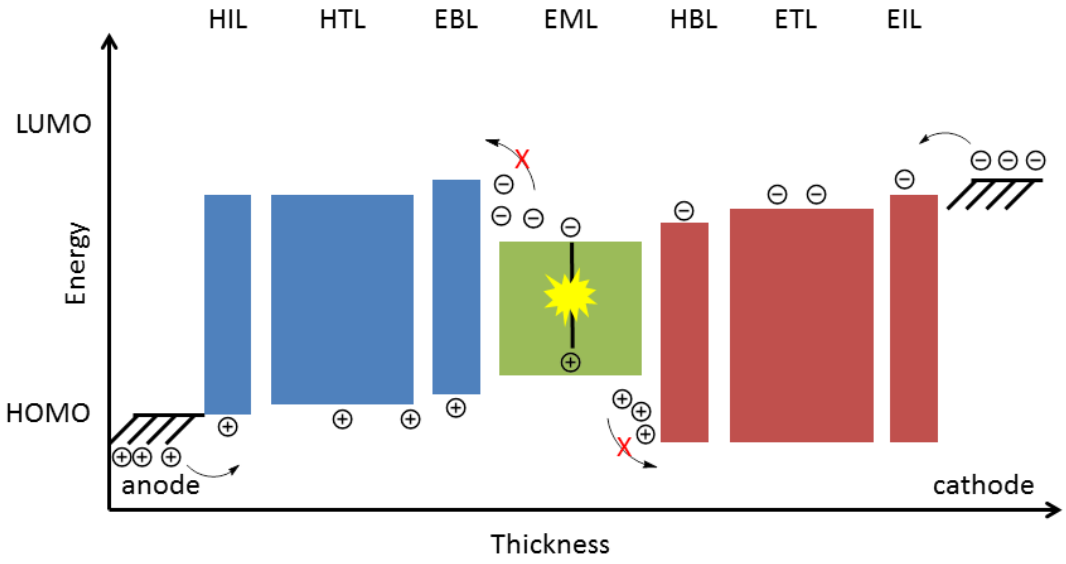

Figure 2. Simplified energy diagram of a multilayer OLED showing the HOMO and LUMO levels of the different layers.[48]

As mentioned before, holes are injected from the anode into the HIL from where they migrate in the electric field of the applied bias towards the HTL into the EML. An optional hole blocking layer (HBL) is introduced with a low-lying highest occupied molecule orbital (HOMO) in order to prevent the holes from reaching the ETL, where the formation of excitons is undesired, or even the cathode, where they would be quenched. The electrons are injected into the lowest unoccupied molecule orbital (LUMO) of the electron injection layer (EIL) and migrate towards the ETL to the EML. The electron blocking layer (EBL) with its high-lying LUMO hinders the electrons from reaching the HTL or even the anode. When an electron-hole pair recombines, it forms an exciton, an excited state on a molecule. It is well known from spin statistics that the probability of forming a singlet exciton is 25%, whereas the probability of forming a triplet exciton is 75% when organic molecules are electrically excited.[49] Due to the fact that transitions from the triplet states to the singlet ground state are forbidden by spin statistics, only the excited singlet states can relax to the ground state by emitting photons. This is usually a very fast process in the order of 1 to 100 ns. The excited triplet states are transformed into heat through vibrational modes and, thus, are lost for the emission. This means, fluorescent OLEDs can only reach a maximum internal quantum efficiency of 25%. To avoid this limit, heavy transition metal complexes can be used as emitters. The strong spin-orbit coupling between the transition metal and the ligands leads to the singlet and triplet states mixing, thus allowing intersystem crossing (ISC) and therefore efficient fluorescence and phosphorescence at room temperature.[50] In theory, an internal quantum efficiency of 100% is possible and many research groups have already claimed to have materials that show 100% internal quantum efficiency in OLEDs.[51-52],[32] Figure 3 illustrates the most important transitions between molecular orbitals (MO) in a modified Jablonski diagram.[53]

Due to an exciton being formed on the molecule, an excited state of the molecule gets populated, thus resulting either in an excited singlet (S_n) or excited triplet state (T_n). In the case of an excited singlet state, the electron will relax to the lowest excited singlet state S_1 through internal conversion (IC). This is a very fast process in the order of 100 fs in which the excess energy of the electronical and vibrational excited molecule is quickly transferred to surrounding molecules (intermolecularly) or intramolecularly due to electron-vibrational interactions.

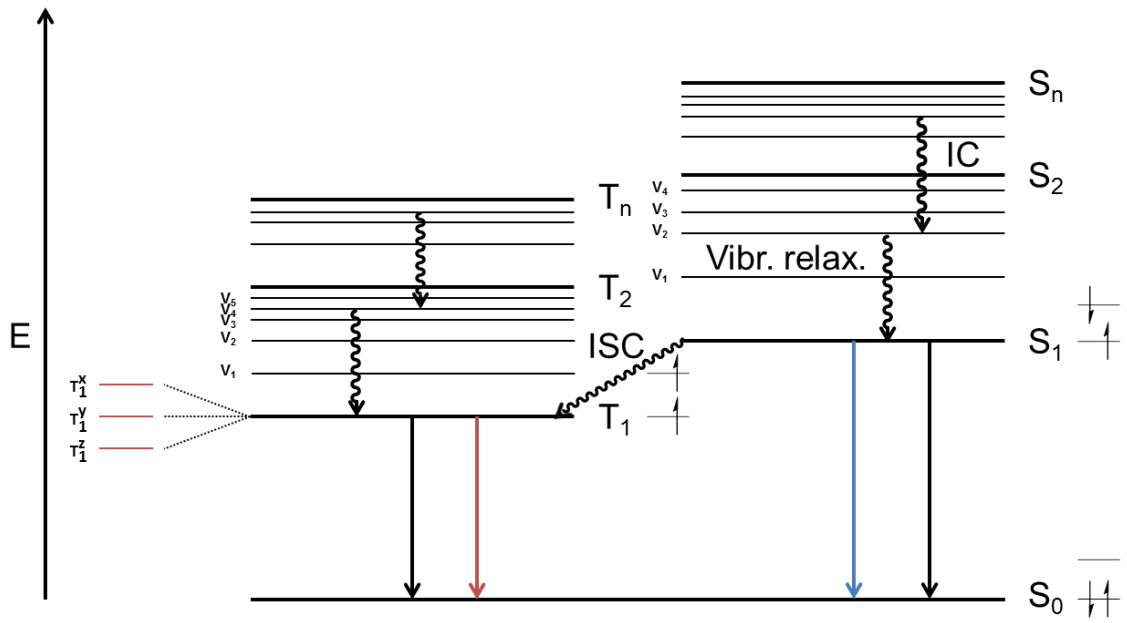

Figure 3. A modified Jablonski diagram showing non-radiative transitions (curved, black lines), spin-allowed radiative transitions (fluorescence, blue) and spin-forbidden radiative transitions (phosphorescence, red). Additional, non-radiative relaxation pathways from S_1 and T_1 to S_0 are indicated by solid black arrows. Electronic singlet states are named S_0…S_n, triplet states are named T_1…T_n. Vibronical states within electronic states are named V_n.

From the lowest excited singlet state (S_1), the further non-radiative transition to the singlet ground-state (S_0) is hindered by a large energy gap and is therefore much slower than the fast radiative relaxation (fluorescence) which usually occurs in the order of nanoseconds. In the case of a triplet exciton being formed, it will quickly decay *via* IC to the lowest triplet state T_1. In the case of a weak spin-orbit coupling, e.g., in hydrocarbons, the radiative transition to the singlet ground state is spin-forbidden (kinetically unfavorable) and therefore orders of magnitude weaker than the fluorescence from excited singlet S_1 states. Thus, the triplet lifetime in hydrocarbons is quite long being in the range of milliseconds or even seconds. During its lifetime, the excited triplet state is very likely to be quenched by bimolecular interactions with other triplet or singlet excitons or charge carriers and therefore wasted for the generation of light.

1.4 Heavy metal transition complexes – harvesting excited triplet states

As described in chapter 1.1, complexes of heavy transition metals like ruthenium, iridium and platinum have been widely used as phosphorescent dopants for OLEDs. This is because they are capable of forming emissive excited states due to efficient mixing of singlet and triplet states.[54] These mixed states are visible in the absorption and emission spectra of the complexes. Figure 4 depicts the chemical structure of an orange light-emitting iridium(III) complex and its normalized absorption and emission spectra in chloroform solution.[55] The absorption spectrum is dominated by strong bands below 300 nm which can be mainly attributed to transitions from the S_0 ground state to various singlet ligand-to-ligand-charge-transfer (^{1}LLCT) and singlet ligand-centered (^{1}LC) states whereas the weaker bands between 400 nm and 550 nm mainly arise from transitions to singlet metal-to-ligand-charge-transfer (^{1}MLCT) states. The emissive T_1 state at 625 nm is of mixed ^{3}LC and ^{3}MLCT character.

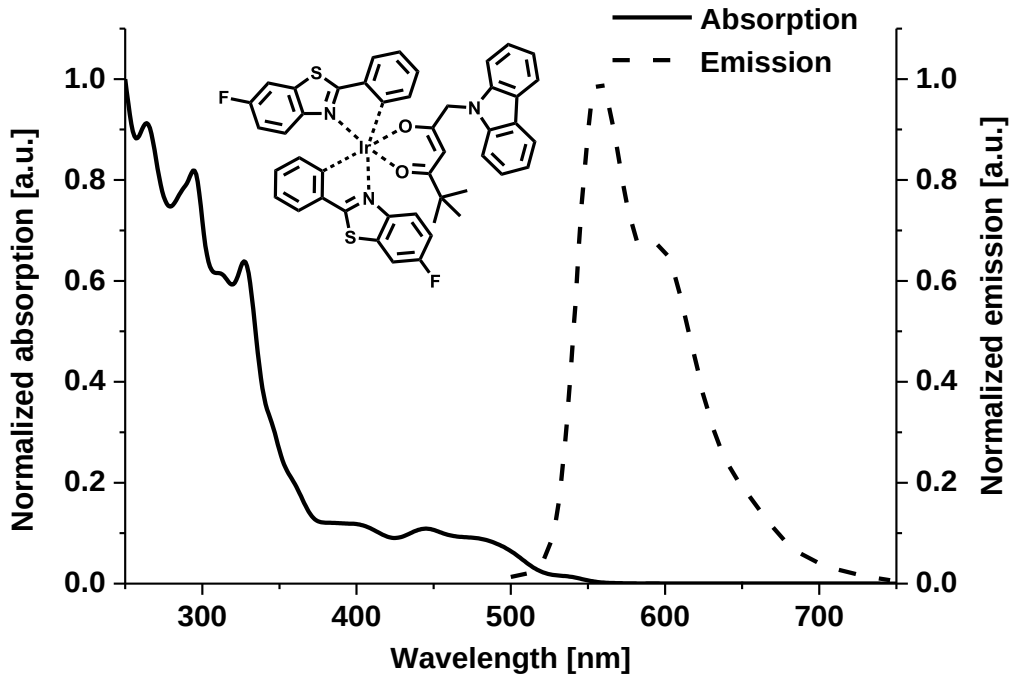

Figure 4. Normalized absorption and emission spectra of an iridium(III) complex (chloroform solution at a concentration of 10^{-5} M).[55]

Due to concentration quenching, pristine layers of iridium(III) complexes in OLEDs usually reveal very low efficiencies.[56] Hence, the phosphorescent dyes are blended into a proper host matrix.[54] Self-evidently, singlet and triplet excitons may be formed directly on the guest or on the host material. In the case of direct exciton generation on the dye, the matrix only functions as a charge transport layer. The phosphorescent dye should then behave as a charge trap and recombination site. In order to reach acceptable device performance, excitons formed on the host material have to efficiently transfer the exciton energy to the guest molecules. Two possible mechanisms of energy transfer

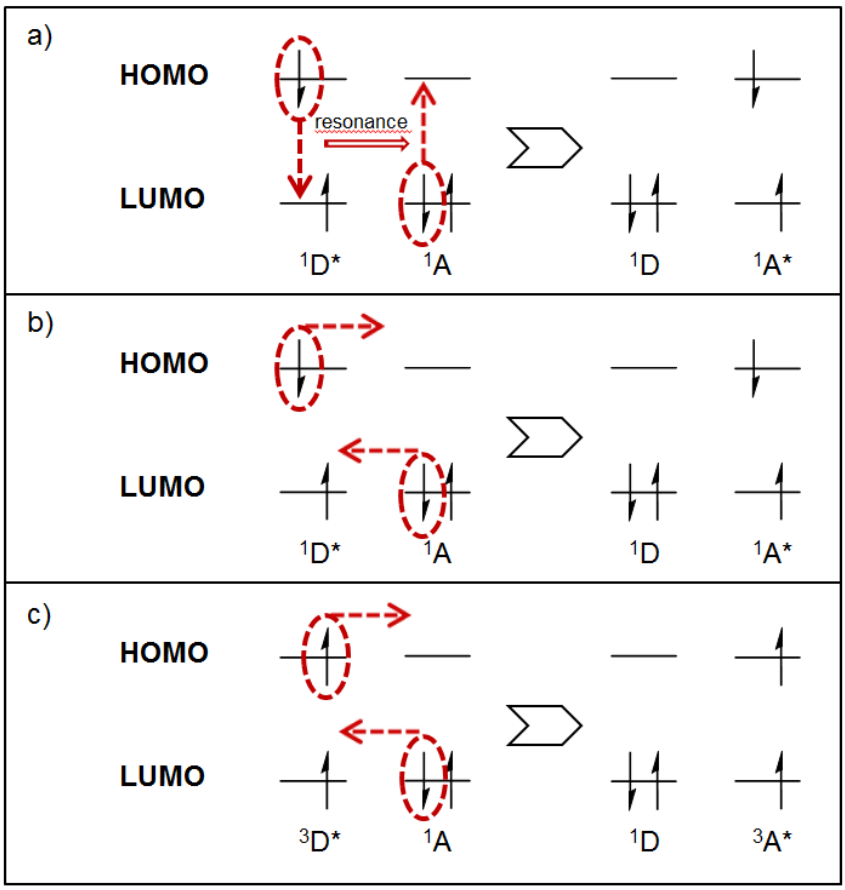

Figure 5. Simplified illustration of energy transfer processes. a) Förster energy transfer; b) Singlet Dexter energy transfer; c) Triplet Dexter energy transfer.[57]

(exciton energy) from the host to the guest are postulated. These are, on the one hand, Förster[58] transfer of singlet excitons and, on the other hand, Dexter[59] transfer of singlet and triplet excitons. In the case of Förster transfer, the absorption band of the phosphorescent dye needs a good overlap with the emission bands of the host. As most dyes have their absorption maximum in the blue region of the electromagnetic spectrum, wide bandgap materials are

commonly used as host materials in order to fulfill this requirement. Regarding Dexter transfer, the crucial requirement is that the energy of the excitons on the host matches the exciton energies on the guest.[60],[61] Figure 5 illustrates a simplified overview of the possible Förster and Dexter energy transfer mechanisms.

In the case of the Förster mechanism (Figure 5a), an excited donor molecule relaxes into the ground-state. The energy that is released during this process is simultaneously transferred non-radiatively *via* resonance to an acceptor molecule. The result is a donor molecule in ground-state and an excited singlet state on the acceptor molecule. This mechanism depends on some prerequisites. Apart from the orientation of the molecules influencing the dipole transition and absorption dipole, the distance between donor and acceptor molecules have to be < 10 nm as the efficiency is reduced with increasing distance by the factor of r^6 due to the Coulombic interaction. Figure 5 b) and c) illustrate the Dexter mechanism for singlet and triplet transfer, respectively. In this case, electrons hop from the LUMO of the donor to the LUMO of the acceptor while, simultaneously, an electron from the HOMO of the acceptor hops to the HOMO of the donor. For the Dexter mechanism, an overlap of the wave functions of the orbitals is necessary. This limits the possible distance between acceptor and donor to approximately 1 nm. In order to investigate the mechanisms of energy transfer in host-guest environments, Cleave *et al*. studied the transfer processes between a phosphorescent porphyrin, platinum(II) 2,3,7,8,12,13,17,18-octaethyl-21*H*,23*H*-porphyrin (PtOEP), and a series of host materials (Figure 6).[62] Based on their results, the following cases can be distinguished:

a) Exciton formation on the guest occures when it acts as a trap for one or both charges. Here, the HOMO of the host is lower than the HOMO of the guest. In consequence, holes will be trapped on the dye.

b) Dexter transfer occures when the guest is doped into a polymer blend where it only forms shallow charge traps so that excitons are predominantly formed on the host material. Besides singlet exciton transfer from host to guest, also triplet exciton energy transfer appears.

c) In case of offset HOMO and LUMO levels and additionly when the offset value is higher than the coulomb binding energy of the exciton, charge separation will occur and neither emission from the dye nor any energy transfer will be observed.

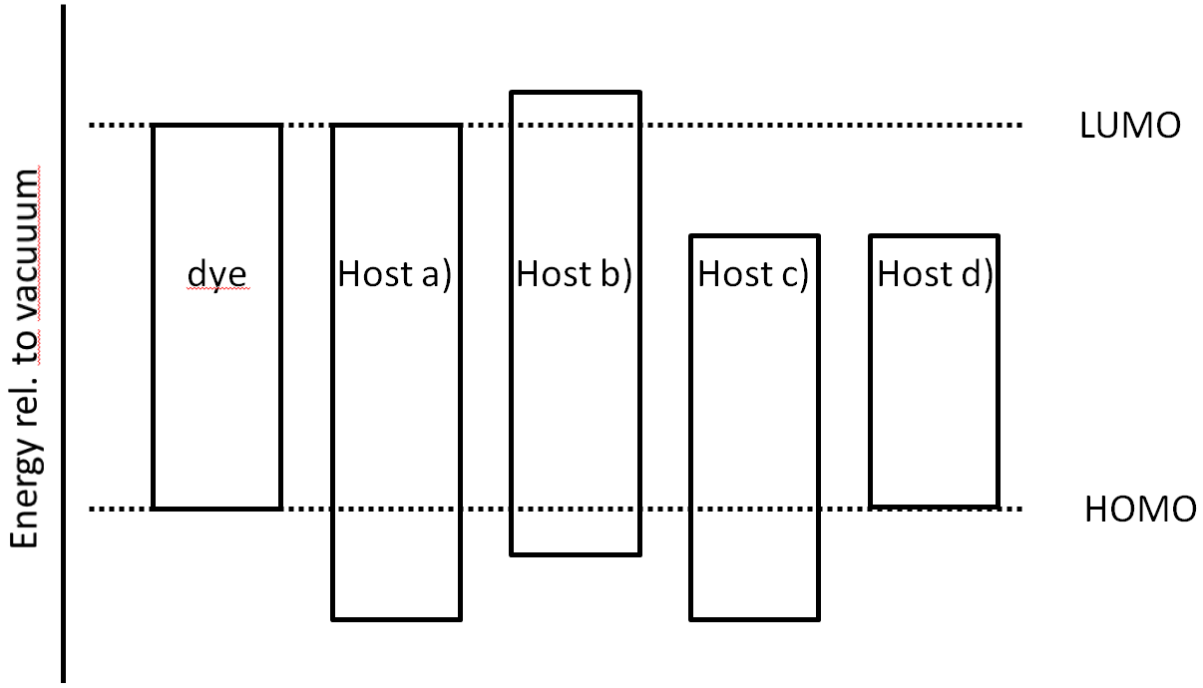

Figure 6. Schematic presentation of HOMO an LUMO levels according to studies of Cleave et al.[62]

d) If the LUMO of the host is lower in energy than the LUMO of the dye, energy back transfer from the guest to the host occurs in this system.

In summary, host and guest materials need to fit in terms of HOMO and LUMO levels to meet the intended operation mode of the device.

1.5 Multicolor OLEDs – approaches to white light-emitting diodes (WOLEDs)

Multicolor OLEDs are of exceedingly interest for lighting and display technology. While monochromatic OLEDs are relatively easy to fabricate and long-term color stability for most applications is of minor importance, multicolor OLEDs are often used as flat panel displays or for lighting applications where long-term stability of the individual colors plays an important role.

White light emission can be realized a) by adding the three basic colors red, green and blue (RGB), b) by utilizing the complementary colors blue and yellow (BY), or c) by a single

broadband emission between 400 nm and 700 nm. In the latter case, pure white light emission could be achieved, similar to daylight. The approach *via* RGB already allows white light emission sufficient enough for industrial use, e.g., in flat panel displays. The color purity of white light emission from blue/yellow devices is not usually sufficient for full color flat panel displays as they are not able to render saturated colors such as red. Thus, approaches for better color rendering by adding a red dye to BY devices have been recently developed.[63]

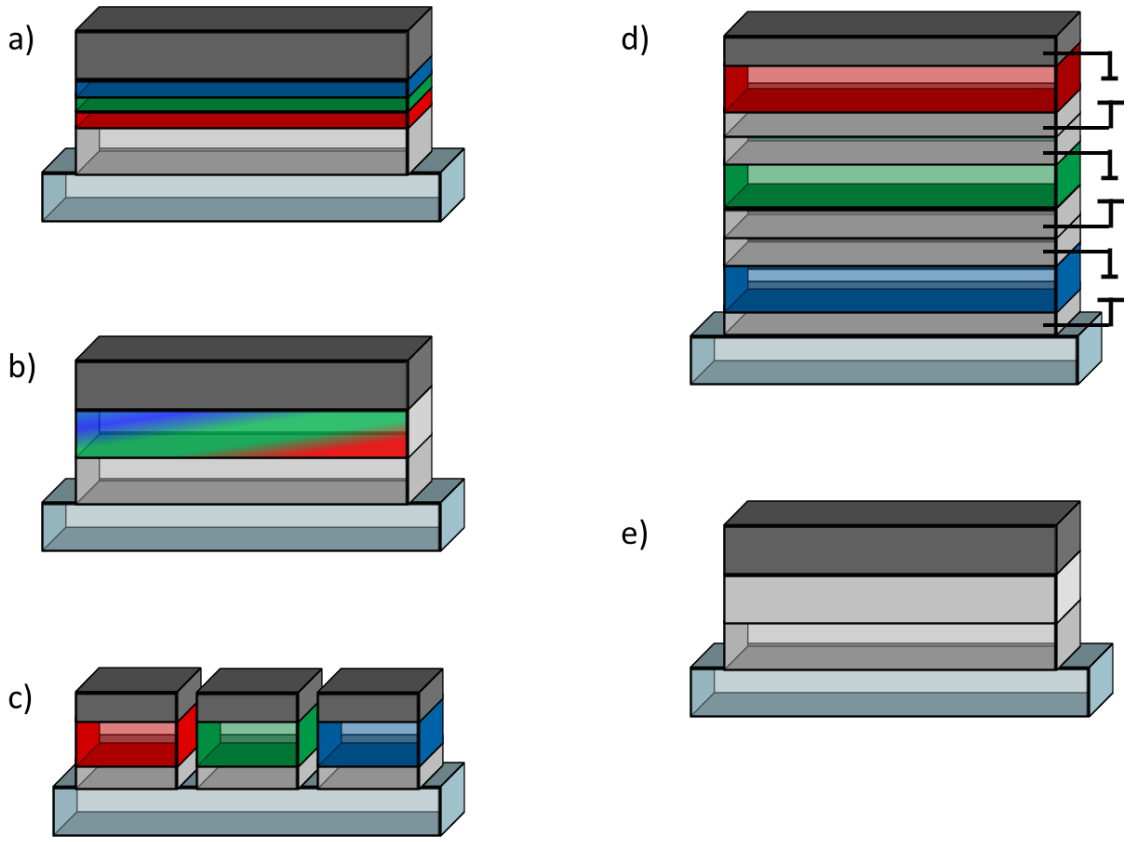

Figure 7. Simplified examples of device architectures for WOLEDs.[48] a) EML with 3 color sub-layers, b) mixture (blend) of RGB emitter molecules, c) pixelated architecture, d) stacked design, e) single component white light-emitting device. Dark grey layers represent reflective electrodes, transparent, light grey layers represent transparent electrodes and the light blue bottom layers represent transparent substrates (glass). For simplicity and better visibility, additional functional layers (HTL, ETL etc.) are not shown.

Figure 7 outlines a selection of white light-emitting OLED architectures. While a), c) and d) represent device architectures with separated red, green and blue light-emitting layers, b) and e) depict concepts of single layer emitter devices. The former allow the use of different host materials in the EML while the latter need to get by with only one host material. In Figure 7 a) three separate sub-layers for each color are casted on top of each other without any

separating functional layers.[64] Figure 7 b) shows a blend of red, green and blue emitters that are applied in a single layer along with a matrix.[65] A pixelated approach as found in multicolor flat panel displays is given in Figure 7 c). Multiple OLEDs can be stacked on top of each other allowing the variation of the current through each emitting layer and therefore tuning the emission color of the whole device as depicted in Figure 7 d).[66] Finally, in Figure 7 e), a single emitter to achieve white light by obtaining radiative decay from the individual excited emitter as well as from an exciplex/excimer is used.[67-68]

1.6 White light polymer organic light-emitting devices (WPLEDs)

In this section the focus will be on white light-emitting devices based on polymers. Therefore, an overview of different approaches utilizing polymer systems is given and some examples are discussed exemplarily.

Polymers can play different roles in OLEDs. They can act as host materials for small emissive molecules as depicted in Figure 8 a). Kido *et al.* published the first device by incorporating three fluorescent dyes in a poly(*N*-vinylcarbazole) (PVK) matrix.[65, 69] Later, Huang *et al.* reported on a device with a poly(fluorene) (PF) host material doped with orange light-emitting rubrene and electron transporting PBD resulting in an efficient WOLED.[70] Kawamura *et al.* gave an account of iridium(III) complexes used as phosphorescent guest materials in a PVK matrix reaching a power efficiency of 1.4 lm/W.[71] Since then, various enhancements in device architecture and materials have been reported.[72-73] Cheng *et al.* reached power efficiencies as high as 25.6 lm/W in devices with two phosphorescent iridium(III) complexes doped into a silane-based wide band-gap polymer.[74]

Furthermore, polymers can also be the light-emitting species. Figure 8 b) outlines a device with two separated polymer layers, one emitting blue light and the other one yellow light. To overcome the difficulties in the device preparation (see chapter 1.2), the first polymer needs to be cross-linked to the underlying functional layer. Moreover, the recombination zone should be close to the interface in order to realize emission from both species.[48]

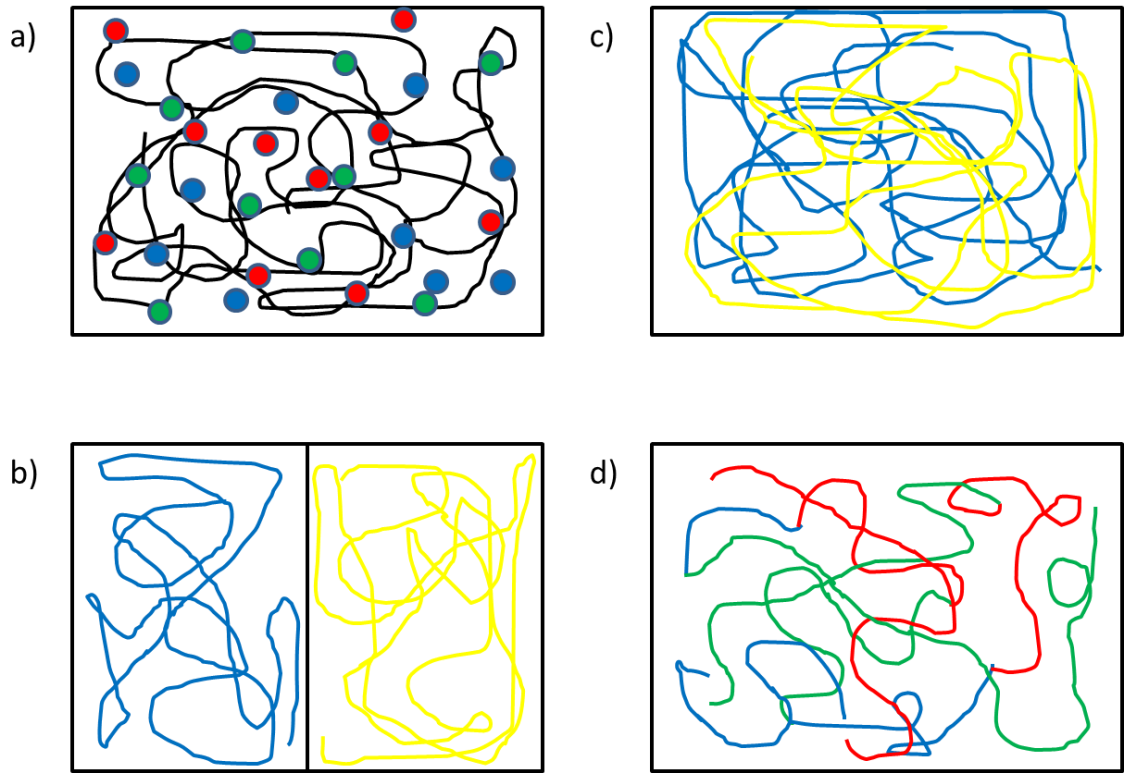

Figure 8. Concepts of polymeric arrangements applied in organic white light-emitting devices. a) polymer as a host material for small emitter molecules. b) separated light-emitting polymers. c) blend of light-emitting polymers. d) single copolymer with red, green and blue light-emitting blocks. [48]

Chao *et al*. described a device with a PVK and poly(2-dodecyl-*p*-phenylene) (C12O-PPP) layer.[75] White light emission was achieved due to exciplex emission at the interface, when toluene was used as good solvent for both layers allowing the mixing of the polymers. When *n*-hexane was used as solvent, no mixing occurred because PVK is insoluble in *n*-hexane, thus resulting in blue fluorescence from C12O-PPP layer only and the PVK acting mainly as a HTL. Further work on this topic was done by Thompson *et al*. who compared a wide range of bilayer devices and also found emission from exciplexes at the interface.[76] Köhnen *et al*. fabricated a device with super yellow[77] as a yellow fluorescent emitter and polyfluorene as a blue fluorescent emitter on top.[78] The yellow layer was cross-linked to the HIL before the polyfluorene layer was applied. All prepared devices revealed good color stability and distinct blue and yellow emission without exciplex emissions.

White light-emission from blended polymers as illustrated in Figure 8 c) was realized by Tasch *et al*., who used a methyl substituted ladder-type polyparaphenylene (*m*-LPPP) as a blue light-emitting polymer blended with orange-red light-emitting poly(perylene-co-

diethynylbenzene) (PPDB).[79] An external quantum efficiency (EQE) of 1.2 % was reported when poly(methylenemethacrylat) (PMMA) was added to the emissive layer in order to reduce the Förster energy transfer.[80] Another approach was realized by Hu *et al*. by using blue and green light-emitting polymers along with a red light-emitting small molecule dye.[81] In an optimized device architecture, an external quantum efficiency of 2.6% was reached. An external quantum efficiency of 6% was achieved by Huang *et al*. by blending polyfluorene as a blue emitter with poly[2-methoxy-5-(2′-ethyl-hexyloxy)-1,4-phenylene vinylene] (MEH-PPV), and optimizing the electronic-energy profile as well as the device architecture with a hole blocking layer of caesium carbonate.[82]

Finally, white light-emitting polymers can either contain blue and orange, or red, green and blue chromophores in the backbone or (partly) in the side chain, as outlined in Figure 8 d) for RGB copolymers. Moreover, either singlet, a mixture of singlet and triplet emitters, or solely triplet emitters can be used. An example for an all fluorescent conjugated RGB copolymer was given by Liu *et al*. in 2005.[83] They synthesized a copolymer *via* Suzuki cross-coupling of 9,9-dioctylfluorene (PF)-based monomers as blue emitter, 4-diphenylamino-1,8-naphthalimide (DPAN)-based monomers as a green emitter and 4,7-bis(5-(4-(*N*-phenyl-*N*-(4-methylphenyl)amino)phenyl)-thienyl-2-)-2,1,3-benzothiadiazole (TPATBT)-based monomers as a red emitter. While TPATBT was incorporated in the main chain, DPAN was attached to the main chain *via* an alkyl chain. Incomplete energy transfer from the fluorene units to the TPATBT and DPAN resulted in red, green and blue emission. The fabricated devices revealed no color dependency on voltage, but the device performance was quite low (0.83 lm/W). Liu *et al*. investigated a WPLED using a polyfluorene-based polymer where a blue dimethylamino-naphthalimide (DMAN) and orange 4-(4-(diphenylamino)phenyl)-7-(4-(*N*-phenyl-*N*-(4-methoxyphenyl)amino)phenyl)-2,1,3-benzothiadiazole fluorescent emitter were attached via alkyl spacers to the polymer backbone.[84] The fabricated device reached an efficiency of 8.5 lm/W. The increase in efficiency was explained by the red shift of the blue emission of DMAN compared to PF and its higher photoluminescence (PL) quantum efficiency.

A coverage of the whole visible spectrum from 400 nm to 700 nm was achieved by Liu *et al*. in 2007 by attaching blue, red and green fluorescent chromophores to a polyfluorene main chain.[85] The fabricated devices revealed good color stability and efficiency as high as 5.4 lm/W. A mixture of fluorescent and phosphorescent chromophores incorporated into the main chain was reported by Zhen *et al*. with a polyfluorene being the backbone as well as the blue fluorescent emitter and benzothiadiazole (BT) as an additional green fluorescent emitter.[86]

An incorporated iridium complex [iridium(III)bis(2-(2'-benzo[4,5-α]-thienyl)pyridinato-N,$C^{3'}$)2,2,6,6-tetramethyl-3,5-heptanedione] ([$(btp)_2$Ir(tmd)]) served as a red triplet emitter. The devices prepared revealed an external quantum efficiency of up to 3.8% and color stable white light emissions independent of the bias. Another approach was published by Jiang *et al*.[87] The reported copolymer consisted of a polyflourene backbone in which BT as green fluorescent emitter units and 3,6-dibromo-9-(iridium(III)bis(2-phenylquinoline-N,$C^{2'}$))-14-trifluoro-11,13-tetradecyldiketone)carbazole[88] as red emitter units being incorporated into the copolymer main chain *via* a carbazole moiety were used. The devices revealed acceptable color stabilities and luminance efficiencies of up to 6.1 cd/A. For deeper insights on other device concepts of WPLEDs, reference is to be taken to the reviews of Wu[89] and Reineke.[48]

1.7 Phosphorescent iridium(III) complexes for OLED applications

Iridium(III) complexes are widely used as phosphorescent emitters in OLEDs (see chapter 1.4). Since the pioneering work of Thompson and Forrest,[31] a wide range of homoleptic iridium(III) complexes with three identical ligands,[90] as tris[2-phenylpyridinato-C^2,*N*]iridium(III) [$Ir(PPy)_3$], on the one hand, and heteroleptic iridium(III) complexes, with at least one different ligand, on the other hand, have been successfully developed and tested in OLEDs. Apart from their already discussed property of harvesting singlet and triplet excitons, their second main advantage is their easy color tuning ability. As figured out by computational studies of *fac*-$Ir(PPy)_3$, this is due to the HOMO of the complex being centered on a iridium(III) d-orbital and the LUMO being localized on the π-orbital of the cyclometalating ligand.[34, 91] By adding electron withdrawing groups (EWG) to its phenyl ring, the HOMO is stabilized resulting in a blue shift of the emission as observed in [$Ir(Fppy)_3$] compared to [$Ir(PPy)_3$] (Scheme 5). In contrast, adding electron releasing groups to the phenyl ring results in a red shift of the emission spectrum by destabilizing the HOMO as observed in tris[1-phenylisoquinoline-C^2,*N*]iridium(III) [$Ir(piq)_3$].[92] A similar effect of color shifting of the emission bands can be achieved by exchanging the ancillary ligand in heteroleptic complexes. Even though the HOMO of the complexes is mostly metal-located and the LUMO is mainly located on the cyclometalating ligands, resulting in the fact that the ancillary ligand is not directly involved in the emissive transition, the ligand structure influences the electron density significantly at the metal center.[93-94] For example, exchanging the acetylacetonate (acac) ligand of FIr(acac) with a stronger electron withdrawing ligand e.g.

picolinate as in Fir(pic), results in a blue shift of the maximum emission wavelength by 20 nm.[95-96]

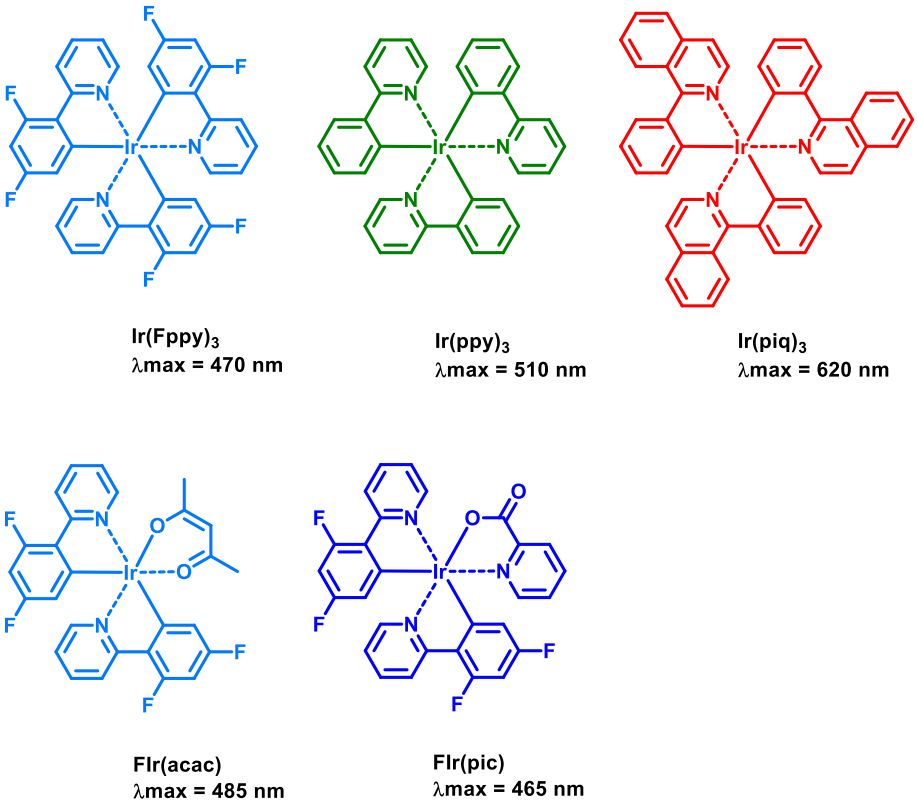

Scheme 5. Chemical structures and corresponding PL maximum of five selected iridium(III) complexes.

The synthesis of homoleptic and heteroleptic Ir(III) complexes is usually carried out by synthesizing a precursor complex of the general formula $[Ir(III)(C\text{^}N)_2\text{-}\mu\text{-}Cl]_2$.[97] There, iridium(III)chloride · x H_2O is treated with 2.5 equivalents of the cyclometalating ligand in a 3:1 mixture of 2-ethoxyethanol and water under inert gas. Biscyclometalated iridium(III) complexes can be obtained *via* the so called bridge-splitting method by stirring the iridium(III) precursor complex with the ancillary ligand and a weak base like potassium carbonate in high boiling point alcohols like 2-ethoxyethanol.[98],[99] The complexes can be purified via column chromatography and recrystallization.

Triscyclometalated iridium(III) complexes are usually obtained by utilizing silver triflate as reagent.[100], [101] Depending on the reaction temperature, thermodynamically favored facial complexes or kinetically favored meridional complexes are obtained (Scheme 6). Microwave assisted synthesis for bis- and triscyclometalated iridium(III) complexes has been reported as

well, allowing shorter reaction times. However, the yields remain lower than those achieved using conventional methods.[102],[103]

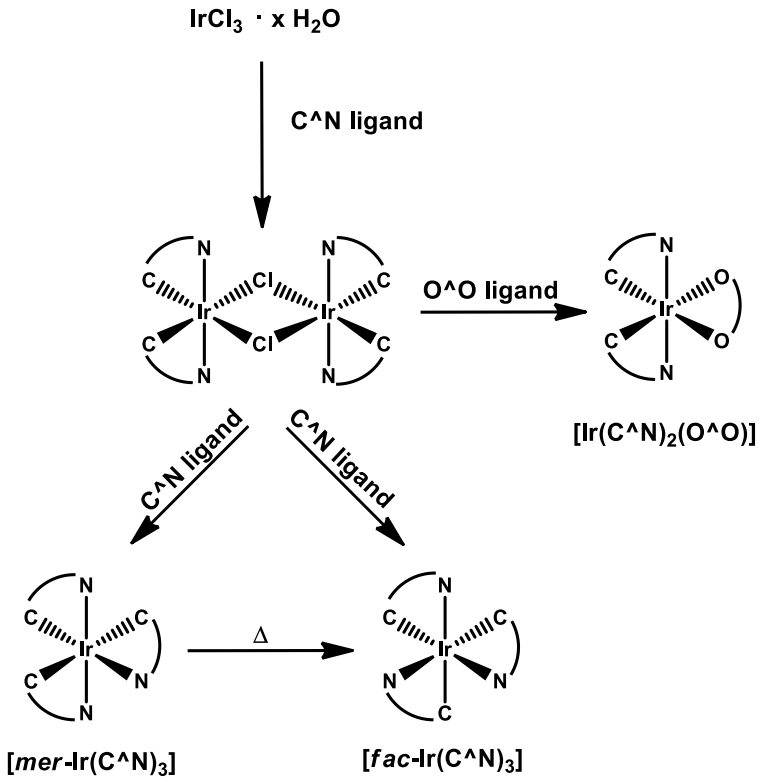

Scheme 6 . Synthesis route to bis- and triscyclometalating iridium(III) complexes.

2. Aim and scope

As outlined in chapter 1, polymers as active layers in OLEDs have advantages in device fabrication regarding costs and simplicity. Following the described design rules, they also show excellent film forming properties and color stability independent of the applied bias. The aim of the project was the synthesis and characterization of emissive copolymers in which iridium complexes are incorporated. Notably, the copolymers had to be suitable for color tuning in the visible spectrum (RGB) and, ultimately, for white light emission. Moreover, facile fabrication properties like good solubility and high thermal stability were crucial requirements.

9,9-dioctyl-9*H*-fluorene **8** has been used in all copolymers as the main repeating unit of the copolymer backbone because polyfluorene-type polymers have proven to be appropriate host materials in OLEDs due to their wide HOMO-LUMO band-gap, high thermal stability, efficient energy transfer and blue emission.[70, 104-105] Moreover, the octyl side chains should enhance the solubility in various organic solvents. In a first series of copolymers, 9*H*-fluorene-9-one was incorporated into the backbone as green emitter along with varying amounts of a red light-emitting phosphorescent iridium(III) complex (Scheme 7).

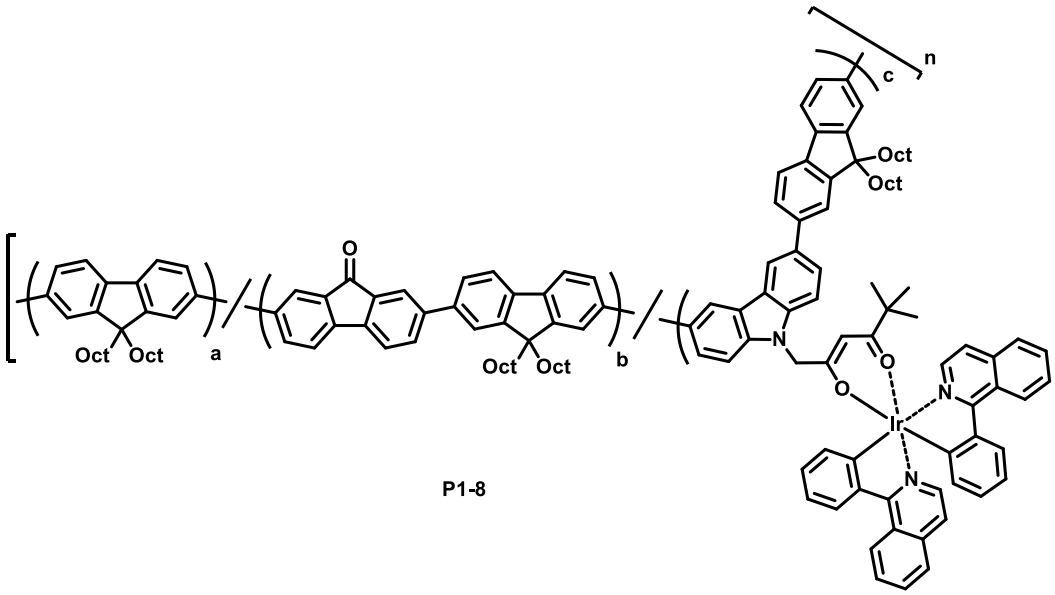

P1-8

Scheme 7. Chemical structure of the planned series of copolymers.

The complex was provided with 2-phenylisoquinoline (piq) as cyclometalating ligands and thus served as a red emitter. A carbazolyl-functionalized ancillary ligand was used to promote hole trapping at the emitter site.[106] The electron rich carbazole moiety should lower the reduction potential of the neighboring 9,9-dioctylfluorene units in the copolymer chain and render the material p-conductive.[107] The electron deficient 9*H*-fluorene-9-one comonomer unit should support electron trapping.[108] Although iridium(III) complexes with 2-phenylisoquinoline (piq) cyclometalating ligands show slightly lower quantum yields as those with 2-naphthylpyridine (npy), piq was favored over npy due to its red-shifted emission, thus allowing a better color tunability for white light emission.[34] As the iridium(III) complex is known to be stable under Suzuki-type cross-coupling conditions, while the reaction conditions of the nickel-mediated Yamamoto protocol appeared to be unsuitable, all copolymers were prepared *via* Suzuki-type cross-coupling.

In order to solve the problem of orthogonal solvents needed when preparing subsequent organic layers from solutions by spin coating or printing, a promising approach by Kanelidis *et al*.[109] was adapted. Microparticle suspensions of the copolymers in water were prepared and evaluated for inkjet printing by Dr. Anke Teichler at the University of Jena, Germany.

White light-emitting copolymers were prepared (Scheme 8) and subsequently corresponding single component WPLEDs were fabricated by M.Sc. D. Abbaszadeh at the University of Groningen, the Netherlands. Notably, enhancement of charge injection is a crucial parameter of single layer devices. Thus, the copolymers for WPLEDs were further optimized by using either triarylamine-functionalized fluorene or 2-ethylhexyl-functionalized carbazole comonomers for incorporation into the copolymer backbone.

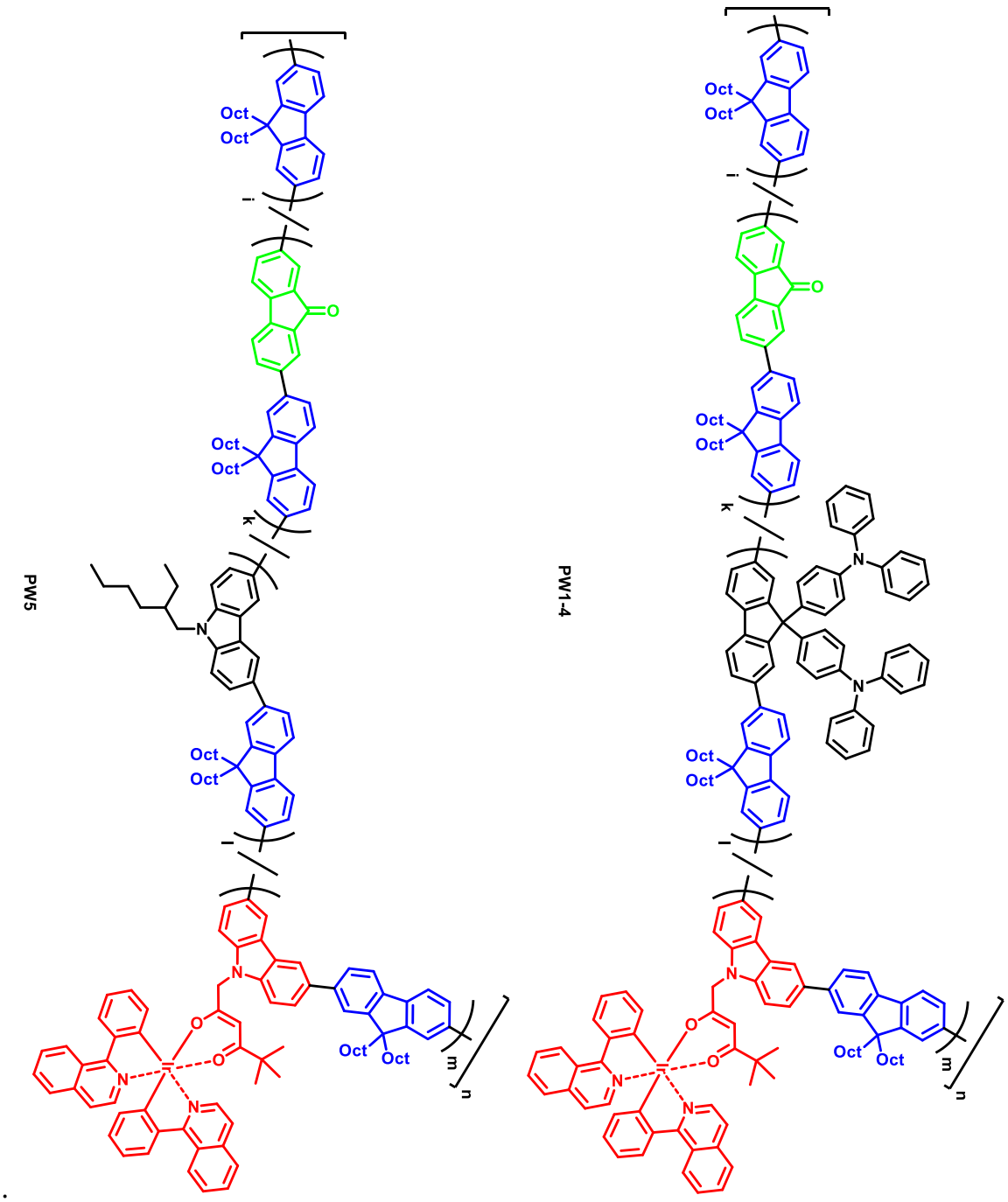

Scheme 8. Chemical structures of copolymers PW1-5.

3. Results and Discussion

3.1 Properties of Ir(piq)$_2$(carbacac)

The monomeric iridium(III) complex [Ir(piq)$_2$(carbacac)] (Scheme 9) that is used as the red light-emitting building block in all copolymers was previously synthesized by N. Tian.[34, 110] It reveals high thermal stability of over 350°C and a luminescence QE of 31%. The PL emission maximum is located at λ_{max} = 624 nm in chloroform solution.

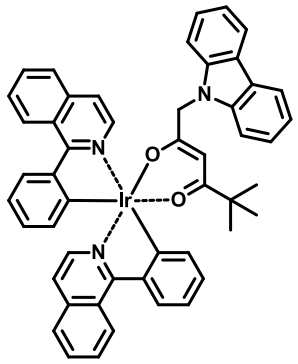

Scheme 9. Chemical structure of iridium(III) complex [Ir(piq)$_2$(carbacac)] as synthesized by N.Tian.[34],[110],[111]

The structural design of the complex allows hole-trapping at the carbazolyl moiety, thus enhancing the probability of exciton formation at the emitter site.[106] Moreover, its 9*H*-carbazol substructure is also the base for incorporation of the complex into the copolymers: 9*H*-carbazol can be easily functionalized in 3- and 6-position due to the mesomeric effect of the nitrogen atom in 9-position, thus activating the 1, 3, 6 and 8-positions, as depicted in Scheme 10. As with diphenylamines, the para-positions with respect to the nitrogen are the most reactive ones, thus allowing the selective functionalization of the 3- and 6-position only. Furthermore, its amine hydrogen is sufficiently acidic, allowing the introduction of a manifold of functionalities by nucleophilic substitution.[112]

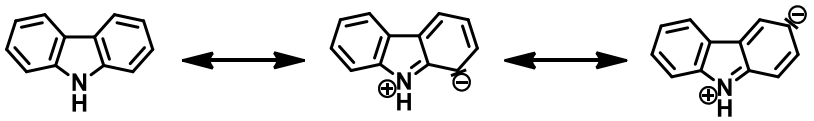

Scheme 10. Aromatic resonance structures of 9*H*-carbazole.

Since conjugation would influence the electron withdrawing effect of the acetylacetonate ligand, a methylene group was introduced as spacer, thus separating the conjugated backbone from the ancillary ligand while keeping the distance of the carbazole unit to the iridium(III) complex as close as possible. Thus, comparable properties of the complex for different polymer backbones should be consectaneous. Furthermore, the bulky *tert*-butyl moiety of the acetylacetonate enhances the solubility of the complex in organic solvents as well as its thermal and chemical stability.[113]

3.2 Synthesis of comonomers

3.2.1 Synthesis of iodine-functionalized Ir- complex [Ir(piq)$_2$(dicacac)]

Our decision was to incorporate the complex into the polymer backbone *via* its carbazole functionality. Obviously, the most efficient route in terms of the synthetic effort would be the introduction of bromine or iodine moieties in the 3- and 6-position of the carbazole. Due to the fact that 3,6-dibrominated 9*H*-carbazoles show reduced reactivity in Suzuki-Miyaura cross-coupling reactions compared to 2,7-dibrominated fluorenes, iodine was preferred over bromine as functional group in 9*H*-carbazol. The synthesis of the iodine-functionalized ancillary ligand was carried out by following the synthetic concept as depicted in Scheme 11. While aromatic hydrocarbons usually cannot be iodinated with elementary iodine, many aromatic heterocycles like 9*H*-carbazole can be easily iodinated with good regio-selectivity. In order to iodinate 9*H*-carbazol to 3,6-diiodo-9*H*-carbazole **1**, a modified method according to Tucker *et al*.[114] was applied which resulted in higher yields compared to microwave-assisted oxidative halogenation with hydrogen iodide and hydrogen peroxide.[115-116]

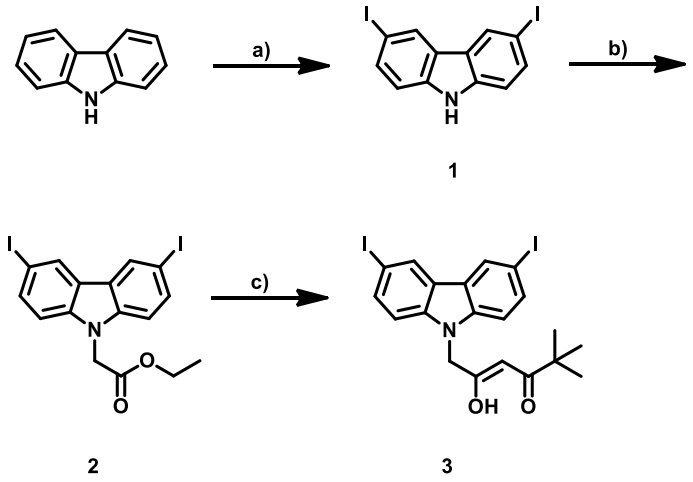

Scheme 11. Synthesis of ancillary ligand 3. a) KI, KIO_3, acetic acid, 80°C 45 min; b) K_2CO_3, ethyl bromoacetate, DMF, 60°C → rt; c) pinacolone, KHMDS, THF, 0°C → rt, overnight.

Here, potassium iodide and 9*H*-carbazole were dissolved in boiling acetic acid, and excess potassium iodate was added in small portions at 80°C. After precipitation with an excess of water, colorless crystals were obtained which were then purified by either recrystallization from ethanol or column chromatography to separate from the by-products, esp. 3-iodo-9*H*-carbazole. 3,6-diiodo-9*H*-carbazole **1** was characterized by NMR spectroscopy and GC-MS measurements.

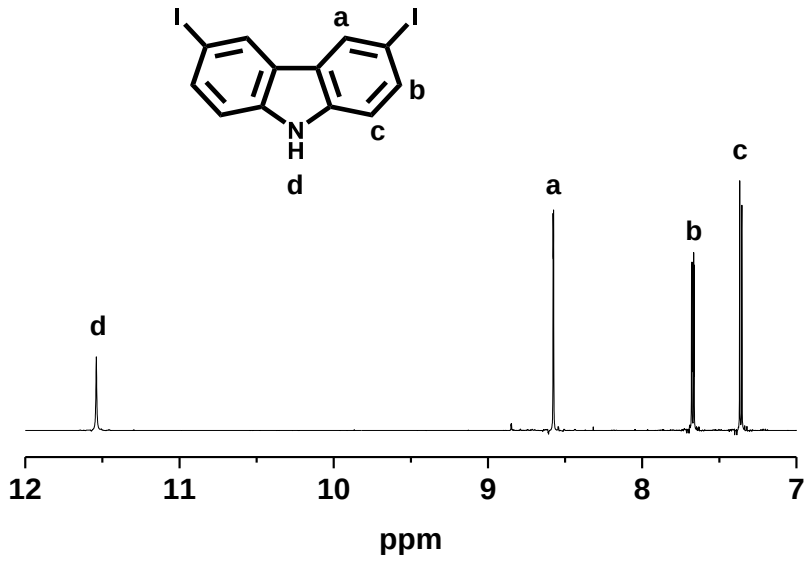

Figure 9. ^{1}H-NMR spectrum of 1 recorded in DMSO-d_6 at room temperature.

The ^{1}H-NMR spectrum of **1** (Figure 9), recorded in DMSO-d_6, shows the expected resonances of the three different remaining aromatic hydrogens. These are a singlet with a chemical shift of δ = 8.57 ppm for the protons in 4 and 5 position and two doublets with a coupling constant of J = 8.5 Hz at δ = 7.67 and 7.36 ppm for the protons in 1 and 8 as well as 2- and 7-positions. Moreover, a broadened resonance of the amine proton is visible at δ = 11.54 ppm. In the ^{13}C{^{1}H}-NMR spectrum the resonances of the carbons in 3 and 6 positions are shifted to higher field from δ = 120 to 81.8 ppm compared to the educt 9*H*-carbazole, due to the combination of mesomeric and inductive effects of the iodine atoms, thus proving the successful introduction of the iodine. Additionally, the molecule mass peak was found in GC-MS measurements at a mass-to-charge ratio of m/z = 419.

Ethyl 2-(3,6-diiodo-9*H*-carbazol-9-yl)acetate **2** was obtained by treating **1** with potassium carbonate in dry DMF in order to abstract the amine hydrogen. In a nucleophilic substitution, the product was formed by adding ethyl bromoacetate to the solution.[117]

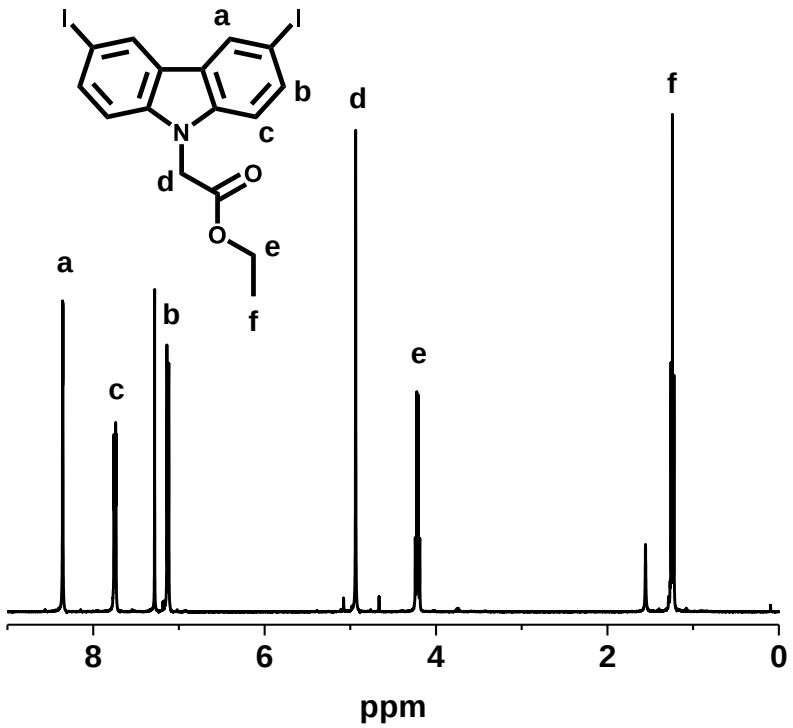

Figure 10. ^{1}H-NMR spectrum of 2, recorded in $CDCl_3$ at room temperature.

After complete precipitation with excess water and drying, the product could be afforded in quantitative yields. Compared to the ^{1}H-NMR spectrum of **1**, the hydrogen of the amine resonance at δ = 11.54 ppm is no longer present (Figure 10). Instead, a triplet at δ = 1.24 ppm with a coupling constant of J = 7.1 Hz and a quartet at δ = 4.22 ppm with corresponding coupling constant are found in the spectrum which are attributed to the ethyl moiety. An additional singlet at δ = 4.94 ppm is assigned to the methylene-bridge. The resonances of the aromatic region are only slightly shifted due to the introduced acetate.

In the ^{13}C{^{1}H}-NMR spectrum the resonances of the aromatic region are barely shifted. Four new signals originate from the ethyl group (δ = 14.11 ppm, δ = 61.93 ppm), the methylene-bridge (δ = 44.75 ppm) and the quaternary carbon of the ester group (δ = 167.70 ppm). The molecule mass peak was found at m/z ([M+Na]$^{+}$) = 527.89.

The last step in the synthetic route towards the ligand is a nucleophilic acylation of pinacolone with **2**. Sterically hindered potassium hexamethyldisilazane (KHMDS) is used as a base in order to abstract an α-proton from the pinacolone.[34] Compared to **2**, the aromatic region of the ^{1}H-NMR spectrum of **3** remains unchanged (Figure 11). Also the singlet at δ = 4.94 ppm, representing the methylene bridge, is found in the same position. The resonances of the ethyl group have been replaced by a singlet at δ = 1.04 ppm with a relative integral of nine hydrogens, representing the nine methyl protons of the introduced *tert*-butyl group. Additionally, a singlet at δ = 5.34 ppm with a relative intensity of one hydrogen atom can be attributed to the keto-enol-tautomer, indicating that the equilibrium is on the side of the enol rather than the diketone. The corresponding alcohol proton resonance is found at δ = 15.43 ppm as a broad singlet. The ^{13}C{^{1}H}-NMR spectrum of **3** is dominated by a resonance at δ = 27.1 ppm which is assigned to the three methyl carbon atoms of the *tert*-butyl group. Moreover, at δ = 200.1 and190.2 ppm, resonances of the carbonyl and alcohol carbons of the keto-enol tautomer are visible. In the recorded mass spectrum, the molecule peak of **3** was found at m/z [M+Na]$^{+}$ = 581.94 g/mol.

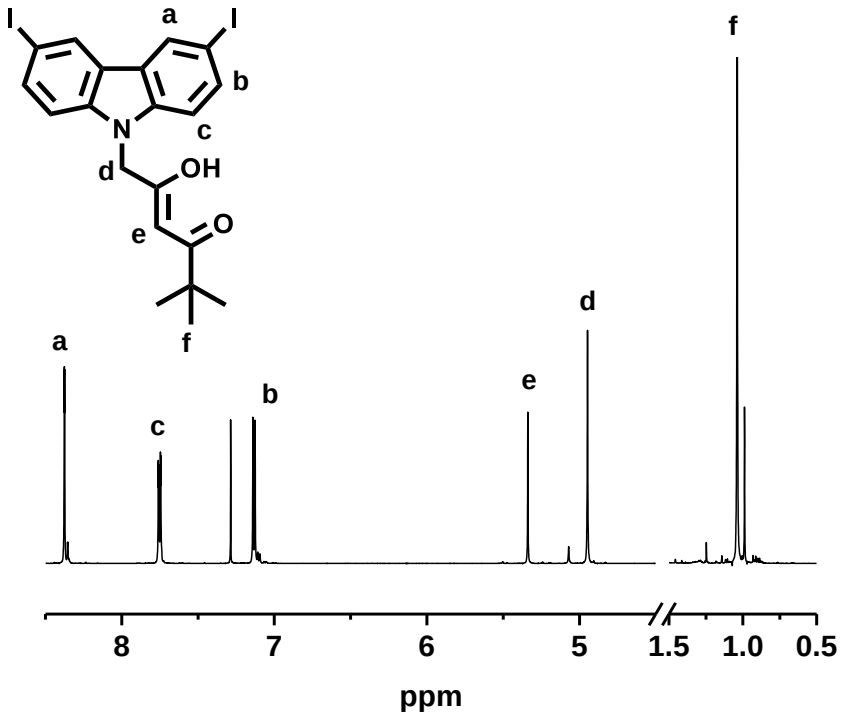

Figure 11. ^{1}H-NMR spectrum of 3, recorded in $CDCl_3$ at room temperature.

1-Phenylisoquinoline **4** as the cyclometalating ligand was synthesized *via* Suzuki cross-coupling of 1-chloroisoquinoline and phenylboronic acid with sodium carbonate as base and tetrakis(triphenlyphsophine)palladium(0) as catalyst (Scheme 12).[34-35, 118] In accordance with the literature, the ^{1}H-NMR spectrum consists of four doublets with a relative intensity of one proton each at δ = 8.65, 8.14, 7.92 and 7.68 ppm as well as two multiplets - one with a relative intensity of three protons at δ = 7.76 - 7.00 ppm and one with a relative intensity of four protons between δ = 7.60 and 7.50 ppm.[119] Doublets at δ = 8.65 and 7.68 ppm can be assigned to the 3 and 4 position of the isoquinoline moiety, respectively. The five protons of the phenyl ring can be assigned to multiplet resonances at δ = 7.56 ppm and δ = 7.73 ppm, respectively. In the ^{13}C{^{1}H}-NMR spectrum of **4** 13 resonances are visible, as expected. The molecule mass peak was found at m/z [M^{+}] = 205.09

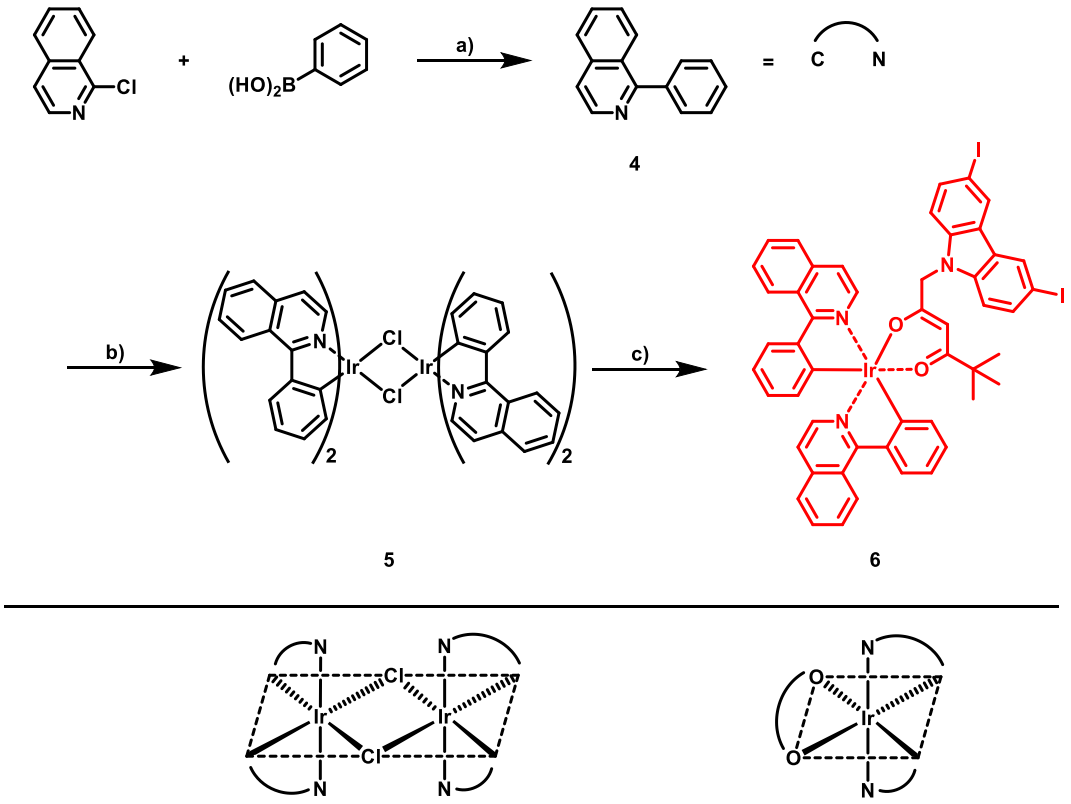

Scheme 12. Top: Synthesis of 1-phenylisoquinoline 5 and [(piq)$_2$Ir(carbacac)] 7. a) Na_2CO_3, $Pd(PPh_3)_4$, toluene/water (3:1 v/v), Aliquat® 336, 85°C, 24h. b) $IrCl_3 \cdot x\ H_2O$, 2-ethoxyethanol/water, 130°C, 24h. c) 3, K_2CO_3, 2-ethoxyethanol, 2h, 130°C. Bottom: Proposed structures of the μ-chloro-bridged iridium(III) precursor dimer complex (edge-sharing bioctahedral) (6) (left) and proposed octahedral structure of the facial [(piq)$_2$Ir(carbacac)] complex (7) (right)[120].

The synthesis of the iridium(III) complex **6** was performed in two steps. First, a μ-chloro-bridged dimer complex **5** was synthesized following a modified route by Nonoyama.[97] Here, iridium(III)chloride hydrate is stirred overnight with **4** in 2-ethoxyethanol at reflux temperature to obtain a red powder which is filtered off and washed with excess ethanol to give **5** in 70.5% yield. At room temperature, the product is insoluble in common organic solvents and water.

(Z)-((1-(3,6-diiodo-9*H*-carbazol-9-yl)-5,5-dimethyl-4-oxohex-2-en-2-yl)oxy)bis(2-(isoquinolin-1-yl)phenyl)iridium(III) **6** was synthesized following a slightly modified protocol developed by Tian *et al.*[7] Precursor complex **5** and ligand **3** were stirred with potassium carbonate in 2-ethoxyethanol at reflux temperature for two hours. After workup and cleaning, a red powder was obtained in 82.3 % yield which revealed good solubility in common organic solvents, e.g, chloroform, dichloromethane and acetone.

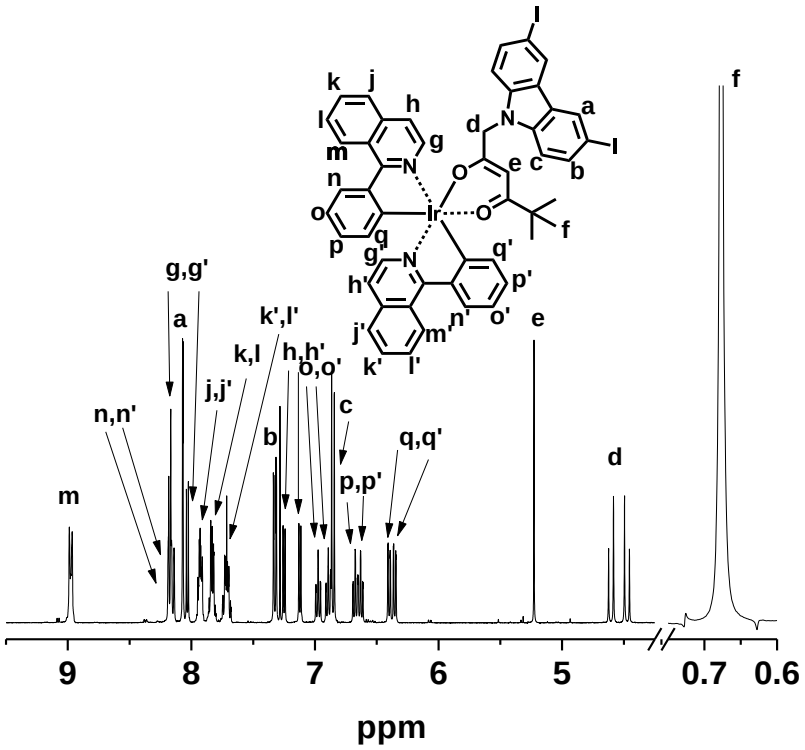

Figure 12. Cuttings of ^{1}H-NMR spectrum of 6. The assignment was done with the assistance of additional ^{1}H-^{1}H-COSY-NMR experiments.

The ^{1}H-NMR spectrum of **6** (Figure 12) revealed the expected resonances, which were assigned with the help of additional ^{1}H-^{1}H-COSY-NMR experiments. Due to the fact that the ancillary ligand is asymmetric, the protons of the 1-phenylisoquinoline cyclometalating ligands are not chemical equivalent. This is apparent in the ^{1}H-NMR spectrum where all resonances of the cyclometalating ligands are split. The resonances of the ancillary ligand are not splitted due to the free rotation of the carbazole as well as the *tert*-butyl group, except for proton d which is part of the rigid structure. With additional ^{1}H-^{13}C-HSQC-NMR experiments, the resonances of the ^{13}C{^{1}H}-NMR spectrum could successfully assigned. The measured infra-red (IR) spectrum revealed the bands for the aliphatic carbon-hydrogen valence vibration at ν = 3040 cm^{-1}, as well as the expected aromatic carbon-hydrogen valence vibration at ν = 3040 cm^{-1}. A weak band at ν = 1710 cm^{-1} occurs due to the carbonyl stretching vibration (Figure 13). In atmospheric pressure laser ionization – mass spectrometry (APLI-MS) measurements, the molecule mass peak was found at a mass to charge ratio of m/z = 1159 with the expected isotope pattern (Figure 14).

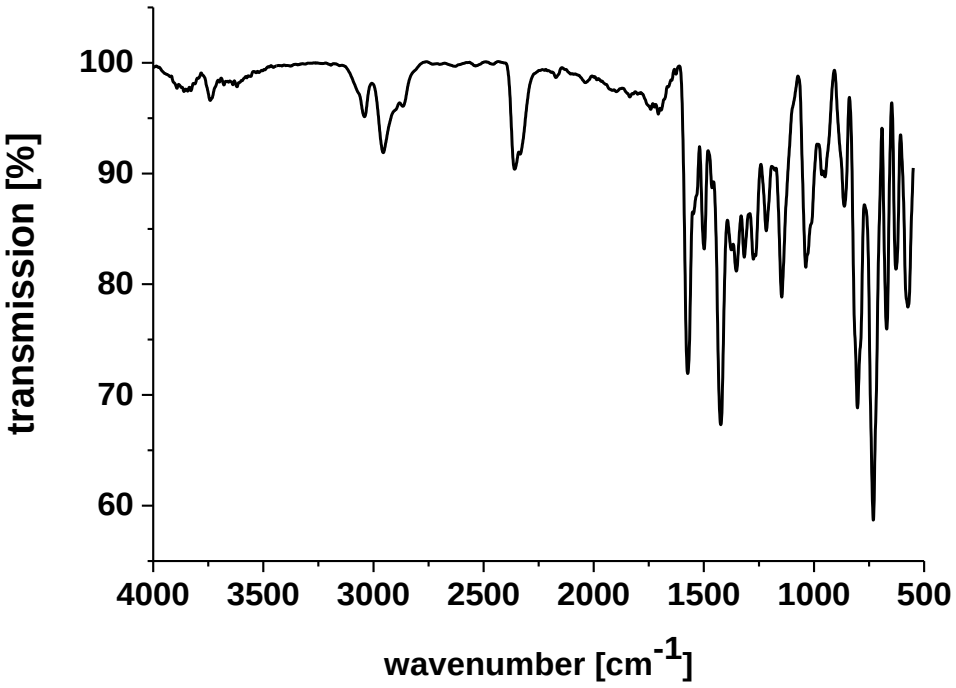

Figure 13. IR (ATR) spectrum of 6.

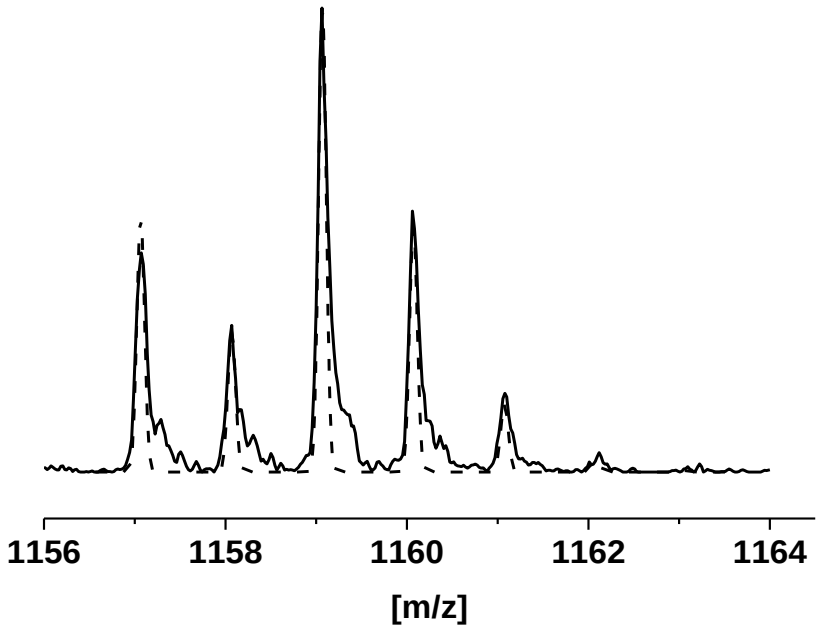

Figure 14. Normalized relevant section of the measured (solid line) and simulated (dashed line) high-resolution mass spectra of 6.

UV/Vis absorption and emission spectra were recorded in chloroform solution and are depicted in Figure 15.

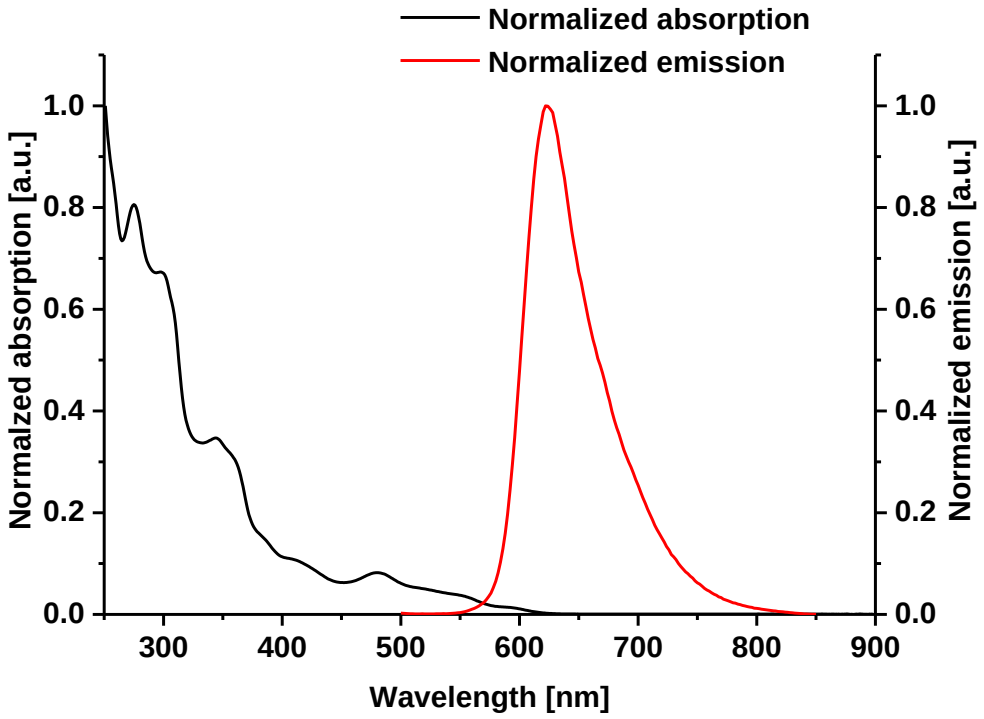

Figure 15. Normalized absorption and emission spectra of 6 in chloroform solution (exc. 480 nm, 10^{-5} M).

The absorption spectrum is dominated by several strong bands between λ= 250 - 300 nm which can be attributed to spin-allowed π → π* transitions of the cyclometalating ligands (inter-ligand, IL). Shoulders between λ = 300 - 500 nm are mainly attributed to ^{1}LC (ligand centered) and ^{1}MLCT (metal to ligand charge transfer) transitions.[121] The tail in the region of λ = 500 - 600 nm can most likely be assigned to ^{3}MLCT and ^{3}LC transitions.[122] As mentioned in the introduction, the cyclometalating piq-ligands own a strong contribution to the emission color of the iridium(III) complex, while the contribution of the ancillary ligand **3** is only low. Therefore, the emission spectrum consists of only one band which is assigned to the transition from the lowest lying triplet state to the ground state and is found at λ_{max} = 622 nm.

3.2.3 Synthesis of fluorene-based monomers

Two fluorene-based monomers were also synthesized (Scheme 13). 4,4'-(2,7-dibromo-9*H*-fluorene-9,9-diyl)bis(*N*,*N*-diphenylaniline) **7** was synthesized to promote hole-injection in the prepared single-layer OLEDs by increasing the HOMO level of the polymer ($HOMO_{PF}$ ~ -5.8 eV; $HOMO_{PF\text{-}Arylamine}$ ~ -5.2 eV – 5.5 eV). Other benefits are the low ionization potential, tridimensional steric and good UV-light harvesting properties.[123-125] The synthesis was carried out by treating 2,7-dibromo-9*H*-fluoren-9-one with *N*,*N*-diphenylbenzeneamine and methanesulfonic acid as catalyst above the melting point of *N*,*N*-diphenylbenzeneamine.[126-127]

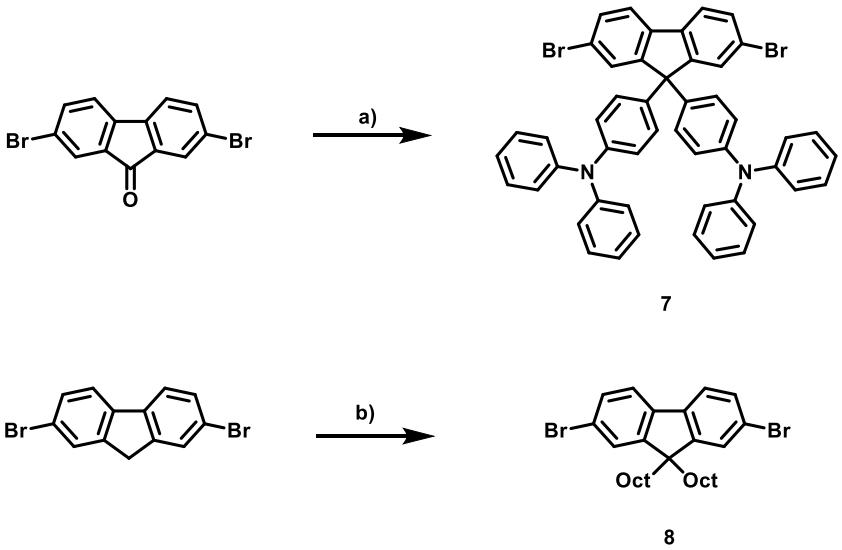

Scheme 13. Synthesis of fluorene-based monomers 7 and 8. a) *N*,*N*-diphenylbenzeneamine, methansulfonic acid, 140°C, 6h, yield 90 %. b) 1-bromooctane, phase transfer catalyst, sodium hydroxide (aq), 60°C, 15h, yield 86%.

2,7-dibromo-9,9-dioctyl-9*H*-fluorene **8** was used as repeat unit of the polymer backbone in all copoloymers for two main reasons: polyfluorenes show efficient electroluminescence and high charge carrier mobility.[128-129] Moreover, especially alkyl-functionalized polyfluorenes reveal good solubility in common organic solvents and are therefore easily processable from their solutions.[130] Fluorenes as well as polyfluorenes not functionalized in the 9-position tend to degrade by autoxidation under fluorene-9-one formation. As a consequence, the PL and EL emissions of fluorene-based materials have a tendency to show red-shifted emission bands in the region of 520 - 560 nm due to the keto defects. Efficient energy transfer to these defects

results in blue-green or even green emission.[131] To avoid degradation, the introduction of alkyl moieties in 9-position is an efficient and facile option.
In thin films, poly(9,9-dioctylfluorenes) show a unique packing behavior apart from the amorphous glassy phase, the so called β-phase, in which stacking of the polymers chains leads to areas of higher organization.[132]

8 was prepared from 2,7-dibromo-9*H*-fluorene by stirring with aq. sodium hydroxide and 1-bromooctane in the presence of tetrabutylammonium bromide (TBABr) as phase-transfer catalyst.[133] While in the introduction the abbreviation 'PF' was used to describe polyfluorene, from now on PF means poly(9,9-dioctylfluornene)

Both monomers **7** and **8** were characterized by ^{1}H-NMR, ^{13}C{^{1}H}-NMR and LC-MS measurements. The data received correspond to common sources of literature.[126, 134]

3.2.4 Synthesis of a 9*H*-carbazole-based monomer

In addition to compound **7**, 3,6-dibromo-9-(2-ethylhexyl)-9*H*-carbazole **9** was synthesized as a comonomer in order to test its adequacy as hole injection-promoting material in single-layer WOLEDs (Scheme 14).

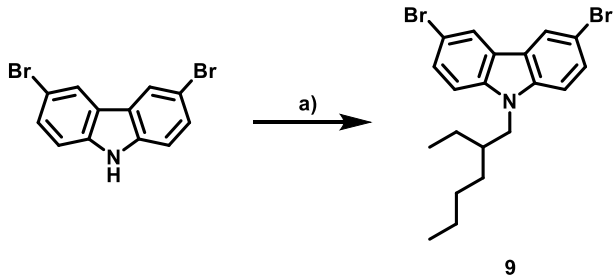

Scheme 14. Synthesis of 3,6-dibromo-9-(2-ethylhexyl)-9*H*-carbazole. a) sodium hydride, THF, 3-(bromomethyl)heptan, rt, 99%.

9 has been used in previous studies about copolymer-based hole injection/transport and revealed good results when applied in OLEDs.[135-136] It was synthesized in a SN2 type reaction by treating 3,6-dibromo-9*H*-carbazole with sodium hydride as base in THF and subsequently adding 3-(bromomethyl)heptan. After work-up and purification, **9** was received

as a colorless oil in 99% yield. It was characterized by NMR spectroscopy and mass-spectrometry.

3.3 Synthesis of orange light-emitting complexes [(F-bt)$_2$Ir(carbacac)]

In 2011, Wang *et al.* reported an orange light-emitting iridium(III) complex with a fluoro-functionalized benzothiadiazole ligand which was used as an emitter in monochromatic OLEDs (Scheme 15).[137]

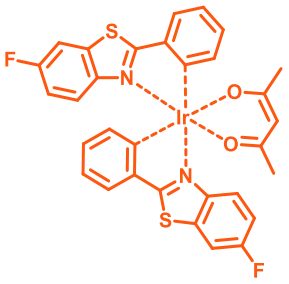

Scheme 15. Chemical structure of the orange light-emitting iridium(III) complex as reported by Wang *et al.*[137]

Devices with the following structure were presented: ITO/PEDOT:PSS (40 nm)/Ir:CBP (5 wt%, 30 nm)/TPBI(45 nm)/LiF (1 nm)/Al, with 'Ir' being the iridium complex and CBP being 4,4'-bis(carbazol-9-yl)biphenyl.

The OLEDs exhibited the highest efficiencies reported to date at that time with 71.6 cd · A^{-1} and efficacy of 44.9 lm · W^{-1} at a voltage of 5V. Additionally, two-element WOLEDs were fabricated via an additional blue-emitting Firpic:CBP layer. In an optimized WOLED-structure of ITO/PEDOT:PSS (40 nm)/Ir:CBP (1 wt%, 10 nm)/Firpic:CBP (10 wt%, 20 nm)/TPBI (45 nm)/LiF (1 nm)/Al, an efficiency 68.6 cd · A^{-1} and efficacy of 34.0 lm · W^{-1} at 6V were achieved.

This encouraged us to substitute the ancillary acetylacetonate ligand of [(F-bt)$_2$Ir(acac)] with our carbazole-functionalized acetylacetonate ligand **3** in order to investigate the photophysical properties of the nre complex as well as its suitability as dye in OLEDs. The synthesis route is outlined in Scheme 16.

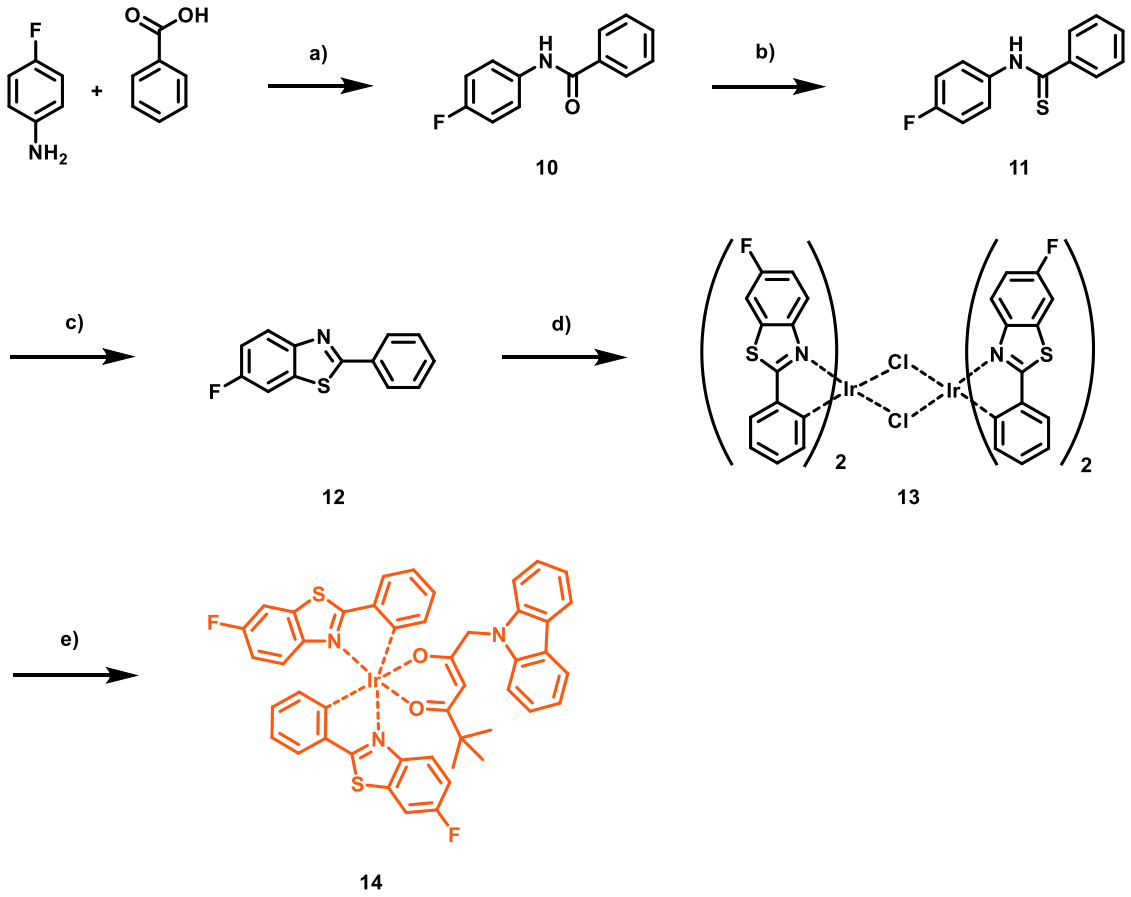

Scheme 16. Synthetic route to the orange light-emitting complex 15. a) PCL_3, toluene, reflux, 6h. b) Lawesson's reagent, toluene, reflux, 15h. c) $K_3Fe(CN)_6$, NaOH, water, reflux, 3h. d) $IrCl_3 \cdot x\ H_2O$, 2-ethoxyethanol, water, reflux, 12h. e) (3), 2-ethoxyethanol, Na_2CO_3, reflux, 2h.

The synthesis of the fluoro-functionalized benzothiadiazole ligand (F-bt) was carried out following the synthesis route by Wang[137] and Singh[138]. First, *N*-(4-fluorophenyl)benzamide **10** was synthesized by treating 4-fluoroaniline and benzoic acid with phosphorus trichloride in boiling toluene. The colorless solid was isolated in yields of 62% and was characterized by ^{1}H-NMR, ^{13}C{^{1}H}-NMR and LC-MS measurements. Additional ^{1}H-^{1}H-COSY-NMR as well as ^{1}H-^{13}C-HSQC-NMR experiments were performed in order to assign all resonances. The ^{1}H-NMR spectrum reveals the expected doublet (δ = 7.89 ppm) and triplet (δ = 7.52 ppm, δ = 7.59 ppm) resonances for the non-substituted phenyl ring. The fluoro substituent leads to multiplet resonances of the protons in 3- and 5-position of the fluorophenyl ring (δ = 7.63 ppm, δ = 7.10 ppm). Finally, the resonance of the amine proton shows a broad singlet δ = 7.82 ppm. In the ^{13}C{^{1}H}-NMR spectrum, the quaternary carbon bond to the fluoro atom appears as a doublet at δ = 159.6 ppm with J = 244.1 Hz . Additional doublets of

the carbon atoms of the fluoro substituted phenyl ring show signals at δ = 122.1 ppm (*J* = 7.9 Hz) and δ = 115.8 ppm (*J* = 22.7 Hz) due to ^{5}J and ^{4}J coupling, respectively. Furthermore, the carbonyl carbon resonance appears at δ = 165.7 ppm. In the mass spectrum, the expected molecule peak $[M+H]^+$ was found at m/z = 216.07.

The synthesis of *N*-(4-fluorophenyl)benzothioamide **11** was carried out by treating **10** with a small excess of the sulfonation reagent "Lawsesson's Reagent" in dry toluene at reflux overnight. After work-up and purification, the colorless material was obtained in 82% yield.

In the ^{1}H-NMR spectrum no noteworthy shifts of the aromatic hydrogen atoms occur; the amine proton resonance appeared at δ = 9.01 ppm. The $^{13}C\{^{1}H\}$-NMR spectra recorded showed similar chemical shifts for the aromatic carbon atoms compared to compound **10**. Most significantly, the new resonance at δ = 198.9 ppm for the thioketone and the missing resonance around δ = 165 ppm for the carbon of the carbonyl group both proved successful conversion. The LC-MS mass spectrum revealed the molecule mass peak $[M+H]^+$ at m/z = 232.1.

Finally, 6-fluoro-2-phenylbenzo[*d*]thiazole **12** was synthesized via an oxidative ring closure by treating *N*-(4-fluorophenyl)benzothioamide **11** with an aqueous solution of potassium ferricyanid(III) in the presence of sodium hydroxide.[139] The product was purified by recrystallization from methanol and was obtained in 94 % yield.
Compared to **11**, the ^{1}H-NMR spectrum shows just slight differences regarding the non-substituted phenyl ring. A multiplet at δ = 8.11 - δ = 8.07 ppm for the hydrogens in ortho-position and an overlapped multiplet for the *m*- and *p*-hydrogens at δ = 7.52 ppm became evident. For the fluoro-substituted benzene ring, three resonances at δ = 8.04 ppm (dd), δ = 7.60 ppm (dd) and δ = 7.25 ppm (td) were found, indicating the successful ring closure. As expected, the resonance for the amine proton can no longer be found. In the $^{13}C\{^{1}H\}$-NMR spectrum, most significantly, the sulfur double-bonded carbon resonance at δ = 198.9 ppm is not present anymore and instead a new resonance at δ = 167.7 ppm is visible for the sulfide carbon. The ^{13}C-DEPT-NMR now shows six quaternary carbons instead of five for **11**. Moreover, the ligand's mass peak was found at m/z $[M+H]^+$ = 230.1

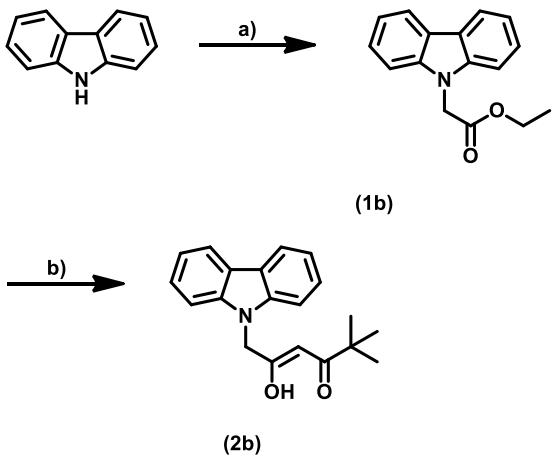

Scheme 17. Synthesis of ancillary ligand 2b. a) K_2CO_3, ethyl bromoacetate, DMF, 60°C → rt,; b) pinacolone, THF, KHMDS, 0°C → rt, overnight.

In order to build up complex **14**, ligand (Z)-6-(9*H*-carbazol-9-yl)-5-hydroxy-2,2-dimethylhex-4-en-3-one **2b** had to be synthesized (Scheme 17). The synthesis was executed based on that of ligand **3** (Scheme 11). Hereby, 9*H*-carbazole was used as starting material and an ethylacetate moiety was introduced in 9-position to yield ethyl 2-(9*H*-carbazol-9-yl)acetate **1b**. In the second step, a claisen-type condensation of pinacolone and **1b** yielded (Z)-6-(9*H*-carbazol-9-yl)-5-hydroxy-2,2-dimethylhex-4-en-3-one **2b** in 67%.

In the aromatic region of the ^{1}H-NMR spectrum of **2b**, four resonances with relative intensities of two protons each at δ = 8.15 (d), 7.50 (t), 7.37 (d) and 7.32 (m) represent the hydrogens of the aromatic 9*H*-carbazol moiety. A new singlet at δ = 15.54 ppm is assigned to the alcoholic proton of the acetylacetate's enol tautomer. Moreover, a singlet at δ = 5.36 ppm is caused by the proton of the methin bridge of the keto-enol tautomer. The relative intensity of both hydrogen resonances is close to one (0.95 and 0.97), which indicates that the equilibrium of the keto-enol-tautomerism is almost completely on the enol side. Finally, the three methyl groups of the *tert*-butyl group appear as a singlet at δ = 1.00 ppm with an intensity of 9 protons in accordance to the literature[7, 111]

Subsequently, complex **14** was prepared in the same two-step synthesis route as for complex **6**. μ-Chloro-bridged precursor complex **13** was obtained by stirring iridium(III) chloride hydrate and ligand **12** in 2-ethoxyethanol and water at reflux temperature for 12 hours. The raw product was washed with excess ethanol before drying. As **5**, **13** appeared to be insoluble

in common organic solvents at room temperature. Subsequently, **13** was treated with sodium carbonate and **2b** in 2-ethoxyethanol as solvent at 130°C for two hours to yield **14** in 67%.

The ^{1}H-NMR spectrum of complex **14** is shown in Figure 16. The proton resonances of the F-bt ligands are split due to the asymmetry of the complex. While proton m of the ancillary ligand is part of the rigid system, and thus, appears as a split resonance, proton n and protons h-k are allowed to rotate free and therefore the ^{1}H-NMR spectrum shows unsplit resonances.

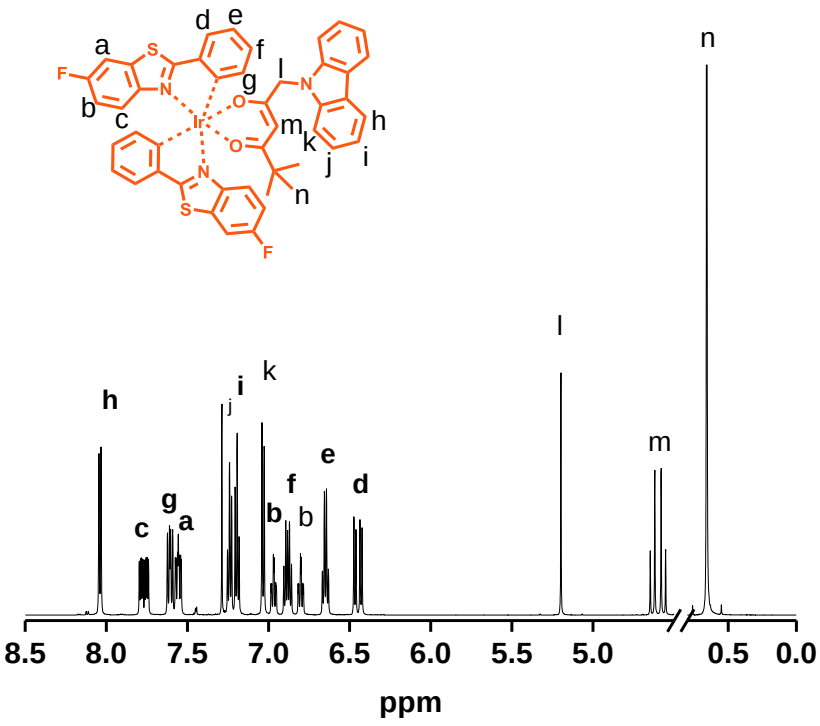

Figure 16. ^{1}H-NMR spectrum of complex 14, recorded in $CDCl_3$ at room temperature. Assignments of the resonances were conducted with the assistance of additional ^{1}H-^{1}H-COSY-NMR measurements.

The UV-Vis absorption spectrum of complex **14** in chloroform solution is presented in Figure 17. According to DFT calculations, the local maximum at $\lambda = 327$ nm can be assigned to ligand-centered (LC) $\pi \rightarrow \pi^*$ transitions of the cyclometalating ligands.[55] Additional shoulders appear at $\lambda = 405$, 445 and 485 nm. The band at $\lambda = 405$ nm is originating from spin-allowed transitions from the ground state to singlet metal-to-ligand charge transfer (^{1}MLCT) states, while the other bands $\lambda > 445$ nm are due to spin-forbidden transitions from the ground state to triplet metal-to-ligand charge transfer (^{3}MLCT) states. The emission band reveals a maximum at $\lambda_{max} = 560$ nm and a shoulder at $\lambda = 595$ nm. The quantum yield of

Φ = 29% was determined according to the method of Demas and Crosby.[140] Table 1 summarizes the photophysical properties in chloroform solution.

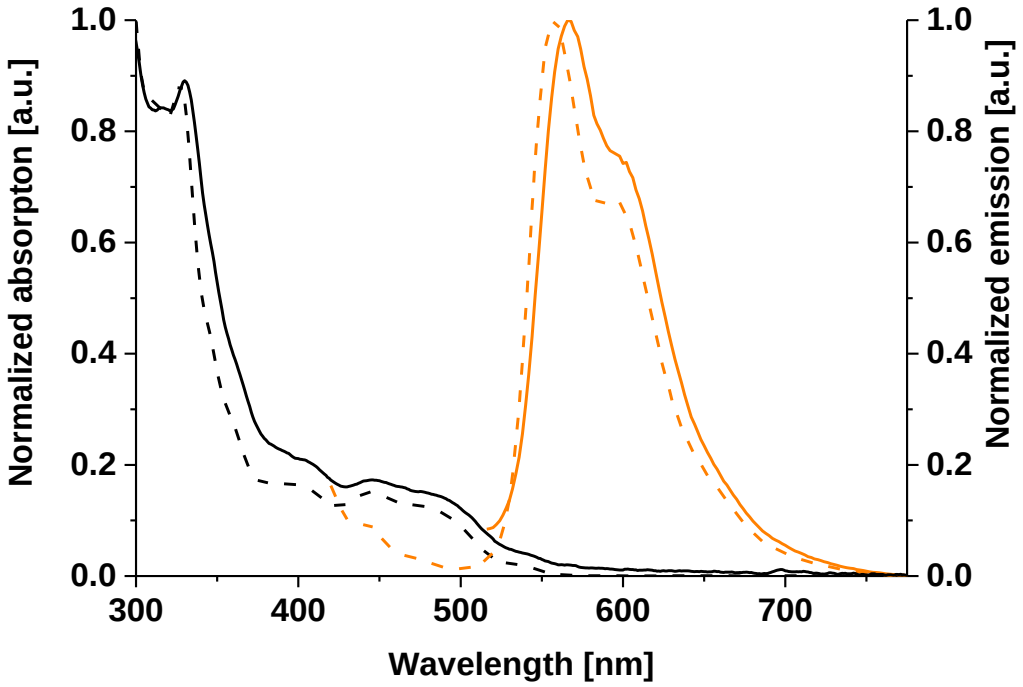

Figure 17. Normalized absorption and emission spectra of complex 14 in chloroform solution (room temperature, 10^{-5}M, dashed line) and in the solid state (room temperature, spin-casted from 5 mg · L^{-1} chloroform solution, solid line). Excitation wavelength: λ = 460 nm.

In the solid state, an absorption maximum was found at λ_{max} = 330 nm, again assigned to $\pi \rightarrow \pi^*$ transitions of the cyclometalating ligands. The photoluminescence spectrum shows a maximum at λ_{max} = 568 nm with a shoulder at λ = 598 nm.

Moreover, APLI-MS measurements were performed. Figure 18 presents the measured isotopic pattern of complex **14** as well as a corresponding simulation.

Table 1. Optical properties of complex 14 recorded in chloroform solution (10^{-5} M).

Absorbance [nm] (log ε, [L · mol^{-1} · cm^{-1}])	Maximum Emission λ [nm]	Quantum yield Θ [%]
264 (4.79), 294 (4.74), 328 (4.63), 400 (3.94), 445 (3.94), 488 (3.82)	558	29

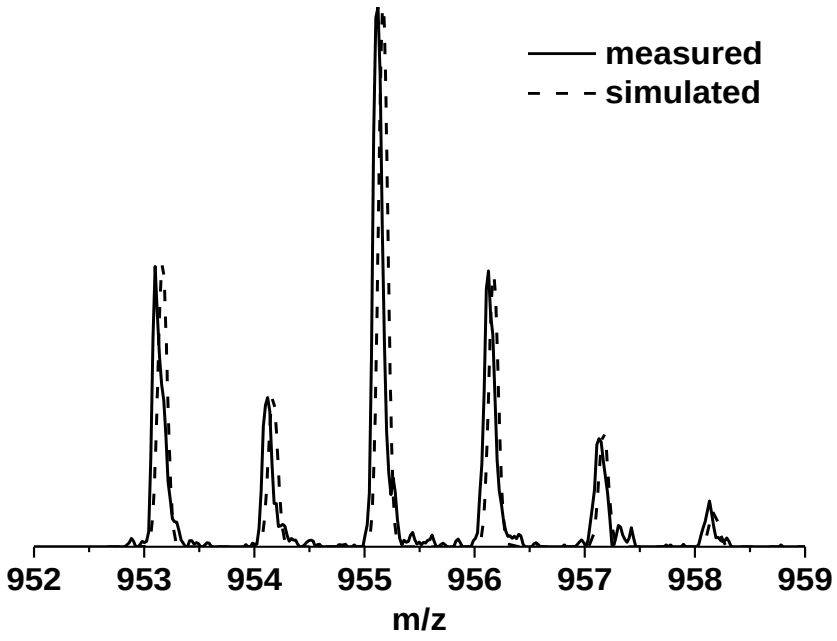

Figure 18. Normalized relevant section of the measured (solid line) and simulated (dashed line) high-resolution mass spectra of 14.

3.4 Synthesis and characterization of statistical copolymers for OLED applications

As already stated in the introduction, the need of orthogonal solvents in the fabrication of OLEDs by spin coating and printing is one of the most challenging problems. Vacuum deposition of organic materials is commonly used to circumvent this problem. However, this technique has some requirements regarding the material. For example, it must be stable at elevated temperatures. It also has to be evaporable, which consequently limits this technique to small molecules. Hence, high molecular weight polymers are precluded from vacuum deposition. The third method of circumventing orthogonal solvents is cross-linking the layers to each other and therefore rendering them insoluble. Then again, this technique also has some disadvantages, such as additional synthetic effort in preparation of cross-linkable materials. Hence, there is a demand for a technique that allows the forming of thin films of organic compounds and polymers from polar solvents. Water-soluble copolymers have already been evaluated and OLEDs were prepared from ionic polymers.[141] In this chapter, the synthesis and characterization of a series of copolymers is described. Subsequently, a

concept of printing thin films of the copolymers from aqueous micro-particle suspensions is presented which allows printing of non-polar copolymers from water. Finally, the results of preliminary attempts of printing the copolymers from their solutions is presented as well as results from their application in OLEDs.

3.4.1 Synthesis of statistical RGB copolymers for application in OLEDs

A series of copolymers **P1-8** were prepared *via* Suzuki cross-coupling condensation with different ratios of the monomers. This protocol was used due to the stability of the iridium(III) complex under these conditions in contrast to the conditions of the Yamamoto protocol in which the complex decomposes.

The copolymer backbone mainly consists of 9,9-dioctylfluorene units. Fluorene-9-one was used as green fluorescent emitter and the above described iridium(III) complex **6** was incorporated as red phosphorescent emitter. Depending on the feed-ratio of the emitter molecules in respect to the fluorescent blue polyfluorene backbone and taking the energy transfer into account, the synthesis of copolymers with distinctive emission colors from red to blue is possible. The copolymers were end-capped with bromobenzene and phenylboronic acid. Scheme 18 depicts the monomers used in the synthesis and the structure of the statistical copolymers. In this first series, no further charge injection enhancing components were added. 2,7-dibromo-9*H*-fluorene-9-one and 9,9-dioctyl-9*H*-fluorene-2,7-diboronic acid bis(1,3-propanediol) ester were bought from commercial sources. After purification by precipitation and Soxhlet-extraction with acetone, the phosphorescent metallo-copolymers were received with number average molar masses (M_n) ranging from 4000 to 17300 $g \cdot mol^{-1}$ with polydispersity indices of 1.7 to 2.3. The copolymers reveal high thermal stability of at least 354 °C (at 5% weight loss). The molecular weight appears to be mainly determined by the feed-ratio of the iridium(III) complex monomer. **P5** and **P6** (no iridium(III) complex) possess the highest molecular weights, while **P1**, **P7** and **P8** (feed-ratio of 5 mol% iridium(III) complex) reveal molecular weights (M_w) below 10000 $g \cdot mol^{-1}$. The monomer feed-ratios, copolymer composition and GPC results are summarized in Table 2.

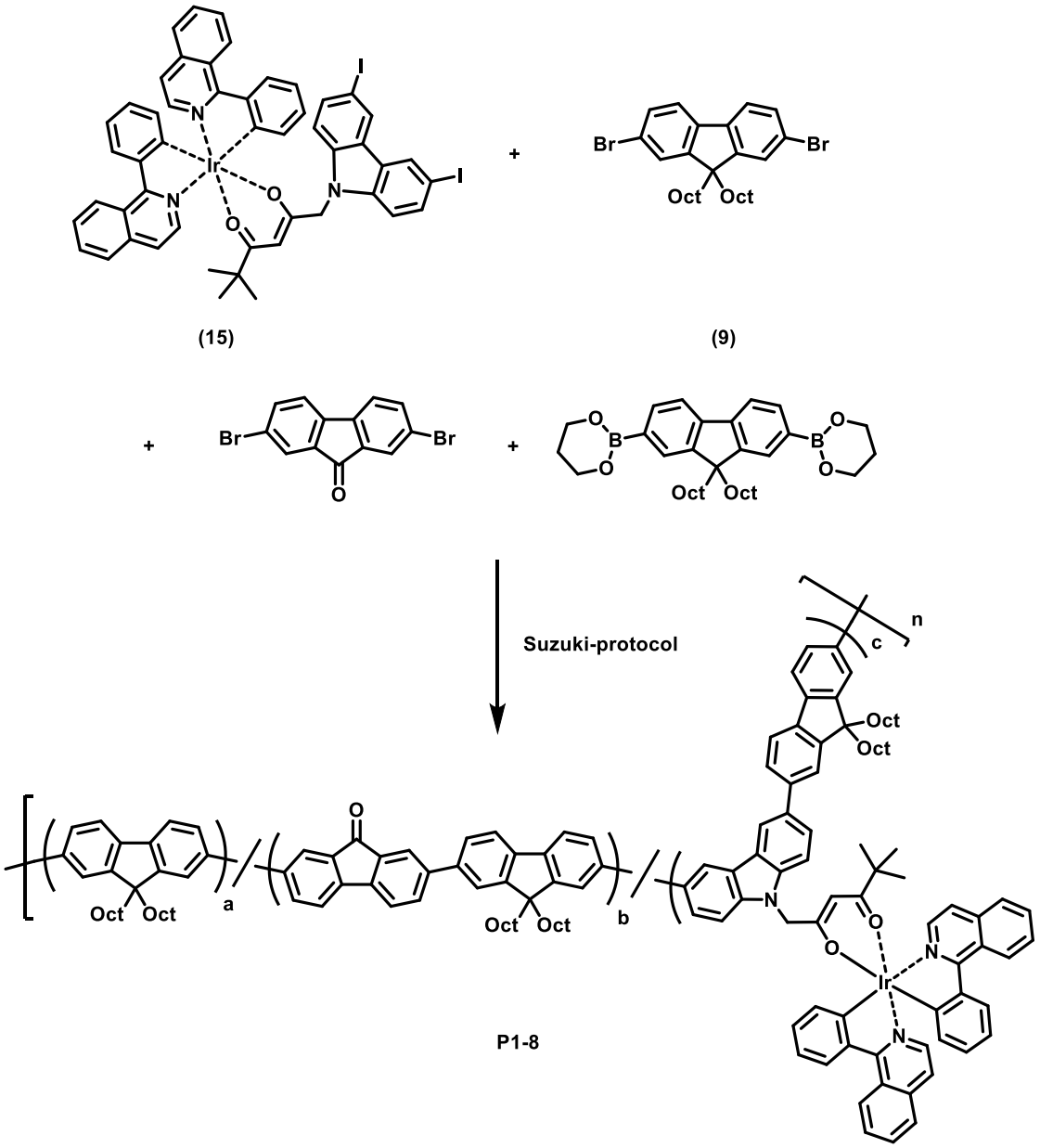

Scheme 18. Synthesis of the first copolymer series containing phosphorescent iridium(III) complex 6.

Table 2. Monomer feed-ratio, GPC results and PLQE of metallo-copolymers (P1-8). The copolymer composition, estimated by ^{1}H-NMR measurements, is given in parentheses.

Entry	Fluorene [mol%]	Fluoren-9-one [mol%]	Ir(III) complex [mol%]	M_n [g·mol^{-1}]	M_w [g·mol^{-1}]	PDI	PLEQ$^{\#}$ [%]
P1	90 (90.6)	5 (6.1)	5 (3.3)	4100	9300	2.3	n.m.
P2	92 (93.3)	5 (5.6)	3 (1.1)	10600	17900	1.7	n.m.
P3	93 (94.4)	5 (5.0)	2 (0.6)	9200	15900	1.7	n.m.
P4	94 (94.4)	5 (5.3)	1 (0.3)	9100	19200	2.1	25.0
P5	95 (94.7)	5 (5.3)	0 (0.0)	14600	29200	2.0	21.4
P6	98 (97.7)	2 (2.3)	0 (0.0)	17300	33700	1.9	n.m.
P7	93 (93.4)	2 (3.3)	5 (3.3)	4000	8000	2.0	n.m.
P8	95 (97.1)	0 (0.0)	5 (2.9)	4300	8800	2.0	25.9

$^{\#}$ measured in chloroform solution at room temperature. n.m.: not measured.

The copolymers **P1-8** reveal glass transition temperatures (T_g) ranging from 65.4 °C to 87.5 °C. The decomposition temperature (T_d) at 5% weight loss was found at around 400°C (Table 3).

Table 3. Glass transition temperatures (T_g) and decomposition temperatures (T_d) of copolymers P1-8.

Entry	T_g [°C]	T_d (5% weight loss) [°C]
P1	87.5	354
P2	72.8	391
P3	68.9	416
P4	79.8	416
P5	73.5	415
P6	66.2	419
P7	68.9	395
P8	65.4	397

T_g of pristine poly(9,9-dioctylfluorene) is usually in the range of 70°C – 80°C.[142]

^{1}H-NMR spectra were recorded for all copolymers **P1-8**. Figure 19 shows an overlay of the ^{1}H-NMR spectra of **P1** and of the iridium(III) complex-monomer **6**. Several common resonances can be found in both spectra, e.g., at δ = 9.0, 5.2, 4.6 and 0.7 ppm, these showing the successful incorporation of monomer **6** into the copolymer chain.

The fluorene-9-one resonances are mostly overlaid by the resonances of the dioctylfluorene units, but one resonance at 8.1 ppm can be distinguished from the others. To calculate the copolymers composition, the areas under the resonances at 9.0 ppm (Ir(III) complex) and 8.1 ppm (fluorene-9-one) were compared to those of the two α-methylene groups of the

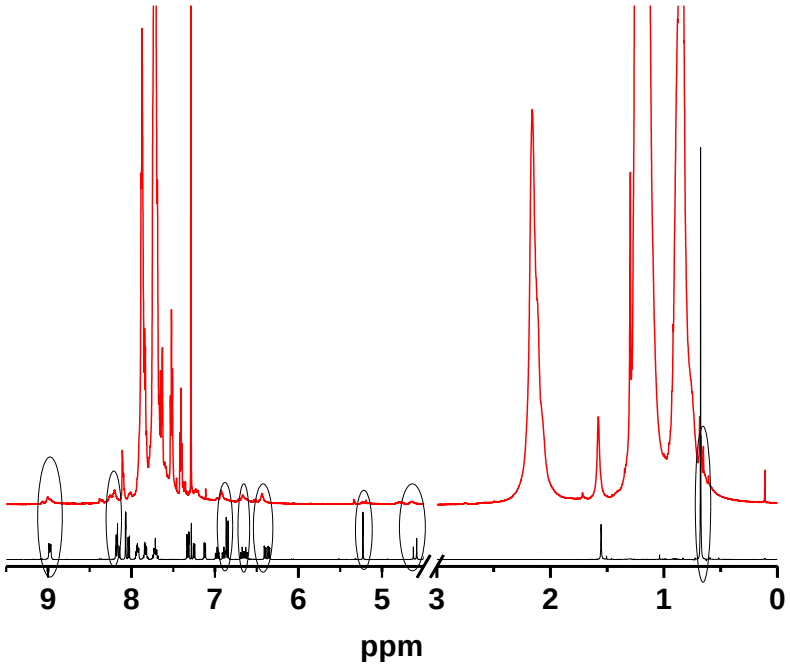

Figure 19. Overlay of ^{1}H-NMR spectra of monomer 7 (black line) and copolymer P1 (red line). Both spectra were recorded in $CDCl_3$ at room temperature. The intensity of the spectrum of P1 is magnified for clarity.

fluorene's octyl chains. The results are summarized in Table 2. While the content of fluorene-9-one units found in the copolymers varies only slightly with the different feed-ratios, the amount of incorporated Ir(III) complex units is lower than expected, which can be attributed to the reduced coupling reactivity of 3,6-halogenated 9*H*-carbazoles (see 3.2.1).

Photoluminescence quantum efficiencies (PLQE) in chloroform solution were determined for **P4**, **P5** and **P8** as examples for copolymers containing only fluoren-9-one (**P5**), only Ir(III) complex (**P8**) or both guest units (**P4**) (Table 2).

UV/Vis absorption and emission spectra were recorded in solution as well as the solid state. The thin films were prepared on quartz-glass substrates from $7\ mg \cdot ml^{-1}$ solutions in toluene/*ortho*-dichlorbenzene (ODCB) (80/20 v/v) on a spin coater at 1500 rpm for 60 seconds. The solution spectra of the copolymers were measured in toluene/ODCB (80/20 v/v) at a concentration of $c = 10^{-5}$ M. The absorption spectra in solution (Figure 20) are

dominated by one broad absorption band for each copolymer at λ_{max} = 371 - 386 nm which can be assigned to $\pi \rightarrow \pi^*$ transitions of the polyfluorene backbone.

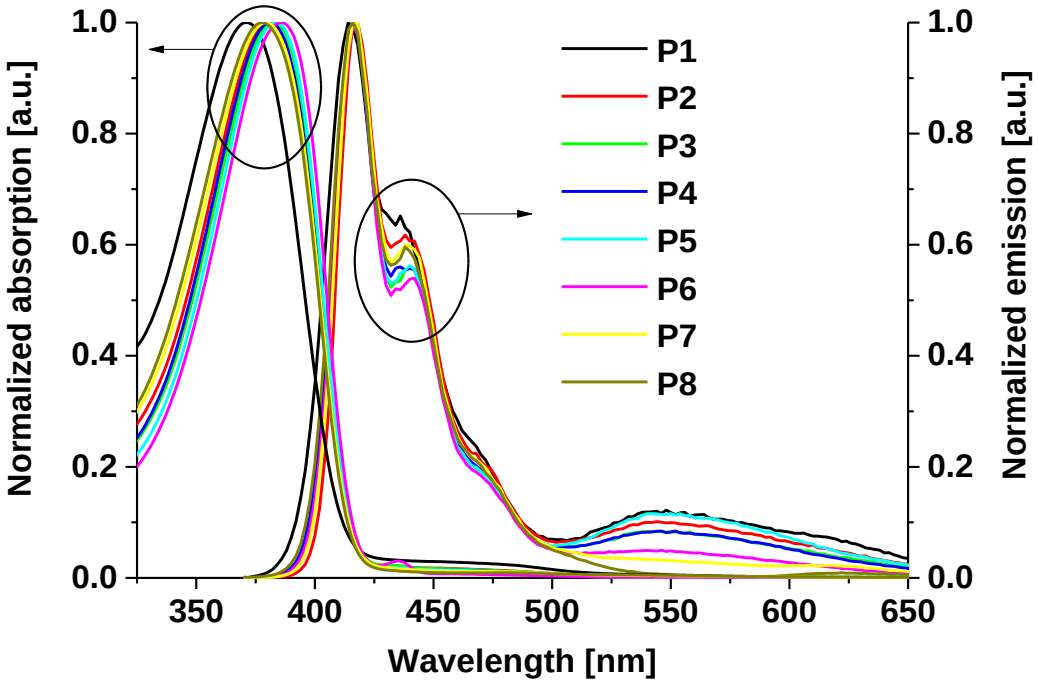

Figure 20. Normalized absorption and emission spectra of copolymers P1-8, recorded in toluene/ODCB (80/20 v/v) at concentration of 10^{-5} M. Excitation wavelength: 350 nm.

Comparing the feed-ratios of the iridium(III) complex comonomer with the maximum absorption wavelength shows that increasing the feed-ratio of the iridium(III) complex monomer shifts the maximum absorption wavelength to higher energy: the complex units partially break the conjugation of the polyfluorene backbone, raising its $\pi \rightarrow \pi^*$ transition energy.

Consequently, the feed-ratio of the fluoren-9-one comonomer does not have a visible influence on the absorption maximum of the copolymers.

In the normalized emission spectra, two dominant transitions at λ = 415 and a shoulder at 440 nm appear. The former is typical for fluorene-based (co)polymers and originates from $S_0 \leftarrow S_1$ transitions in accordance with Kasha's rule. The latter as well as the small shoulder at λ = 470 nm are side bands.[143-144] All copolymers contain fluoren-9-one units except for **P8**. It is well known for PF-based copolymers with fluoren-9-one on-chain units that Förster energy

transfer occurs from the polyfluorene to the fluoren-9-one units resulting in an emission band at around 550 nm.[145]

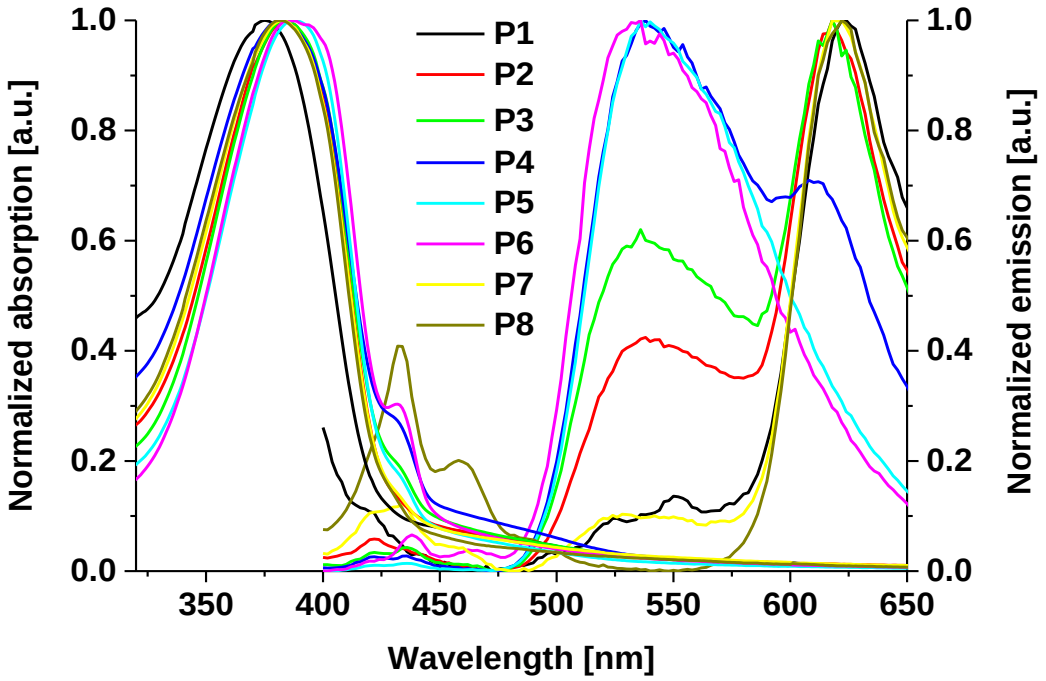

Figure 21. Normalized absorption and emission spectra of copolymers P1-8 recorded in solid state. Excitation wavelength: 350 nm.

In solid state (Figure 21), the absorption spectra of copolymers **P1-8** remain similar to those of the solutions. The absorption maxima are slightly bathochromically shifted. Small shoulders appear at λ = 430 nm, indicating a β-phase formation.[146]

In the emission spectra, efficient Förster energy transfer from the polyfluorene backbone to the two different guest moieties results in a decreased emission from the host. Depending on the amount of fluoren-9-one and triplet emitter in the backbone, the two emission bands of the polyfluorene at λ = 430 and 460 nm appear in different intensities. **P8**, for instance, synthesized with a feed-ratio of 5 mol% iridium(III) complex and no fluoren-9-one, incomplete energy transfer results. Thus, emission in the blue region of the spectrum still appears. In case of **P5**, synthesized with a feed-ratio of 5 mol% of fluoren-9-one and no iridium(III) complex, the energy transfer is almost complete, resulting in almost no blue emission around λ = 450 nm. The energy transfer to the fluoren-9-one appears to be more efficient than to the iridium(III) complex. A reason for this may be that the fluoren-9-one is

incorporated directly into the chain, minimizing the distance to excited states on the polyfluorene blocks, while the iridium(III) complex is situated in the periphery of the chain.[36] **P1-5** were synthesized with a feed-ratio of 5 mol% fluoren-9-one and decreasing feed-ratios of iridium(III) complex of 5 mol% (**P1**), 3 mol% (**P2**), 2 mol% (**P3**), 1 mol% (**P4**) and 0 mol% (**P5**), respectively. In the case of **P5**, as mentioned above, the energy transfer to the guest is almost complete, resulting in greenish emission at λ = 550 nm. By increasing the feed-ratio of the iridium(III) complex, the red phosphorescence at λ = 620 nm arises. While in case of **P4** the green emission is still dominant, at a feed-ratio of 2 mol% in case of **P3** the phosphorescence at λ = 620 nm is dominant. For **P1**, the greenish emission is almost completely vanished in favor of the phosphorescence. An additional energy transfer from the fluoren-9-one to the iridium(III) complex may take place due to the spectral overlap of the emission band of the fluoren-9-one with the ^{1}MLCT and ^{3}MLCT absorption bands of the iridium(III) complex. **P1**, **P7** and **P8** were synthesized with a constant feed-ratio of 5 mol% for the triplet emitter and 5 mol%, 2 mol% and 0 mol% of fluoren-9-one, respectively. The blue emission bands are reduced with increasing feed-ratio of fluoren-9-one relative to the emission of the triplet emitter. For **P1**, almost no emission was measured, indicating a complete energy transfer to the guest units. For **P7**, weak emission bands appear in the blue region. The greenish emission is approximately equal to the emission of **P1** relative to the red phosphorescence of the triplet emitter, indicating a saturation of the fluoren-9-one emission already at a feed-ratio of 2 mol%.

In conclusion, eight statistical copolymers based on a polyfluorene backbone were synthesized. Varying feed-ratios of fluoren-9-one and iridium(III) complex led to copolymers that exhibit tunable photoluminescence from green to red. The energy transfer from the host to the fluorene-9-one guest in copoylmers without Ir(III) complex is already saturated at feed-ratios of 2 mol%. The results were used to estimate the monomer feed-ratios for the design of white light-emitting copolymers for OLED applications (see chapter 3.4.5).

3.4.2 Microparticle suspensions of copoylmer P8

Solution processing of polymer-based materials during multilayer OLEDs fabrication requires the need of orthogonal solvents. Thus, the consecutive materials need to be soluble in contrarily polar solvents. This presupposes the utilization of polar materials which can be made by the introduction of polar side-groups like polyglycol groups or even ionic moieties,

both resulting in higher synthetic efforts. In order to solve the problem of the need of orthogonal solvents in the fabrication of polymer-OLEDs (PLEDs), an aqueous solution of a non-polar organic copolymer would be needed. The preparation of a microparticle-based suspension of a non-polar polymer may be a promising and sufficient alternative to circumvent this problem.

The preparation of the microparticle suspensions was performed by following a slightly modified method of Kanelidis.[109] First, the copolymer was diluted in THF which is miscible with water. 1 ml of the THF solution was drawn up into a syringe and was quickly injected through a micro porous filter into a round bottom flask filled with water under ultra-sonication. In this process, the copolymer chains collapse immediately and form particles. Without ultra-sonication, the copolymer precipitates due to aggregation. The suspension was left in the ultra-sonic bath for another two minutes. Subsequently, the THF was removed in vacuum. The result is a suspension of the copolymer with no visible particles, in contrast to the experiments without ultra-sonication, with streaks and visible particles. A maximum concentration of 50 $mg \cdot L^{-1}$ was possible. Experiments with higher concentration led to precipitation and the formation of streaks. The suspensions are stable at least for several days, although the emission spectra reveal reduced phosphorescence from the iridium(III) complex emitter over time, presumably due to absorption of THF residues. The suspensions obtained were investigated by UV/Vis spectroscopy and the results are presented in Figure 23. While the THF solution does not emit a visible red phosphorescence under UV light, the aqueous suspension appears red under UV irradiation, indicating an efficient energy transfer from the copolymer backbone to the iridium(III) emitter. Thus, the PL maximum is found at $\lambda = 620$ nm, originating from the iridium(III) complex, and shoulders at $\lambda = 436$ and 464 nm originating from the backbone, respectively.

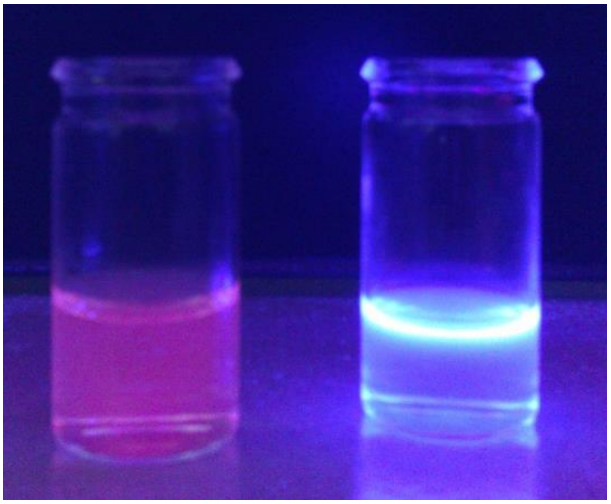

Figure 22. Aqueous suspension of P8 (left) and corresponding solution in THF (right) under UV irradiation.

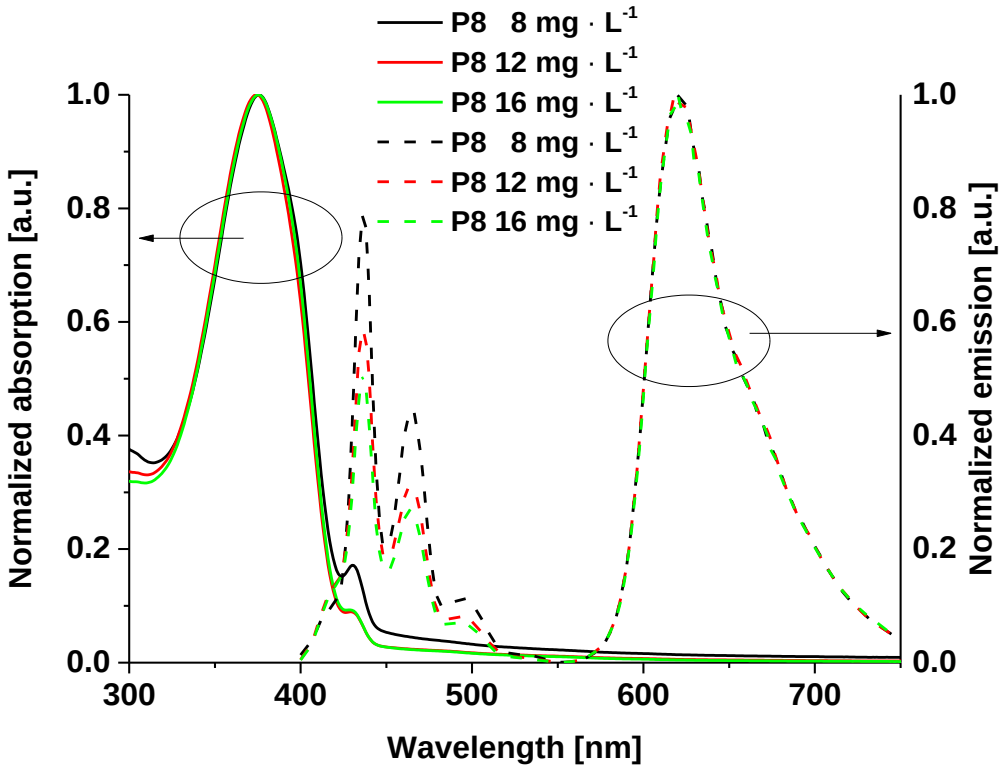

Figure 23. Normalized UV/Vis absorption (solid) and emission (dashed) spectra of aqueous copolymer suspensions of P8 at concentrations of 8, 12 and 16 mg · L^{-1}.

The UV/Vis absorption spectra of the aqueous suspensions of **P8** at concentrations of 8, 12, and 16 mg · L^{-1} revealed a maximum absorbance at 376 nm. Compared to the measurements in solid state, the absorption band is blue-shifted by 6 nm. Compared to those of the toluene/ODCB (80/20 v/v) solutions, no change in in the maximum absorption wavelength can be observed. The spectra reveal shoulders at λ = 430 nm which are typical for the β-phase that usually occurs in the solid state, e.g., thin films, and reveal the solid state character of the microparticles. In preliminary attempts, Dr. Anke Teichler of the group of Prof. Dr. U. S. Schubert at the University of Jena, Germany, was able to inkjet print the aqueous suspension on glass substrates, but printing on organic layers remains difficult due to dewetting.

3.4.3 Printing results of copolymers P1-8

For the fabrication of multilayer devices, e.g., for OLEDs, organic thin film transistors (OFETs) or organic solar cell applications, (co)polymers cannot be processed by vacuum deposition techniques due to their high molecular weights (see chapter 1.2). While spin coating is just suitable for small area devices, the fabrication of large area devices with controllable layer thickness is mostly conducted by inkjet printing techniques.[147]

The copolymers **P1-8** described in the last preceding paragraphs were investigated for their suitability for inkjet printing. All measurements in this chapter were performed by Dr. Anke Teichler of the group of Prof. Dr. U. S. Schubert at the University of Jena, Germany. The printing was performed on 6 mm × 6 mm glass substrates at room temperature from toluene/*o*-DCB (80/20 v/v) solution (7 mg/mL). The printing was performed on an Autodrop professional system from microdrop technologies (Norderstedt, Germany) equipped with piezo-based micropipettes with an inner nozzle diameter of 70 μm.

Table 3. Varied Inkjet Printing Parameters of the printed Films of P1-8.

Copolymer	Dot spacing [μm]	Substrate temperature [°C]	Film thickness [nm]	Surfaces roughness [nm]
P1	225	35°C	60	10
P2	215	RT	45	8
P3	240	RT	35	9
P4	140	RT	180	28
P5	180	RT	110	35
P6	205	RT	70	9
P7	220	RT	55	12
P8	220	RT	60	11

The resulting films revealed low surface roughness of 8 to 35 nm. Table 3 summarizes the printing parameters and results.

Figure 24 shows the normalized absorption and emission spectra of the printed thin films. Compared to the photophysical results of the spin-coated films, the absorption spectra of the copolymers **P1**-**P8** from inkjet printing reveal reduced shoulders at $\lambda = 435$ nm that are supposed to originate from β-phase aggregation. It is also significant that emission at

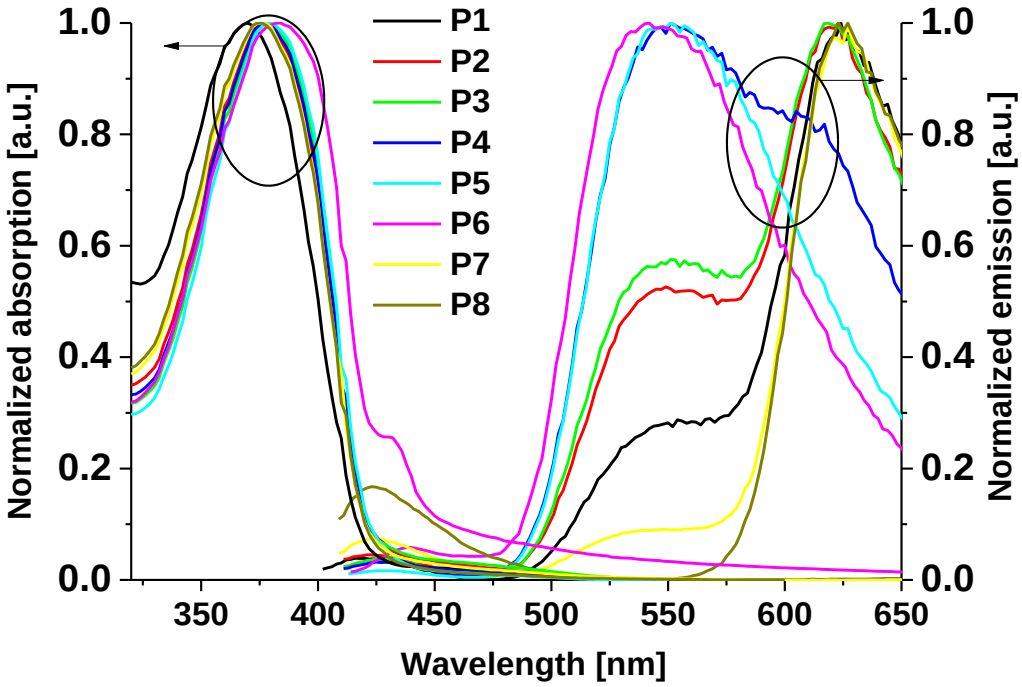

Figure 24. Normalized absorption and emission spectra of metallo-copolymers 1-8 inkjet printed on glass substrate from toluene/*o*-DCB (80/20 v/v) solution (7 mg/mL).

λ = 550 nm is slightly increased relative to the red phosphorescence from the iridium(III) complex in copolymers **P1** and **P2**.

Optical profiler images of printed copolymers **P5** and **P6** are presented in Figure 25, revealing the low roughness of the printed films.

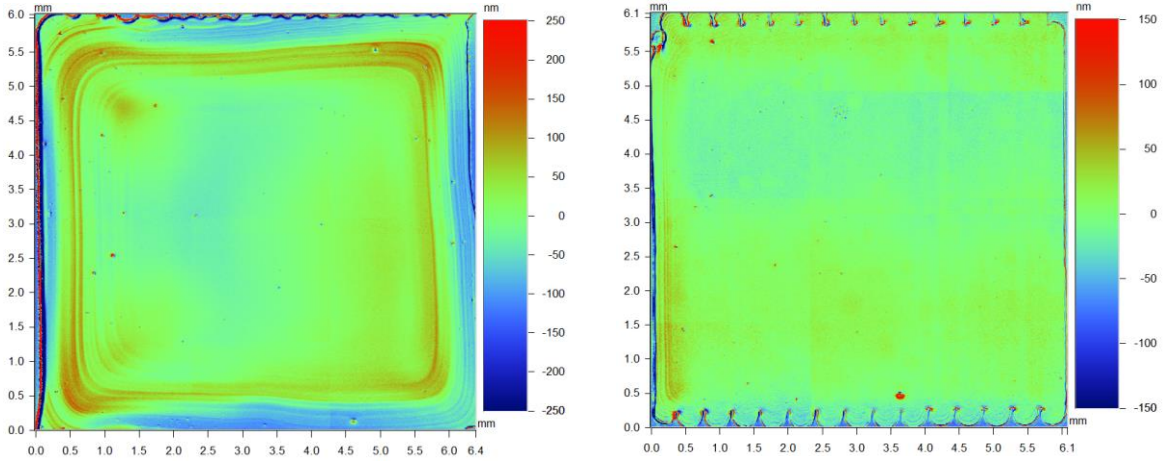

Figure 25. Optical profiler images of inkjet printed polymers P5 (left) and P6 (right). Film size: 6 by 6 mm2.

3.4.4 P1-8 and their application in OLEDs

Copolymers **P1-8** were designed to be used as active materials in OLEDs. In order to investigate their properties in OLEDs, samples of the copolymers were sent to the group of Prof. P. Blom, University of Groningen, Netherlands. All measurements presented within this chapter were done by M. Sc. D. Abbazadeh.

For all copolymers **P1-8**, OLEDs of the device structure glass\ITO\PEDOT:PSS (60 nm)\copolymer\Ba (5 nm)\Al(100 nm) were fabricated (Figure 26). It should be noted that neither an HTL nor an ETL layer was applied, supposing that the carbazole functionality of the iridium(III) complex already promotes hole transport. The layer thicknesses of the active copolymer layers of the devices varied from 80 nm to 230 nm. Table 4 depicts the layer thicknesses of the active material.

The electroluminescence spectra of devices with copolymers **P2-5** are shown in Figure 27. In these materials, the feed-ratio of the fluoren-9-one is kept constant at 5 mol%, while the feed-ratio of the iridium(III) complex is decreased from 3 to 0 mol%. For all materials, no EL-emission in the polyfluorenes region is observed which may be due to charge trapping effects at the metal complexes or efficient energy transfer from the copolymer backbone to the guest moieties.

Table 4. Thicknesses of the active layers in the prepared OLEDs.

Copolymer (feed-ratio)	Active layer thickness [nm]
P1 (PF90PFO5Ir5)	80
P2 (PF92PFO5Ir3)	105
P3 (PF93PFO5Ir2)	130
P4 (PF94PFO5Ir1)	170
P5 (PF95PFO5Ir0)	230
P6 (PF98PFO2Ir0)	100
P7 (PF93PFO2Ir5)	90
P8 (PF95PFO0Ir5)	110

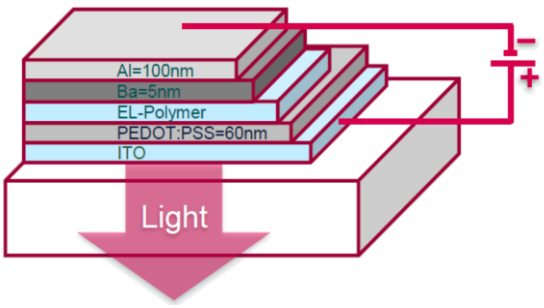

Figure 26. Schematic illustration of the device architecture prepared with copolymers P1-8.

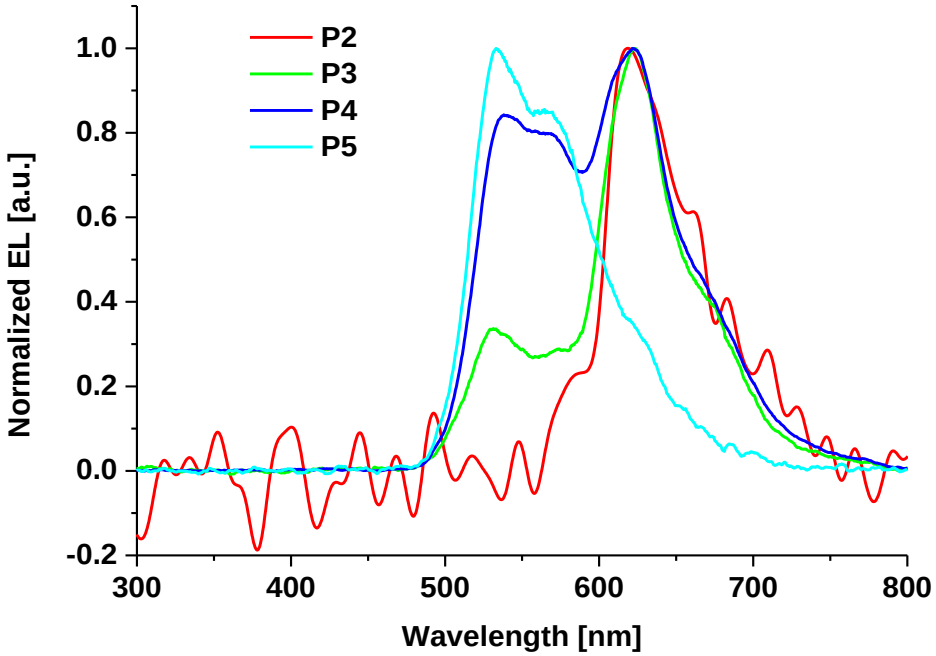

Figure 27. Normalized electroluminescence spectra of OLED devices with copolymers P2-5 as active layers.

The emission spectrum of **P2** reveals an emission maximum of λ_{max} = 620 nm that can be assigned to $T_1 \rightarrow S_0$ transitions in the complex. **P3** shows the same maximum absorption band as **P2**, but reveals an additional emission at λ = 530 nm. For **P4**, the emission bands in the green region are increased compared to **P3**, according to the lowered feed-ratio of iridium(III) complex. For **P5**, no emission in the red (620 nm) is observed, the emission band maximum is found at λ = 533 nm with a shoulder at λ = 565 nm. The shoulder may be a result of interface defects.[148]

Figure 28 depicts the EL spectra of devices containing **P1**, **P7** and **P8**. Due to the high Ir(III) complex content, the emission band is located at 624 nm for all three copolymers. While **P1** and **P7** show low emission in the green region, **P8**, which was synthesized without fluorene-9-one, inexplicably, exhibits notably high emission at 530 nm.

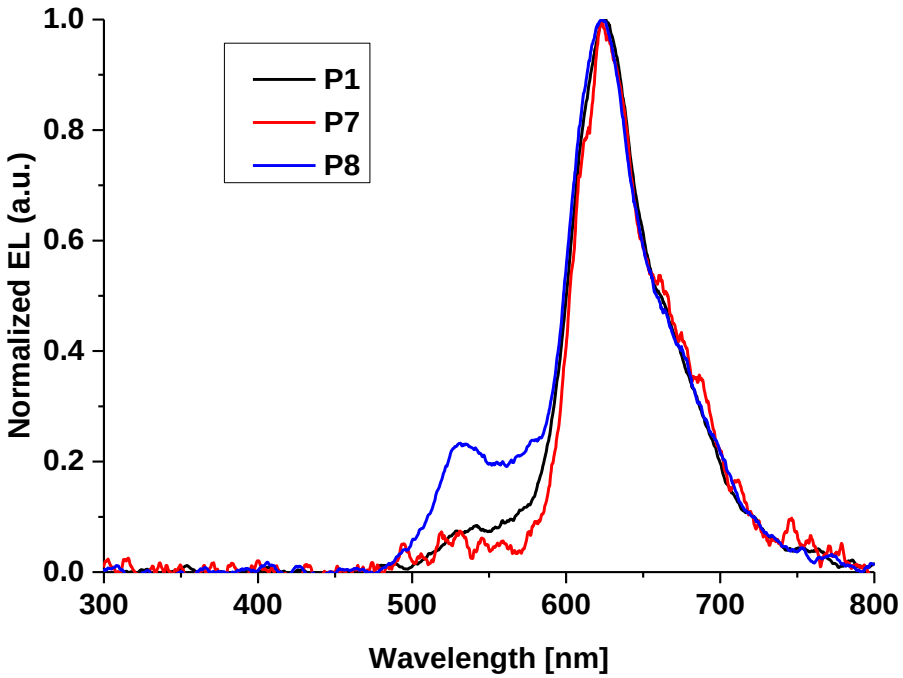

Figure 28. Normalized electroluminescence spectra of OLED devices with copolymers P1, P7 and P8 as active layers.

Figure 29 and 30 show current-voltage (*J*-V) curves and corresponding detector photocurrents of two series of devices containing the copolymers. In Figure 29, **P1**, **P7** and **P8** are compared. These copolymers were synthesized with a constant feed-ratio of 5 mol% of the iridium(III) triplet emitter complex and feed-ratios of 0, 2 and 5 mol% for the fluoren-9-one component, respectively. It can be observed that the current density as well as the detector photocurrent increases with the feed-ratio of fluoren-9-one.

The turn-on-voltage is decreased from 5.8 V for **P8** to 4.6 V for **P1**. The turn-on-voltage is essentially determined by the emission color (photon energy) and other factors such as thermal relaxation energy Stokes shift, injection barriers at different interfaces and potential drops due to charge transport.[149]

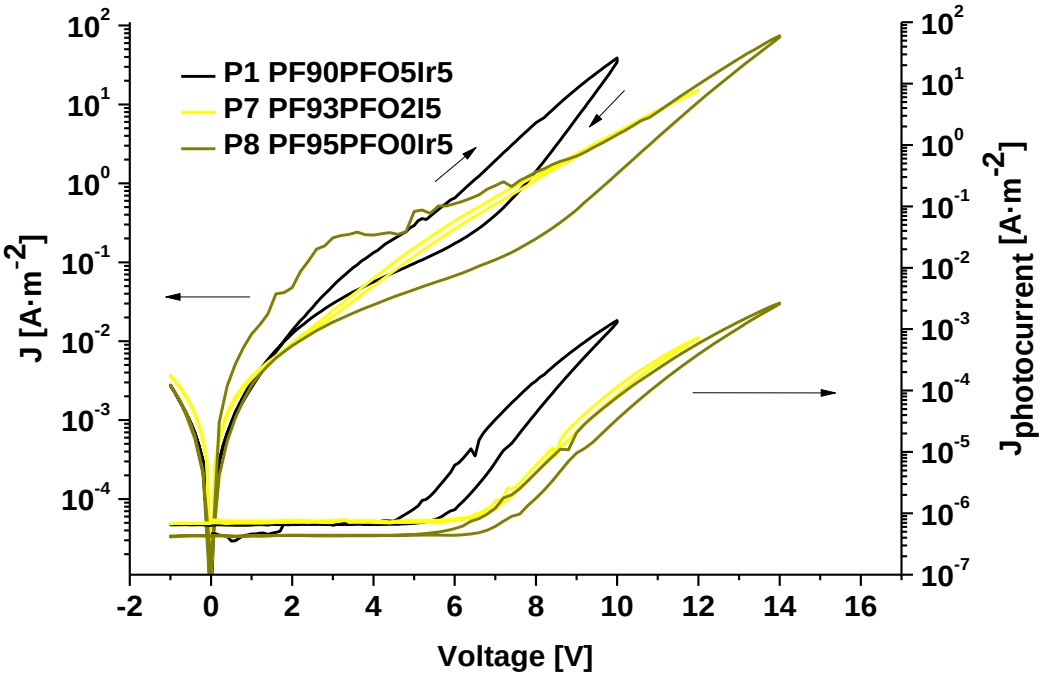

Figure 29. J-V curves and detector photocurrent measured for devices containing P1, P7, P8.

Figure 30 depicts the current-voltage characteristics of a second series of devices. Here, the feed-ratio of the fluorene-9-one moiety was kept constant at 5 mol% whereas the feed-ratio of the triplet emitter complex **7** was varied from 3 (**P2**) over 2 (**P3**) to 1 mol% (**P4**).

While the device fabricated with **P4** as active layer revealed the lowest current density measured, the devices with **P3** and **P2** showed higher current densities, respectively. The photocurrent of the devices also increased with higher amounts of iridium(III) complex feed-ratio. Furthermore, the turn-on voltage decreased from 7.4 V (**P4**) to 6.0 V (**P2**) showing similar behavior compared to the previous measurements.

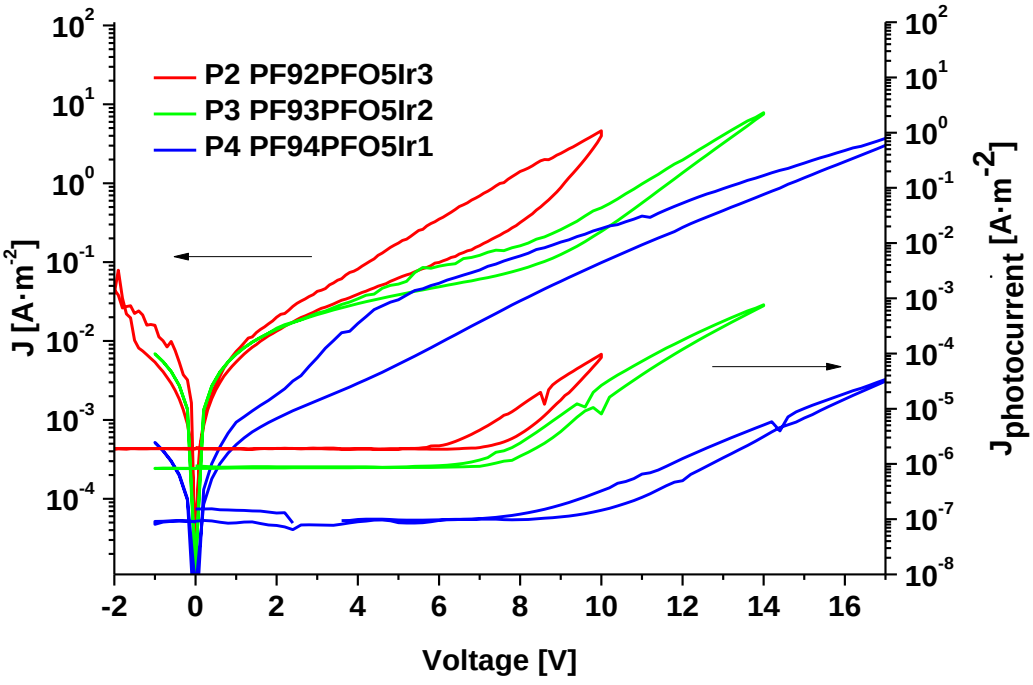

Figure 30. ***J*-V curves and detector photocurrent measured for devices containing P2-4.**

3.4.5 Synthesis of statistical copolymers for (WOLEDs)

As already stated in the introduction, white OLEDs are expected to play an important role in future ambient lighting applications. The concept of using RGB dyes to produce white light allows pure white emission compared to e.g., blue/yellow dye combinations. The same concept of fluorescent blue and green dyes and a phosphorescent red dye as presented in chapter 3.4.1 was used to prepare copolymers that should emit white light. Furthermore, 4,4'-(2,7-dibromo-9*H*-fluorene-9,9-diyl)bis(*N*,*N*-diphenylaniline) **7** was also incorporated in order to further improve hole-injection and transport properties. The synthesis was carried out according to the previously described route of RGB copolymers (chapter 3.4.1). The necessary feed-ratios of the monomers, especially of the dyes, were estimated on the basis of the electroluminescence spectra of the RGB copolymers as well as empirical values. The amount of **7** was fixed and chosen to be 10 mol%. The structure of the statistical copolymers as well as the comonomer feed-ratios are shown in Scheme 19 and Table 5.

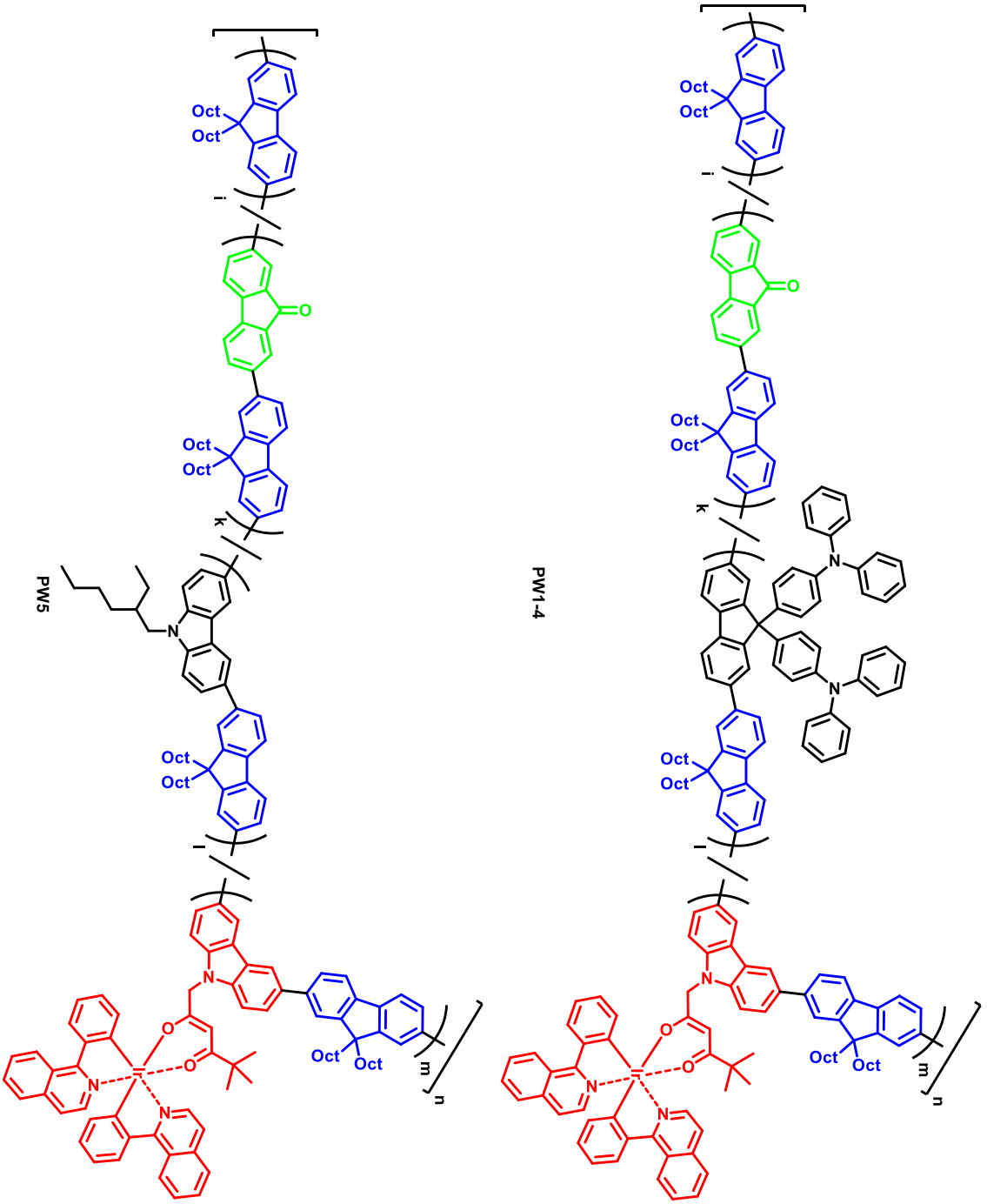

Scheme 19. Top: Chemical structures of the statistical copolymers PW1-4 with triarylamine-functionalized fluorene units. Bottom: chemical structure of the statistical copolymer PW5 with 2-ethylhexyl-functionalized 9*H*-carbazole units.

Table 5. Monomer feed-ratios for the synthesis of copolymers PW1-4.

Name	Dioctylfluorene **8** [mol%]	Fluoren-9-one [mol%]	Ir(III) complex **6** [mol%]	Triarylaminfluorene **7** [mol%]
PW1	99.0	0.8	0.2	0
PW2	89.4	0.2	0.4	10.0
PW3	89.25	0.25	0.5	10.0
PW4	89.1	0.3	0.6	10.0

Additionally, the ethylhexyl-functionalized 9*H*-carbazole **9** was used instead of the triarylamine-functionalized fluorene **7** in copolymer **PW5**. The feed-ratio of monomer **9** was 10 mol%, too (Table 6).

Table 6. Monomer feed-ratios for the synthesis of copolymer PW5.

Name	Dioctylfluorene **8** [mol%]	Fluoren-9-one [mol%]	Ir(III) complex **6** [mol%]	Carbazol **9** [mol%]
PW5	89.3	0.2	0.5	10.0

The GPC results as well as glass transition temperatures (T_g) and decomposition temperatures (T_d) of all white copolymers are presented in Table 7.

Table 7. GPC results of copolymers (UV detector, $CHCl_3$) and corresponding glass transition- and decomposition temperatures.

Name	M_n [g·mol^{-1}]	M_w [g·mol^{-1}]	PDI	T_g [°C]	T_d* [°C]
PW1	11300	17500	1.55	64.8	421
PW2	7300	11400	1.56	70.7	405
PW3	11400	15800	1.39	80.7	412
PW4	8500	14700	1.73	68.3	406
PW5	11600	16200	1.40	71.1	413

* @ 5% weight loss

The ^{1}H-NMR spectra (exemplarily for **PW1**, Figure 32), recorded in $CDCl_3$ at room temperature, showed the same broadened resonances of the dioctylfluorene chains in the aromatic region at δ = 7.85 ppm and δ = 7.70 ppm as for copolymers **P1-8**. The phenyl end-groups were found at a chemical shift of δ = 7.65 - 7.62 ppm (m), 7.51 ppm (t, 7.3 Hz) and 7.40 ppm (t, 7.4 Hz), respectively. The resonances of the Ir(III) complex as well as the fluorene-9-one units were too weak compared to the noise of the signal to allow for an estimation of the copolymer's composition. As already described for **P1-8**, the resonances of the octyl side chains were found at δ = 2.13 , 1.15 and 0.84 ppm, respectively. For the

copolymers **PW2-4**, with incorporated triarylamine-functionalized fluorene, the additional resonances of the phenyl ring protons appear as three multiplets between δ = 7.29 – 7.02 ppm in accordance with similar copolymers reported in the literature.[126, 150] For **PW5**, the resonance of the aliphatic α-CH_2 in the ethylhexyl-functionalized 9*H*-carbazole is represented by a broadened signal at δ = 4.17 ppm (Figure 33).

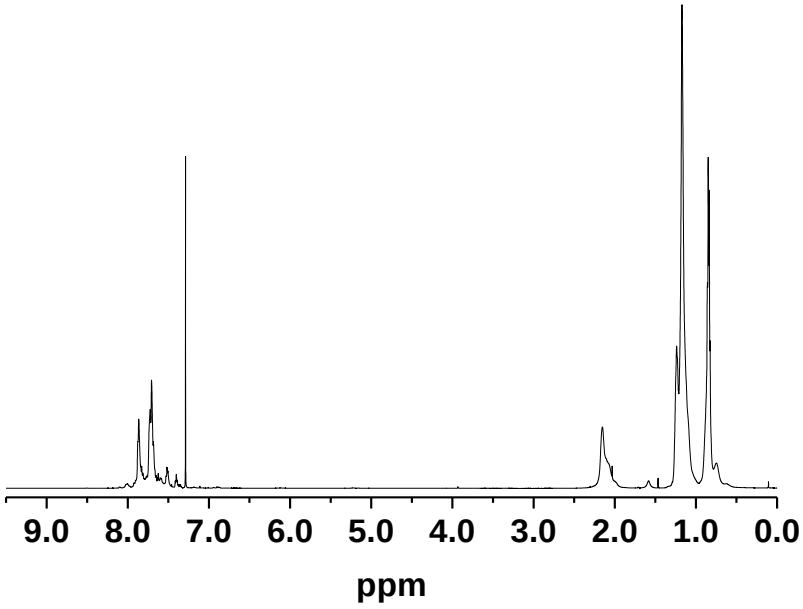

Figure 31. ^{1}H-NMR spectrum of PW1 recorded in $CDCl_3$ at room temperature.

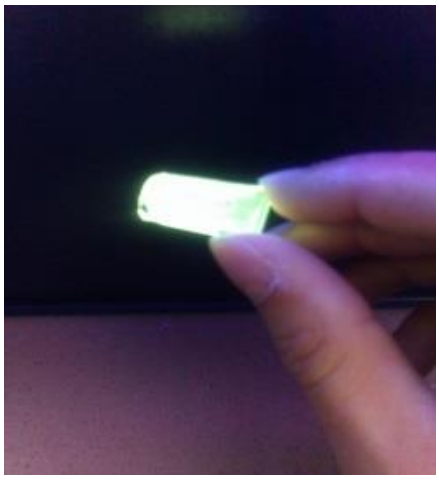

Figure 32. Picture of photoluminescence of PW2, spin-coated from chloroform solution on a glass substrate.

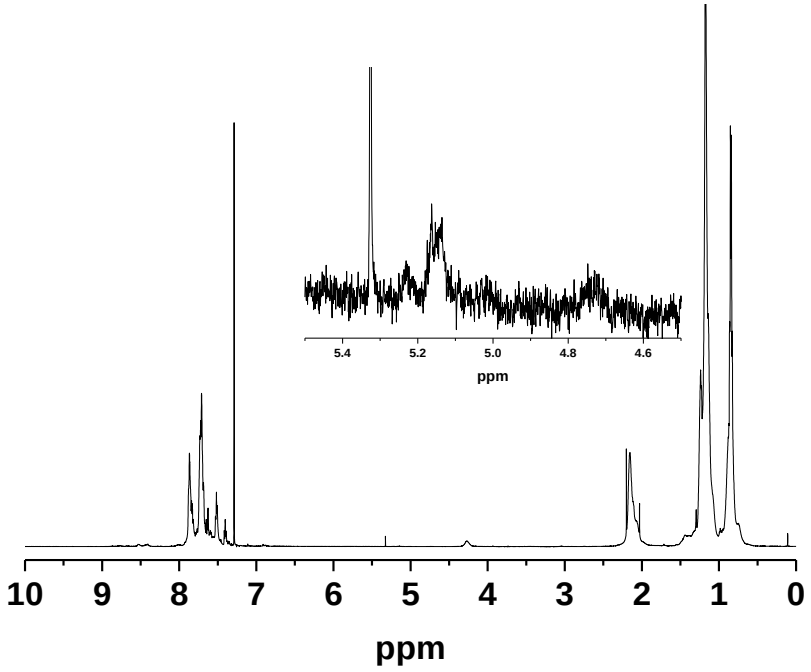

Figure 33. ^{1}H-NMR spectrum of PW5 recorded in $CDCl_3$ at room temperature.

The ^{3}J coupling to the aliphatic *tert*. carbon can be seen in the two-dimensional ^{1}H-^{1}H-COSY-NMR spectrum (Appendix A). Its resonance is overlapped by the resonances of the α-CH_2 protons of the octyl side chains which is located at δ = 2.15 ppm. The resonances of the α-CH_2 and CH group of the Ir(III) complex's ancillary ligand were found at δ = 5.17 and 4.17 ppm, respectively (insert of Figure 33). Other resonances of the Ir(III) complexes' cyclometallating ligands were too weak.

The normalized absorption spectra in solid state are dominated by a strong band with a maximum located at λ = 380 nm which represents $S_0 \leftarrow S_1$ transitions of the 9,9-dioctylfluorene backbone (Figure 34).

The normalized PL spectra recorded in thin-film state are shown in Figure 35. **PW1** was synthesized with a feed-ratio of 0.2 mol% of the red light-emitting iridium(III) complex, resulting in insufficient emission at λ = 650 nm. The spectrum is dominated by an emission band at λ = 535 nm which is assigned to the fluoren-9-one moieties. The emission bands at λ = 420 nm as well as the shoulder at λ = 445 nm originate from fluorescence of the copolymer backbone (see chapter 3.4.1). Accordingly, the feed-ratio of the triplet emitter **6** in

PW2 was increased to 0.4 mol%, while the feed-ratio of the fluoren-9-one monomer was reduced to a fourth.

Simultaneously, monomer **7** was introduced. This results in an enhanced emission in the blue and red region of the spectrum relative to the greenish fluorescence. For **PW3** and **PW4**, the feed-ratios of the fluorene-9-one and triplet emitter were raised slightly which, as expected, translates into lower blue emission in favor of increased greenish and red emission. Surprisingly, **PW4** showed increased bluish emission over green and red if compared to **PW2** and **PW3**.

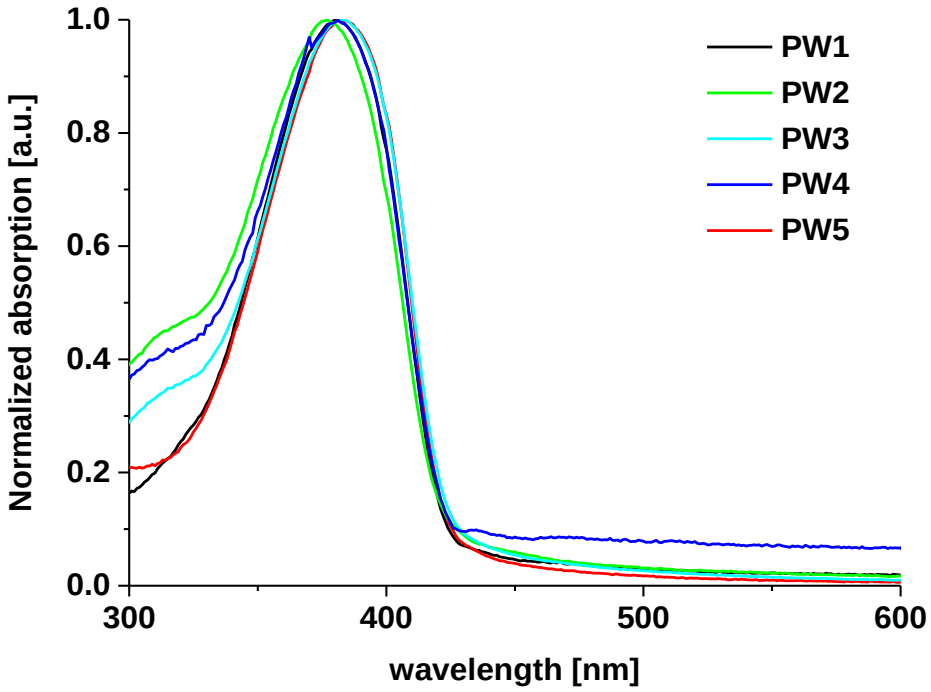

Figure 34. Normalized absorption spectra of copolymers PW1-5 recorded in solid state.

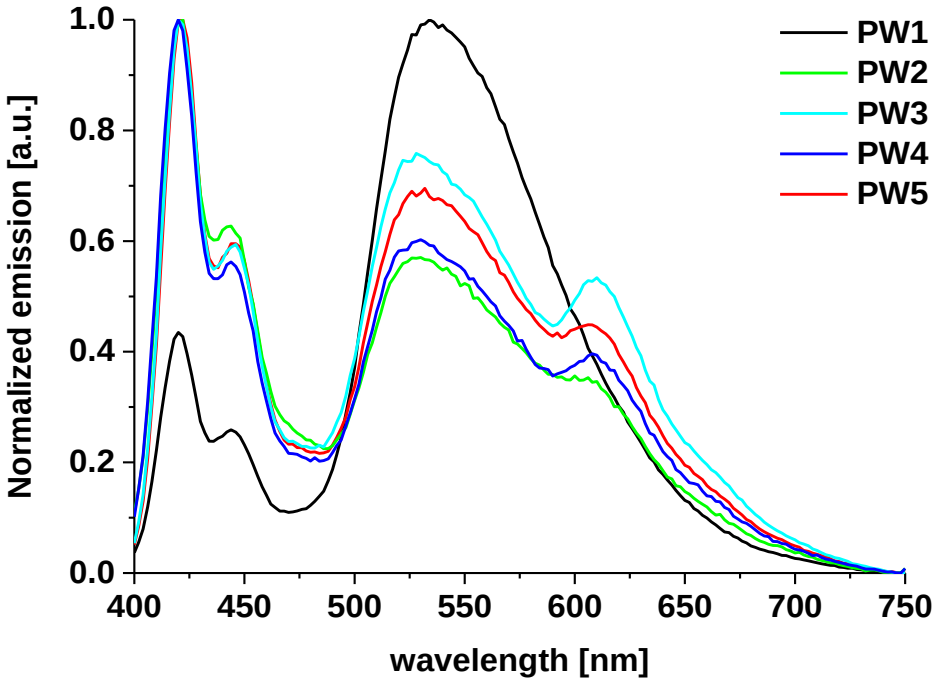

Figure 35. Photoluminescence spectra of PW1-5 solid state films, spin-coated from chloroform solutions.

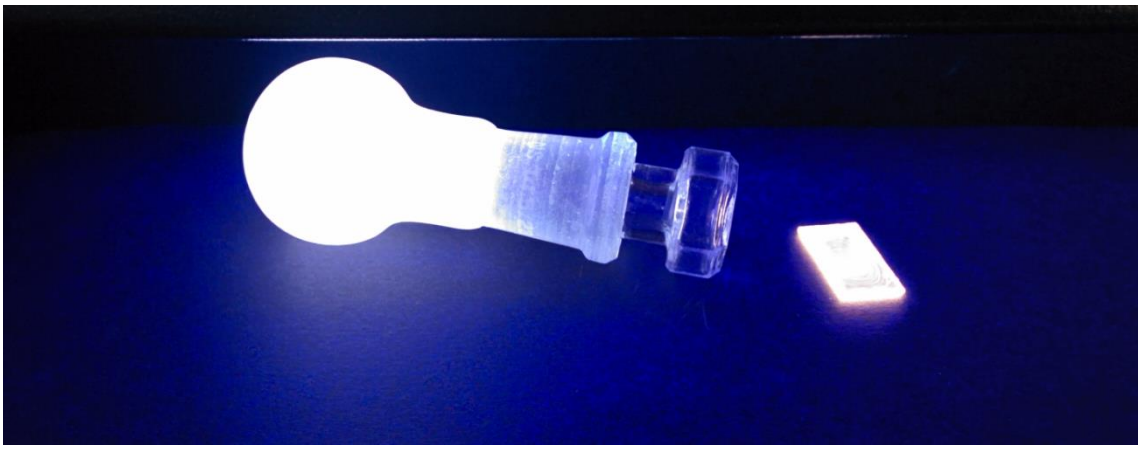

Figure 36. Picture of a flask containing an aqueous suspension (16 mg · L^{-1}) of PW2 (left) and glass substrate with a thin film of PW2, drop-casted from chloroform solution (right) under UV irradiation.

To study the properties of **PW1-5** in electroluminescent devices, the polymeric materials were sandwiched between an ITO/PEDOT:PSS anode and a Ba/Al cathode by M. Sc. D.

Abbazadeh of the group of Prof. P. Bloom at the University of Eindhoven, Netherlands. The electroluminescence spectra (Figure 37) revealed almost no blue emission, indicating the absence of electroluminescence from the dioctylfluorene backbone. It turns out that such OLEDs containing **PW3-5** exhibit promising ratios of red and green emission that can fulfill the requirements for suitable WOLED. Unfortunately, due to the missing blue emission, all devices are dominated by the green and red components and thus appear greenish/red to the human eye. In order to prepare real RGB WOLEDs with this concept, the overall feed-ratios of fluorene-9-one and triplet emitter would need to be lowered even more, by preserving the fluorene-9-one to iridium(III) complex ratio.

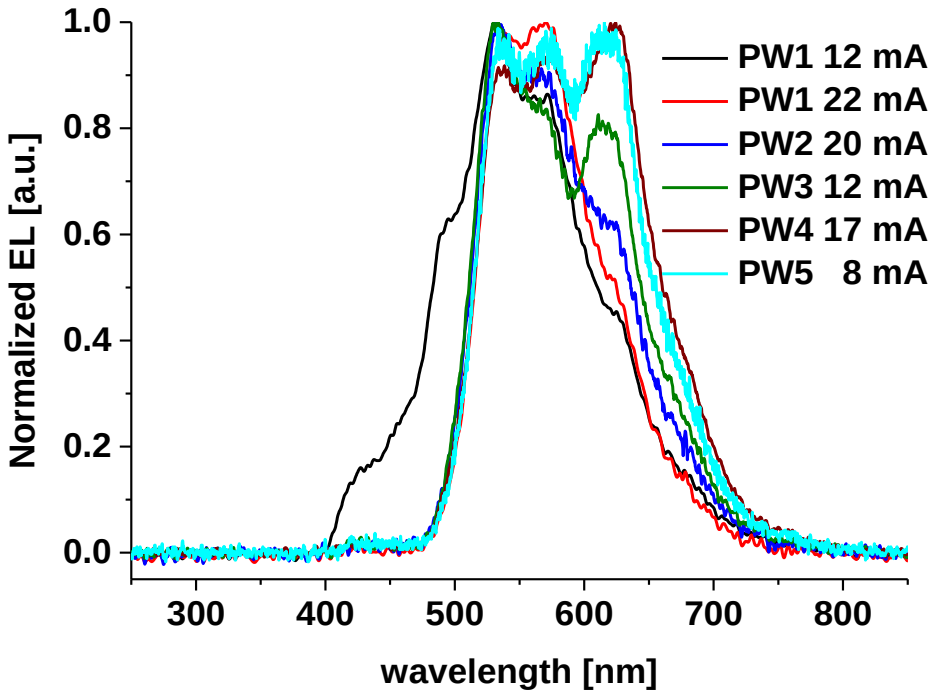

Figure 37. Normalized electroluminescence of devices prepared with copolymers PW1-5.

3.5 Results of OLED with a novel orange triplet emitter

The orange Ir-triplet emitter complex **14** introduced in chapter 3.3 was tested as an emitter in an OLED device prepared by the group of Prof. H. Bolink at the University of Valencia,

Spain. Additional theoretical studies on the complex were executed by the group of Prof. Dr. W. Thiel at the Max-Planck-Institut für Kohlenforschung, Mühlheim / Ruhr, Germany.

The devices were prepared by spin coating an 100 nm PEDOT:PSS layer onto pre-cleaned ITO coated glass substrate and subsequently applying a layer of poly(*N*,*N*,(diphenyl)-*N*',*N*'di-(4-hexylphenyl)-4,4'-biphenyldiamine (pTPD) as hole transport layer and electron blocking layer. The orange complex **14** was used as a dye in the *N*,*N*'-bis(1-naphtalenyl)-*N*-*N*'-bis(phenylbenzidine) (NPB) layer at a ratio of 10 wt%. 2,9-dimethyl-4,7-diphenyl-1,10-phenanthroline (bathocuproine, BCP) was thermally evaporated on top as a hole blocking layer. Finally, caesium carbonate was co-evaporated together with BCP (17 wt%) to serve as an electron transport and injection layer and aluminum was evaporated as cathode material.[151] Figure 38 illustrates the device architecture and corresponding layer thicknesses.

The prepared device revealed a maximum brightness of 13800 cd · m^{-2} at 6.8 V that decreased with higher applied voltage (Figure 39). Due to the low turn-on voltage of 2.1 V, the device showed higher brightness levels compared to the reference device at low voltages. The reference device published by Wang *et al.* was reported with a turn-on voltage of 4 V. and a maximum brightness of 64800 cd · m^{-2} at 11 V.[137]

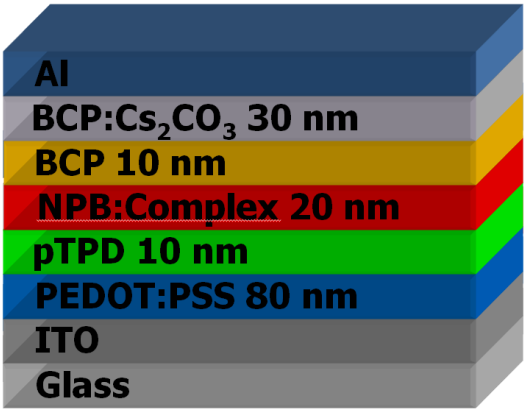

Figure 38. Device architecture of fabricated OLEDs and corresponding layer thicknesses.

The measured maximum luminous efficiency of 9.5 cd · A^{-1} @ 3.1 V (Figure 40) is lower than that of the reference device (71.6 cd · A^{-1} @ 5 V), so further device optimization is needed.

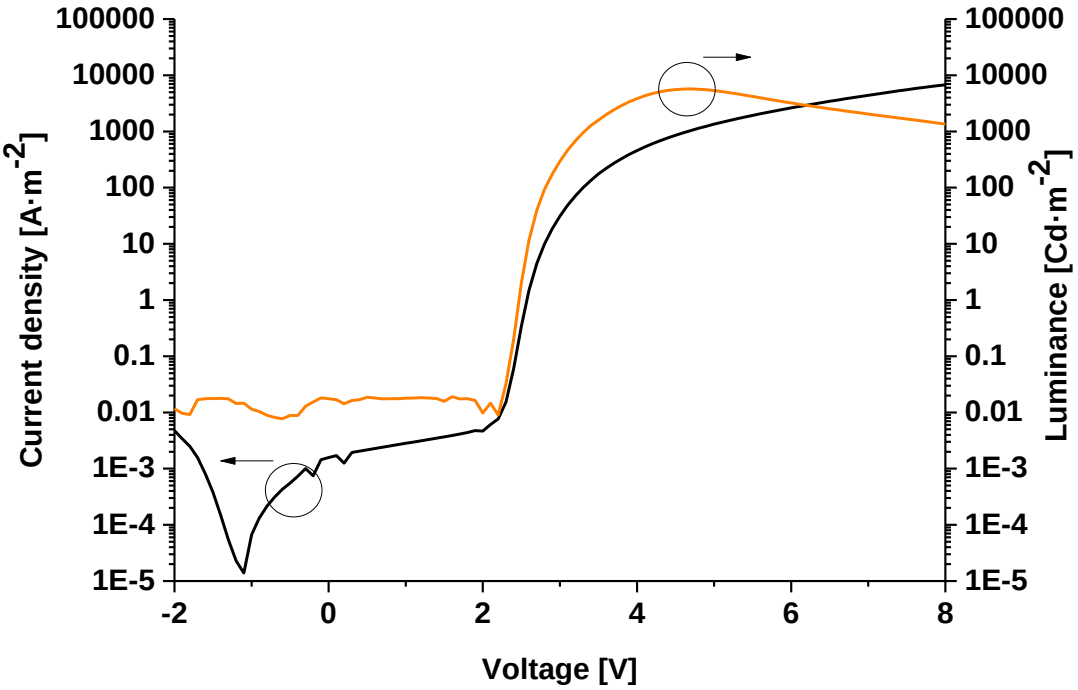

Figure 39. Luminance and current density of an OLED containing complex 14.

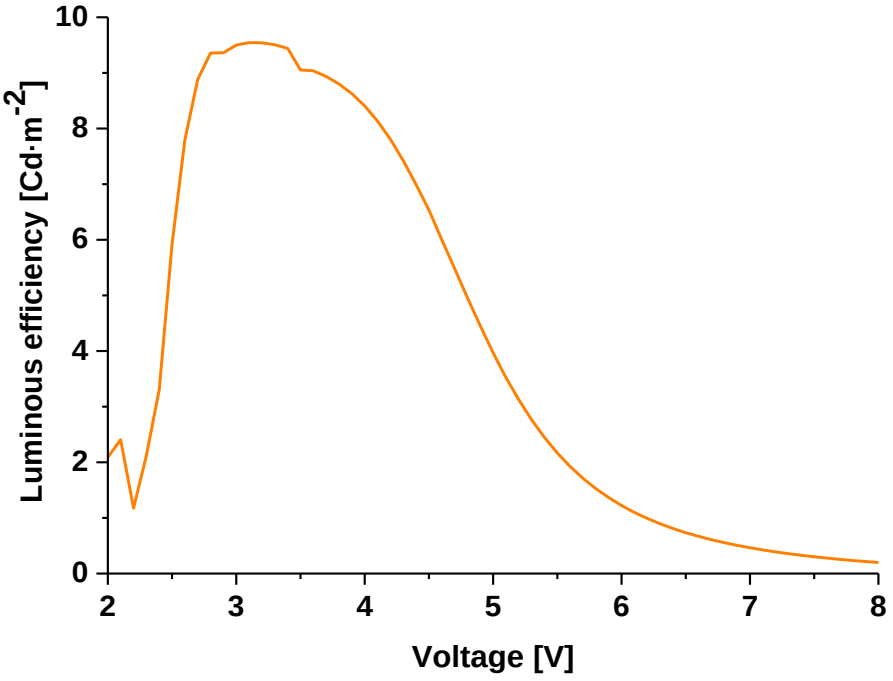

Figure 40. Luminous efficiency of OLED, fabricated with complex 14.

4. Summary and Outlook

A series of statistical copolymers containing red, green and blue light-emitting units were successfully synthesized for application as active emitting layer in OLEDs. Full color tune ability from green to red was realized by careful estimation of the monomer feed-ratios. The copolymers were suitable as single-layer OLEDs due to 9*H*-carbazole moieties attached to the polymer backbone, thus, possibly allowing for charge trapping at the emitter side. The phosphorescent iridium(III) complex should enhance the internal quantum efficiency of the devices due to its ability to harvest triplet as well as singlet excitons. Excellent solubility and film forming properties were ensured by using 9,9-dioctylfluorene as the copolymer backbone. Printed films from toluene/*o*-DCB solutions of the copolymers showed good film forming properties with low surface roughness.

In an attempt to facilitate the processing of subsequent organic layers in PLED fabrication, which usually requires either orthogonal solvents (and therefore water-soluble components) or an additional cross-linking step, aqueous suspensions of copolymer **P8** were prepared. The suspensions turned out to be stable for at least several days and could be prepared in concentrations of up to 50 mg · L^{-1}. Printing the suspensions on glass substrates proved to be successful, but printing on organic layers suffered from dewetting. Provided this problem can be solved in the future, interesting fabrication processes for OLEDs may be developed.

The series of copoylmers **P1-8** were applied in OLEDs and the properties of the devices were investigated. It could be proved that the current density and turn-on voltages of the devices are dependent on the feed-ratios of fluoren-9-one and iridium(III) complex.

In an attempt to synthesize copolymers for WOLEDs, a third series of copolymers was synthesized. The monomer feed-ratios were varied towards balanced intensities of blue, green and red light emission. The fabricated devices, however, revealed insufficient emission in the blue region, thus appearing greenish. On the other hand, with lower fluorene-9-one and iridium(III) complex feed-ratios, white light emission following the applied design rules may be possible.

Finally, an orange emitting iridium(III) complex was synthesized. The OLED containing the complex revealed a low turn-on voltage of 2.1 V and high brightness of up to 13800 cd · m^{-2} at 6.8 V. Nevertheless, the maximum luminous efficiency of 9.5 cd · A^{-1} @ 3.1 V needs further optimization.

5. Experimental

5.1 Materials

All commercially available reagents and starting materials were used without further purification. Unless otherwise specified, all reactions were carried out using standard Schlenck techniques under argon as inert protective gas.

2,7-dibromofluorene-9-one was prepared by M.Sc. Eduard Preis and was recrystallized from ethanol prior to use.

5.2 Solvents

Solvents were used in commercial p.a. quality. Dry THF and DMF were purchased from Acros GmbH or SigmaAldrich GmbH. Degassed solvents were prepared applying sparging[152] or vacuum degasification techniques.

5.3 Instrumentation

Preparative column chromatography

For purification, column chromatography was performed utilizing silica-gel by either Merck (particle size 40 – 63 µm) or Acros (0.06 – 0.2 mm).

LC-MS

LC-MS measurements were performed on a Bruker Daltonics MICROTOF with Agilent 1100 series HPLC unit.

APLI-MS

APLI-MS measurements were carried out on a Bruker Daltronics MICROTOF with APLI unit (APCI source by Bruker Daltronics) and KrF – Laser ATLEX-SI by ATL.

GC-MS

GC-MS measurements were executed on either a GC 17A QP 5050 by Shimadzu or 7890 GC gas chromatograph with 5975C MSD by Agilent Technologies.

NMR-spectroscopy

NMR measurements were conducted on Bruker Avance 400 or Avance III 600 spectrometer.

IR-spectroscopy

IR-spectroscopy was performed on a Jasco FT/IR-4200 spectrometer with an ATR unit from Specac.

UV-Vis-spectroscopy

UV-Vis absorption spectra were recorded on a Jasco V-670 UV/Vis spectrometer.

Fluorescence spectroscopy

Fluorescence spectra were measured using a Varian Cary Eclipse fluorescence spectrometer. PLQE was measured on Horiba FluoroMax 4 with F-3029 Quanta-φ accessory.

Gel permeation chromatography (GPC)

GPC measurements were carried out on a Agilent SECurity System with PSS as standard and VWD G1329A ALS UV-detector and a C1362A RI-detector. Columns: MZ Gel SDplus 5 µm, 30 · 0,8 cm (2x), 5 · 0,8 cm precolumn.

Thin-layer chromatography (TLC)

For TLC, silica gel plates with 0,2 mm layer thickness and fluorescence indicator from Macherey-Nagel were used. The spots were visualized with a UV-lamp at λ = 254 nm or 366 nm, respectively.

Thermogravimetric analysis (TGA)

TGA was conducted using a Mettler/Toledo TGA/DSC1 STAR System with SDTA Sensor in a small oven.

Differential Scanning Calorimetrie (DSC)

DSC was performed on a Mettler/Toledo DSC1 STAR System at a heat-/cooling rate of 10K·min^{-1}.

5.4 Monomer Synthesis

5.4.1 3,6-diiodo-9*H*-carbazole (1)[114]

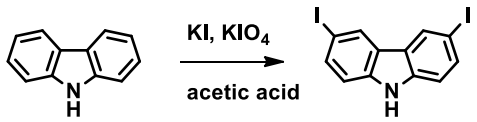

(1)

9*H*-carbazol (8.35 g, 50 mmol) was dissolved in 180 ml boiling acid in a two necked flask equipped with reflux condenser. KI (11.0 g, 70 mmol) was added and the solution was allowed to cool down to 80°C. Subsequently, KIO_4 (16.0 g, 70 mmol) was added in small portions over 5 min. The mixture was stirred for 30 min at 80°C, heated to 120°C and stirred for another 15 min. Subsequently, the solution is allowed to cool down to room temperature. The precipitated brownish crystals are filtered off and washed with excess water. The filtrate is poured into excess water and the precipitated crystals are filtered off and washed with excess water. The combined crystals are purified by column chromatography (*n*-hexane/ethyl acetate 10:3 (v/v)) to yield 14.1 g (34 mmol, 67.4 %) colorless crystals.

^{1}H-NMR (600 MHz, DMSO-d_6): δ [ppm] = 11.54 (s, 1H), 8.58 (d, *J* = 1.7 Hz, 2H), 7.67 (dd, *J* = 8.5, 1.7 Hz, 2H), 7.36 (d, *J* = 8.5 Hz, 2H). ^{13}C-NMR (150 MHz, DMSO): δ [ppm] = 138.8, 134.1, 129.2, 123.8, 113.5, 81.8. GC-MS: m/z $[M]^+$ calcd.: 418,87, found: 419. IR (ATR): ν [cm^{-1}] = 3450 – 3200 (N-H), 3055 (C_{arom-H}), 1597 (C=C), 1457, 1422, 1274, 1124, 1041, 890.

5.4.2 ethyl 2-(3,6-diiodo-9*H*-carbazol-9-yl)acetate (2)[106]

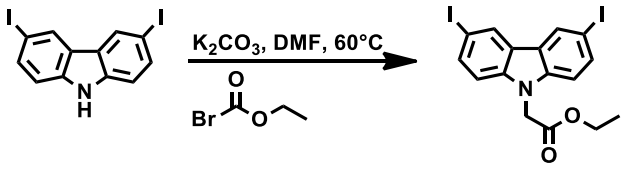

(1) (2)

3,6-diiodo-9*H*-carbazole (**1**) (9.6 g, 22.9 mmol) was dissolved in 100 ml dry DMF and stirred with K_2CO_3 (6.3 g, 45.7 mmol) at 60°C for 1.5 hours. The solution was cooled down to rt and ethyl 1-bromoacetate (8.4g, 50.3 mmol) was added via a syringe. The mixture was stirred at rt for 2 hours and subsequently heated to 50°C. After one hour, the flask was cooled down to rt, the reaction quenched with 150 ml water and the mixture poured into ice-cooled water. The precipitate was filtered off, washed with excess water and dried in vacuum to yield 11.5 g (22.9 mmol, 99.6 %) of a colorless solid.

^{1}H-NMR (400 MHz, $CDCl_3$): δ [ppm] = 8.36 (d, *J* = 1.5 Hz, 2H), 7.75 (dd, *J* = 8.6, 1.7 Hz, 2H), 7.13 (d, *J* = 8.6 Hz, 2H), 4.94 (s, 2H), 4.22 (q, *J* = 7.1 Hz, 2H), 1.24 (t, *J* = 7.1 Hz, 3H). ^{13}C-NMR (101 MHz, $CDCl_3$): δ [ppm] = 167.7, 139.7, 134.9, 129.5, 124.4, 110.6, 82.7, 61.9, 44.8, 14.1. LC-MS: $[M+Na]^+$ calcd.: m/z = 527.89, found: m/z = 527.89.

5.4.3 (Z)-1-(3,6-diiodo-9*H*-carbazol-9-yl)-4-hydroxy-5,5-dimethylhex-3-en-2-one (3)[106]

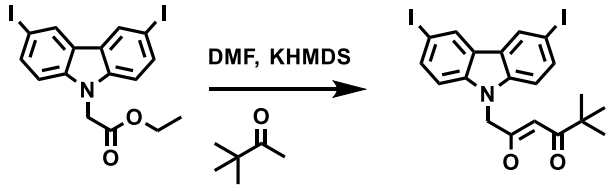

(2) (3)

3,3-dimethylbutan-2-one (4.3 g, 43.6 mmol) were dissolved in 150 ml dry DMF and cooled down in an ice-bath. KHMDS (0.7M solution in toluene, 81.8 g, 65.4 mmol) was added drop wise to the solution over 10 minutes. The ice-bath was removed and the mixture stirred for one hour at rt. Subsequently, a solution of ethyl 2-(3,6-diiodo-9*H*-carbazol-9-*yl*)acetate (**2**) (11.0 g, 21.8 mmol) in 50 ml dry DMF was added drop wise within 10 minutes and stirred overnight at rt. The reaction mixture was poured into excess water, acidified with 2M HCl and extracted three times with chloroform. The united organic phase was dried over $MgSO_4$ and

subsequently the solvent removed in vacuum. The residue was purified by silica column chromatography (ethyl acetate/*n*-hexane 1:3 (v/v)) to yield a colorless solid (11.0 g, 90.6 %).

^{1}H-NMR (600 MHz, $CDCl_3$): δ [ppm] = 8.38 (d, *J* = 1.5 Hz, 2H), 7.75 (dd, *J* = 8.5, 1.6 Hz, 2H), 7.13 (d, *J* = 8.6 Hz, 2H), 5.34 (s, 1H), 4.95 (s, 2H), 1.04 (s, 9H). ^{13}C-NMR (151 MHz, $CDCl_3$): δ [ppm] = 200.1, 190.2, 139.7, 135.0, 129.6, 124.3, 110.8, 92.6, 82.8, 48.6, 38.8, 27.1. IR (ATR): ν [cm^{-1}] = 3054, 2970, 2877, 1707, 1582, 1467, 1424, 1352, 1275, 1202, 1144, 984, 921, 868, 783, 623, 549. LC-MS calcd.: m/z = 558.95, found: m/z $[M+Na]^+$ = 581.94.

5.4.4 1-phenylisoquinoline (4)[118]

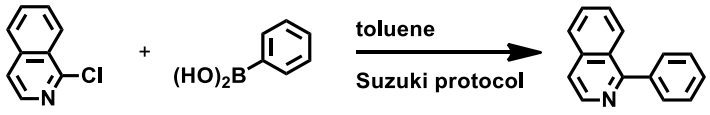

(4)

Phenylboronic acid (2.46 g, 20.2 mmol), 1-chlorisoquinoline (3.0 g, 18.3 mmol), Tetrakis(triphenylphosphine)palladium(0) (1.06 g, 0.92 mmol) and 50 ml degassed toluene were placed in a 2-necked flask with magnetic stirring and septum. 25 ml of a degassed 2M aqueous solution of Na_2CO_3 and 5 ml degassed ethanol were added via syringe and subsequently the mixture was vigorously stirred at 80°C for 15 hours. After cooling to rt, 150 ml chloroform were added and the organic phase was washed with brine (100 ml), water (2x 100 ml) and dried over $MgSO_4$. The solvents were removed in vacuum and the residue was purified by column chromatography (*n*-hexane:ethyl acetate (3:1 v/v)) to yield a colorless solid (2.97 g, 78.9%).

^{1}H-NMR (600 MHz, $CDCl_3$): δ [ppm] = 8.65 (d, *J* = 5.7 Hz, 1H), 8.14 (dd, *J* = 8.5, 0.8 Hz, 1H), 7.92 (d, *J* = 8.3 Hz, 1H), 7.75 – 7.70 (m, 3H), 7.68 (d, *J* = 5.6 Hz, 1H), 7.59 – 7.55 (m, 3H), 7.55 – 7.50 (m, 1H). ^{13}C-NMR (151 MHz, $CDCl_3$): δ [ppm] = 160.7, 142.0, 139.4, 136.9, 130.1, 129.9, 128.6, 128.3, 127.6, 127.2, 127.0, 126.7, 119.9. LC-MS: calcd.: $[M+H]^+$ m/z = 206.09, found: $[M+H]^+$ m/z = 206.11.

5.4.5 $[(piq)_4Ir_2Cl_2]$ complex (5)[97]

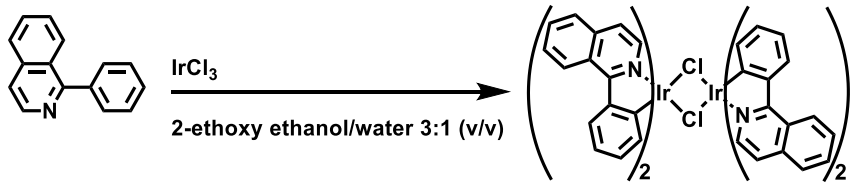

(4) (5)

1-phenylisoquinoline (**4**) (1.20 g, 5.85 mmol) and iridium(III) chloride hydrate (0.76 g, 2.54 mmol) were refluxed in 30 ml degassed 2-ethoxyethanol and 10 ml degassed water for 15 hours. After cooling to rt, the precipitated product was filtered off, washed with excess water and ethanol and dried in vacuum to yield a deep-red powder (1.14 g, 70.5%).

^{1}H-NMR (600 MHz, DMSO): δ [ppm] = 9.76 (d, *J* = 6.1 Hz, 1H), 9.60 (d, *J* = 6.3 Hz, 1H), 8.94 (d, *J* = 8.5 Hz, 1H), 8.88 (d, *J* = 8.5 Hz, 1H), 8.25 (dd, *J* = 13.9, 8.1 Hz, 2H), 8.20 (d, *J* = 8.2 Hz, 1H), 8.15 (d, *J* = 7.9 Hz, 1H), 8.04 (d, *J* = 6.4 Hz, 1H), 7.99 – 7.82 (m, 5H), 7.03 (t, *J* = 7.4 Hz, 1H), 6.93 (t, *J* = 7.4 Hz, 1H), 6.80 (t, *J* = 7.3 Hz, 1H), 6.65 (t, *J* = 7.3 Hz, 1H), 6.34 (d, *J* = 7.6 Hz, 1H), 5.59 (d, *J* = 7.4 Hz, 1H). IR (ATR): ν [cm^{-1}] = 3042, 1570, 1533, 1499, 1437, 1375, 1266, 1155, 1038, 812, 729, 670, 582. APLI-MS: $[M]^+$ calcd.: m/z = 1272.19, found: m/z $[M]^+$ = 1272.17.

5.4.6 $[(piq)_2Ir(carbacac)]$ complex (6)

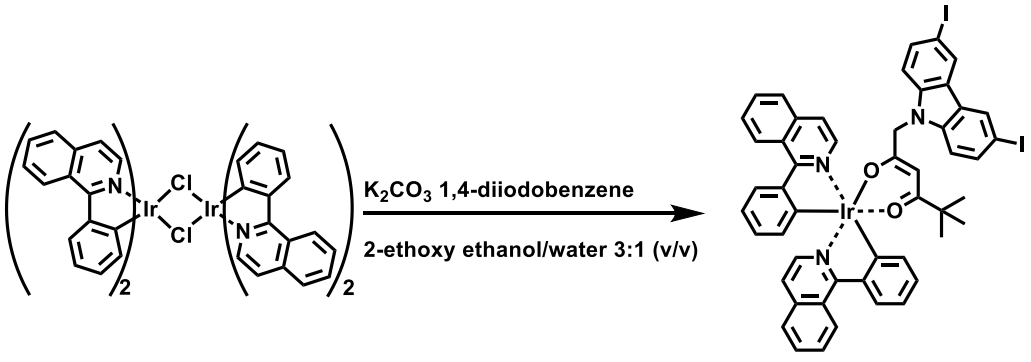

(5) (6)

$[(piq)_4Ir_2Cl_2]$ (**5**) (1.2 g, 0.94 mmol), (Z)-1-(3,6-diiodo-9*H*-carbazol-9-*yl*)-4-hydroxy-5,5-dimethylhex-3-en-2-one (**4**) (1.16 g, 2.07 mmol), K_2CO_3 (0.91 g, 6.60 mmol) and 1,4-diiodobenzene (6.22 g, 18.90 mmol) were placed in a Schlencktube and dissolved in 50ml

degassed 2-ethoxyethanol. The mixture was stirred at 110°C for 2 hours and subsequently allowed to cool down to rt. The red solution was carefully neutralized with 2M HCl and poured into 150 ml chloroform. The organic phase was washed three times with water and dried over $MgSO_4$. The solvents were removed in vacuum and the residue was purified by column chromatography (*n*-hexane/ethyl acetate (3:1 v/v)) to yield a deep-red solid (1.80 g, 82.3 %).

^{1}H-NMR (600 MHz, $CDCl_3$): δ [ppm] = 8.98 (d, *J* = 8.0 Hz, 2H), 8.18 (d, 1H), 8.18 (d, 1H), 8.15 (d, *J* = 8.0 Hz, 1H), 8.07 (s, 2H), 8.03 (d, *J* = 6.2 Hz, 1H), 7.98 (d, 1H), 7.98 (d, 1H), 7.83 (t, 1H), 7.83 (t, 1H), 7.7 (t, 1H), 7.7 (t, 1H), 7.33 (d, *J* = 8.5 Hz, 1H), 7.25 (d, *J* = 6.3 Hz, 1H), 7.12 (d, *J* = 6.2 Hz, 1H), 6.97 (t, *J* = 7.5 Hz, 1H), 6.89 (t, *J* = 7.6 Hz, 1H), 6.86 (d, *J* = 8.5 Hz, 2H), 6.67 (t, *J* = 7.3 Hz, 1H), 6.63 (t, *J* = 7.4 Hz, 1H), 6.39 (d, *J* = 7.6 Hz, 1H), 6.35 (d, *J* = 7.7 Hz, 1H), 5.25 (s, 1H), 4.61 (d, *J* = 16.2 Hz, 1H), 4.49 (d, *J* = 15.7Hz, 1H), 0.67 (s, 9H). ^{13}C-NMR (101 MHz, $CDCl_3$): δ [ppm] = 197.0, 179.4, 169.1, 168.7, 151.6, 151.4, 146.4, 146.3, 140.3, 140.1, 139.6, 137.0, 137.00, 134.1, 134.0, 130.7, 130.6, 129.7, 129.4, 128.9, 128.6, 127.8, 127.6, 127.3, 127.2, 126.7, 126.1, 126.0, 123.8, 120.4, 120.2, 119.5, 119.3, 111.3, 93.1, 81.9, 77.3, 77.0, 76.7, 51.3, 41.1, 27.6. IR (ATR): ν [cm^{-1}] = 3041, 2955, 1707, 1573, 1498, 1423, 1354, 1318, 1276, 1217, 1146, 1038, 863, 802, 731, 670, 627, 574. APLI-MS: clacd.: $[M]^+$ m/z = 1159.07, found: $[M]^+$ m/z = 1159.05. UV-VIS: Abs. ($CHCl_3$): λ_{max} [nm] = 242, 275, 298, 344, 412, 480. PL ($CHCl_3$, Ex. 480 nm): λ_{max} [nm] = 622 nm.

5.4.7 4,4'-(2,7-dibromo-9*H*-fluorene-9,9-diyl)bis(*N*,*N*-diphenylaniline) (7)[126]

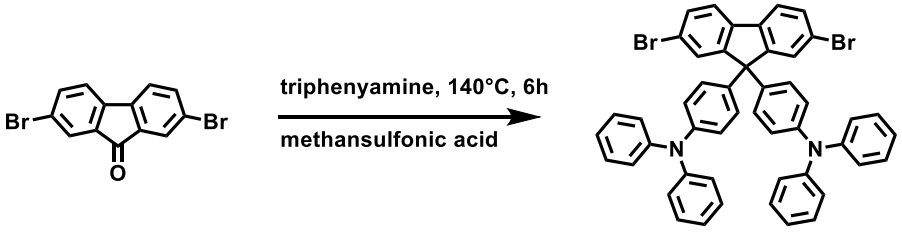

(7)

2,7-dibromo-9*H*-fluorene-9-one (5.0 g, 14.8 mmol), Triphenylamine (36.3 g, 148 mmol) and methansulfonic acid (1.42 g, 14.8 mmol) were stirred at 140°C for 6 hours. After cooling to rt, the solid is dissolved in 200 ml CH_2Cl_2 and the solution washed three times with 50 ml of a saturated aqueous Na_2CO_3 solution and finally with 50 ml of water. The organic phase is dried over $MgSO_4$ and subsequently the solvent is removed in vacuum. Column

chromatography with *n*-hexane/CH_2Cl_2 (10:3 → 10:4 (v/v)) yields a colorless solid (10,76 g, 89.7 %).

^{1}H-NMR (400 MHz, $CDCl_3$): δ [ppm] = 7.59 (d, *J* = 8.1 Hz, 2H), 7.55 (d, *J* = 1.6 Hz, 2H), 7.50 (dd, *J* = 8.1, 1.7 Hz, 2H), 7.26 (dd, *J* = 8.3, 7.5 Hz, 8H), 7.13 – 7.09 (m, 8H), 7.06 – 7.00 (m, 8H), 6.96 – 6.92 (m, 4H). ^{13}C-NMR (101 MHz, $CDCl_3$): δ [ppm] 153.5, 147.5, 146.7, 138.0, 137.7, 130.80, 129.4, 129.3, 128.7, 124.7, 123.1, 122.8, 121.8, 121.5. MS (APLI): calcd.: m/z $[M]^+$ = 810.11, found: m/z $[M]^+$ = 810.11.

5.4.8 2,7-dibromo-9,9-dioctyl-9*H*-fluorene (8)

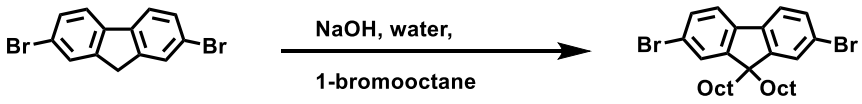

(8)

2,7-dibromo-9*H*-fluorene (10.0 g, 30.9 mmol), a solution of 25.7 g NaOH in 25 ml H_2O and 2 drops of Aliquat® 100 were placed in a 3-necked flask and 1-bromooctane (59.6 g, 309 mmol) was added. The mixture was stirred at 60°C overnight and subsequently 150 ml water were added. After 3x extraction with diethyl ether, the organic phase was washed with brine and water and dried over $MgSO_4$. The solvent was removed in vacuum and the residue was diluted in 100 ml ethanol and subsequently cooled down to -78°C. While cooling down, a colorless solid precipitates that is filtered off, dried and recrystallized from ethanol (yield: 85.7%).

^{1}H-NMR (600 MHz, $CDCl_3$): δ [ppm] = 7.54 (dd, *J* = 7.6, 0.7 Hz, 2H), 7.48 (d, *J* = 1.8 Hz, 2H), 7.47 (s, 2H), 1.95 – 1.90 (m, 4H), 1.30 – 1.04 (m, 20H), 0.86 (t, *J* = 7.3 Hz, 6H), 0.66 – 0.58 (m, 4H). ^{13}C-NMR (151 MHz, $CDCl_3$): δ [ppm] = 152.6, 139.1, 130.2, 126.2, 121.5, 121.1, 55.7, 40.1, 31.7, 29.8, 29.1, 29.1, 23.6, 22.6, 14.0. MS (APCI): calcd.: $[M]^+$ m/z = 548.15, found: m/z $[M]^+$ = 548.15.

5.4.9 3,6-dibromo-9-(2-ethylhexyl)-9*H*-carbazole (9)[136]

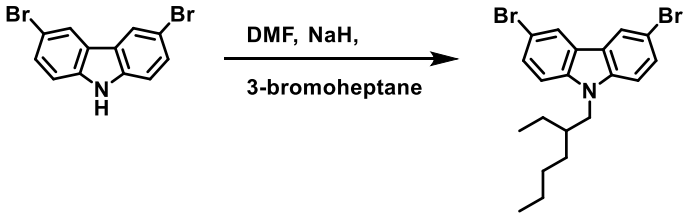

(9)

3,6-dibromo-9*H*-carbazole (2.0 g, 6.15 mmol) and NaH (370 mg, 15.4 mmol) were dissolved in 250 ml dry DMF and stirred for 30 min at 60°C. After cooling to rt, 3-bromoheptane (1.78 g, 9.2 mmol) was added dropwise *via* a syringe and stirred for another 30 min. Subsequently, the mixture was poured into 350 ml ice cooled water and placed in the fridge for 3 hours. The precipitate is filtered off and purified by silica column chromatography (*n*-hexane:ethyl acetate 0:3 (v/v)) to yield a colorless, transparent oil (2,67 g, 99.2%).

^{1}H-NMR (400 MHz, $CDCl_3$): δ [ppm] = 8.16 (d, *J* = 1.9 Hz, 2H), 7.56 (dd, *J* = 8.7, 1.9 Hz, 2H), 7.28 (d, *J* = 1.9 Hz, 2H), 4.12 (dd, *J* = 7.5, 1.7 Hz, 2H), 2.05 – 1.96 (m, 1H), 1.43 – 1.21 (m, 8H), 0.92 (t, *J* = 7.4 Hz, 3H), 0.8 (t, *J* = 7.1 Hz, 3H). ^{13}C-NMR (101 MHz, $CDCl_3$): δ [ppm] =139.8, 129.0, 123.4, 123.2, 111.9, 110.7, 77.3, 77.00, 76.7, 47.7, 39.3, 31.0, 28.7, 24.3, 23.0, 14.0, 10.8. LC-MS: calcd.: m/z $[M]^+$ = 546.02, found: m/z $[M]^+$ = 546.02.

5.4.10 *N*-(4-fluorophenyl)benzamide (10)[137]

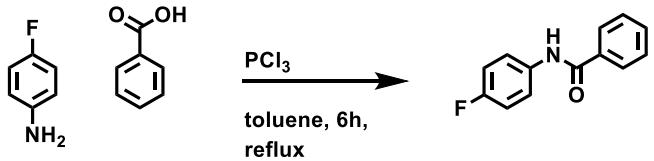

(10)

4-fluoroaniline (5.0 g, 44.5 mmol) and benzoic acid (4.2 g, 34.4 mmol) are dissolved in 80 ml dry toluene and stirred at reflux temperature. Then phosphorous trichloride (5.7 g, 42.2 mmol) is added dropwise within 15 min. The solution is stirred for 2.5 hours and subsequently allowed to cool to rt. The reaction is then quenched with the addition of 10 ml water. After the solvent is evaporated in vacuum, the residue is washed with excess water, dried, and recrystallized from acetone (4.06 g, 62.4%).

^{1}H-NMR (600 MHz, $CDCl_3$): δ [ppm] = 7.91 – 7.87 (m, 2H), 7.82 (s, 1H), 7.65 – 7.61 (m, 2H), 7.61 – 7.57 (m, 1H), 7.52 (t, *J* = 7.6 Hz, 2H), 7.12 – 7.07 (m, 2H). ^{13}C-NMR (151 MHz, $CDCl_3$): δ [ppm] = 165.7, 159.6 (d, *J* = 244.1 Hz), 134.8, 133.9, 132.0, 128.9, 127.0, 122.1 (d, *J* = 7.9 Hz), 115.8 (d, *J* = 22.7 Hz). LC-MS: calcd.: m/z $[M+H]^+$ = 216.07, found: m/z $[M+H]^+$ = 216.07.

5.4.11 *N*-(4-fluorophenyl)benzothioamide (11)[137]

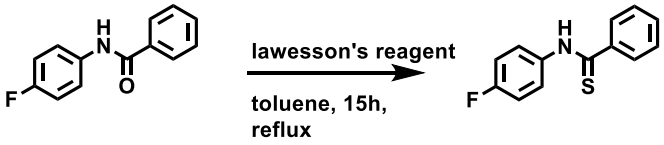

(10) (11)

N-(4-fluorophenyl)benzamide (**10**) (10 g, 46.5 mmol) and Lawsesson's Reagent (10.3 g, 25.6 mmol) were dissolved in dry toluene and heated to reflux over night with constant stirring. After cooling down to rt, the organic phase was washed with water and subsequently dried over $MgSO_4$. The solvent was removed in vacuum and the residue dissolved in 10 ml dichloromethane and subsequently precipitated by adding 50 ml *n*-hexane and removing the dichloromethane under reduced pressure. The flask was kept in the fridge over-night and finally the colorless solid was filtered off, washed with ice-cooled *n*-hexane and dried. The filtrate was collected, the *n*-hexane removed under reduced pressure and the residue purified by column chromatography on silica gel (*n*-hexane:EtAc 10:3 (v/v)). The combined solids added up to 8.79 g (81.8 % yield) of a colorless solid.

^{1}H-NMR (400 MHz, $CDCl_3$): δ [ppm] = 9.01 (s, 1H), 7.85 (d, *J* = 7.4 Hz, 2H), 7.70 (dd, *J* = 7.9, 4.8 Hz, 2H), 7.53 (t, *J* = 7.1 Hz, 1H), 7.45 (t, *J* = 7.4 Hz, 2H), 7.14 (t, *J* = 8.4 Hz, 2H). ^{13}C-NMR (101 MHz, $CDCl_3$): δ [ppm] = 198.9, 160.8 (d, *J* = 247.5 Hz), 142.7, 134.9, 131.4, 128.6, 126.1, 126.0 (d, *J* = 8.2 Hz), 115.8 (d, *J* = 22.8 Hz). LC-MS: calcd.: m/z $[M+H]^+$ = 232.05, found: m/z $[M+H]^+$ = 232.1.

5.4.12 6-fluoro-2-phenylbenzo[*d*]thiazole (12)[137]

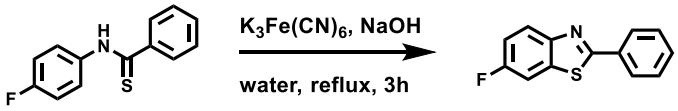

(11) (12)

N-(4-fluorophenyl)benzothiaamide) (**11**) (2.2g, 9.51 mmol) was wetted with a few drops of ethanol and blended with 8 eq. of NaOH (as aqueous 30 wt% solution). Subsequently the mixture is diluted with water to 10 wt%. Subsequently, it is added dropwise to a stirred solution of potassium ferricyanide (III) (12.52 g, 38.04 mmol) in 62.5 ml water at 85°C. After 3 hours, the solution is allowed to cool down to rt and 75 ml water are added. After neutralization with 2M HCl, the mixture is extracted with dichloromethane (3x 50 ml), the combined organic phase is dried over $MgSO_4$ and finally the solvent removed in vacuum. The residue was recrystalized from methanol to yield a colorless solid (2.06 g, 94%).

^{1}H-NMR (400 MHz, $CDCl_3$): δ [ppm] = 8.10 – 8.07 (m, 2H), 8.04 (dd, *J* = 9.0, 4.8 Hz, 1H), 7.60 (dd, *J* = 8.1, 2.5 Hz, 1H), 7.54 – 7.49 (m, 3H), 7.30 – 7.22 (m, 1H). ^{13}C-NMR (151 MHz, $CDCl_3$): δ [ppm] = 167.8 (s), 160.5 (d, *J* = 245.8 Hz), 150.8 (s), 136.1 (d, *J* = 11.4 Hz), 133.4 (s), 131.0 (s), 129.1 (s), 127.5 (s), 124.1 (d, *J* = 9.0 Hz), 115.0 (d, *J* = 24.4 Hz), 107.8 (d, *J* = 26.6 Hz). LC-MS: calcd.: m/z $[M+H]^+$ = 230.04, found: m/z $[M+H]^+$ = 230.05.

5.4.13 $[(F\text{-}bt)_4Ir_2Cl_2]$ complex (13)[137]

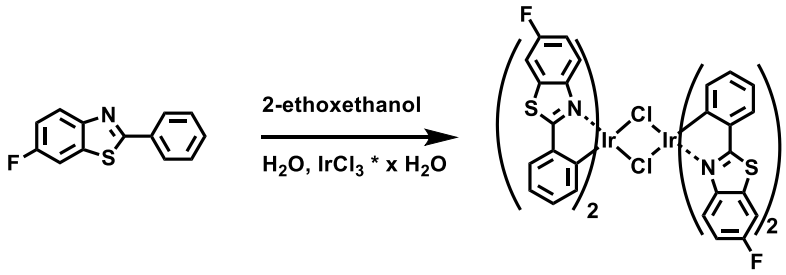

(12) (13)

Iridium(III) chloride hydrate (0.79g, 3.95 mmol) and 6-fluoro-2-phenylbenzo[*d*]thiazole (**12**) (2.00 g, 8.68 mmol) were stirred in a mixture of 30 ml 2-ethoxyethanol and 10 ml water for 15 hours at 130°C. After cooling to rt, the precipitate was filtered off, washed with excess ethanol and dried in vacuum. The crude product was used in the following reaction without further purification.

IR (ATR) [cm^{-1}] 3104, 3047, 2972, 1694, 1570, 1447, 1250, 1190, 1021, 965, 907, 849, 814, 757, 679, 577.

5.4.14 [$(F\text{-}bt)_2Ir(carbacac)$] complex (14)

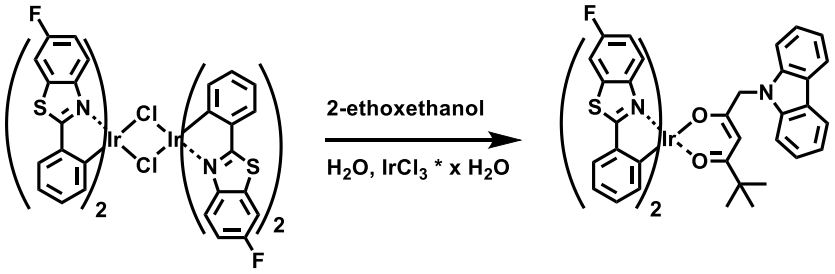

(13) (14)

[$(F\text{-}pbt)_4Ir_2Cl_2$] (**13**) (150 mg, 0.11 mmol), (*Z*)-6-(9*H*-carbazol-9-yl)-5-hydroxy-2,2-dimethylhex-4-en-3-one (84 mg, 0.273 mmol) and K_2CO_3 (106 mg, 0.77 mmol) were placed in a flask and 20 mL degassed 2-ethoxyethanol were added. The mixture was heated to reflux for 2h with constant stirring. After cooling to rt, the solvent was evaporated and the crude product purified by silica column chromatography with *n*-hexane/ethyl acetate (10:3 v/v) as eluent to yield an orange powder (140 mg, 67%).

^{1}H-NMR (600 MHz, $CDCl_3$): δ [ppm] = 8.03 (d, *J* = 7.5 Hz, 2H), 7.78 (dd, *J* = 9.0, 4.7 Hz, 1H), 7.74 (dd, *J* = 9.0, 4.8 Hz, 1H), 7.60 (dd, *J* = 12.2, 7.6 Hz, 2H), 7.58 – 7.53 (m, 2H), 7.23 (t, *J* = 7.3 Hz, 2H), 7.19 (t, *J* = 7.3 Hz, 2H), 7.03 (d, *J* = 8.1 Hz, 2H), 6.96 (td, *J* = 8.8, 2.5 Hz, 1H), 6.92 – 6.85 (m, 2H), 6.79 (td, *J* = 8.9, 2.5 Hz, 1H), 6.64 (q, *J* = 7.2 Hz, 2H), 6.46 (d, *J* = 7.7 Hz, 1H), 6.42 (d, *J* = 7.8 Hz, 1H), 5.19 (s, 1H), 4.59 (dd, *J* = 40.5, 16.7 Hz, 2H), 0.65 ppm (s, 9H). ^{13}C-NMR (100 MHz, $CDCl_3$) δ [ppm] = 27.4, 41.1, 50.8, 94.0, 108.5, 108.7, 108.9, 115.3, 115.5, 115.7, 115.9, 119.0, 120.0, 120.7, 120.8, 120.1, 121.0, 121.2, 121.3, 121.8, 125.5, 125.5, 125.7, 129.8, 130.0, 131.8, 132.0, 132.1, 132.2, 135.0, 135.4, 140.6, 141.4, 141.5, 141.7, 146.9, 147.1, 147.9, 159.0, 159.1, 161.5, 161.6, 181.7, 197.6 ppm. FT-IR (ATR): ν_{max} [cm^{-1}] = 3048 (C-H_{arom}), 2956-2860 (C-H), 1900br, 1575s, 1511, 1457s, 1415s, 1323, 1295, 1244, 1200, 1152, 1048, 1018, 993, 912, 849, 750, 721; UV/Vis: Abs ($CHCl_3$): λ_{max} [nm] = 250, 264, 294, 328, 400sh, 445, 488sh. Abs (film): λ_{max} [nm] = 269, 295, 329, 400sh, 448, 488sh. PL (exc. 460 nm, $CHCl_3$): λ_{max} [nm] = 558, 598sh nm; PL (exc. 460 nm, film): λ_{max} [nm] = 562, 602sh. APLI-MS (ESI): m/z calcd (%) for $IrS_2F_2O_2N_3C_{46}H_{34}$: 953 (20%), 954 (28), 955 (M^+, 39), 956 (20), 957 (8), 958 (3), found: 953 (20%), 954 (28), 955

(M^+, 39), 956 (20), 957 (8), 958 (3) ; elemental analysis calc (%) for $IrS_2F_2O_2N_3C_{46}H_{34}$: C 57.85, H 3.59, N 4.40, S 6.71; found: C 57.46, H 3.66, N 4.27, S 6.24.

5.5 Polymer Synthesis

5.5.1 General procedure for preparation of copolymers P1-8

500 mg 9,9-dioctyl-9*H*-fluorene-2,7-diboronic acid bis(1,3-propandiol)ester (0.90 mmol), 2,7-dibromo-9,9-dioctyl-9*H*-fluorene (**8**), [(Dicacac)Ir(piq)$_2$] (**6**), 2,7-dibromo-9*H*-fluoren-9-one, 72.4 mg Tetrakis(triphenylphosphine)-palladium(0) (0.06 mmol) and two drops of Aliquat® 336 were placed in a 100 ml two-necked flask with reflux condenser and septum. The apparatus was flushed with argon three times and 30 ml degassed toluene and 10 ml of a degassed 2M Na_2CO_3 aqueous solution were added via syringe. The mixture was stirred at 85°C for 48h. The solution was cooled down and 0.13 ml bromobenzene (1.25 mmol) were added and the solution stirred for 24h at 85°C. Afterwards, the solution was again cooled down a bit and 460 mg Phenylboronic acid (3.76 mmol) were added and the solution stirred again for 24h. After cooling down to rt, the mixture was diluted in 150 ml chloroform and the organic layer washed with 50 ml brine (1x) and 50 ml H_2O (2x). The organic layer was dried over $MgSO_4$ and the solvents removed in vacuum. The residue was dissolved in 10 ml chloroform and precipitated in methanol at -78°C. The solid was filtered off, dried, and extracted with acetone for 48h.

P1 (PF90PFO5Ir5)

Yield 441 mg (58.5 %). ^{1}H-NMR (600 MHz, $CDCl_3$): δ [ppm] = 7.87, 7.71, 7.63, 7.52, 7.43, 2.16, 1.18, 0,85. UV/Vis: Abs ($CHCl_3$): λ_{max} [nm], ε [L · mol^{-1} · cm^{-1})] = 371, 186000. PL (exc. 380 nm, $CHCl_3$): λ_{max} [nm] = 414. T_g = 87°C. T_d (5% decomposition) = 354°C. GPC ($CHCl_3$, RID): M_n = 6500 g · mol^{-1}, M_w = 10400 g · mol^{-1}, PDI = 1.6.

P2 (PF92PFO5Ir3)

Yield 334 mg (45.4 %). ^{1}H-NMR (600 MHz, $CDCl_3$): δ [ppm] = 7.87, 7.71, 7.63, 7.52, 7,43, 2.16, 1.18, 0,85. UV/Vis: Abs ($CHCl_3$): λ_{max} [nm], ε [L · mol^{-1} · cm^{-1})] = 380, 740095. PL (exc. 380 nm, $CHCl_3$): λ_{max} [nm] = 418. T_g = 73°C. T_d (5% decomposition) = 391°C. GPC ($CHCl_3$, RID): M_n = 10600 g · mol^{-1}, M_w = 17900 g · mol^{-1}, PDI = 1.7.

P3 (PF93PFO5Ir2)

Yield 446 mg (61.4 %). ^{1}H-NMR (600 MHz, $CDCl_3$): δ [ppm] = 7.87, 7.71, 7.63, 7.52, 7.43, 2.16, 1.18, 0,85. UV/Vis: Abs ($CHCl_3$): λ_{max} [nm], ε [L · mol^{-1} · cm^{-1})] = 383, 465349. PL (exc. 380 nm, $CHCl_3$): λ_{max} [nm] = 418. T_g = 69°C. T_d (5% decomposition) = 416°C. GPC ($CHCl_3$, RID): M_n = 9200 g · mol^{-1}, M_w = 15900 g · mol^{-1}, PDI = 1.7.

P4 (PF94PFO5Ir1)

Yield 376 mg (52.2 %). ^{1}H-NMR (600 MHz, $CDCl_3$): δ [ppm] = 7.87, 7.71, 7.63, 7.52, 7.43, 2.16, 1.18, 0,85. UV/Vis: Abs ($CHCl_3$): λ_{max} [nm], ε [L · mol^{-1} · cm^{-1})] = 381, 396897. PL (exc. 380nm, $CHCl_3$): λ_{max} [nm] = 416. T_g = 80°C. T_d (5% decomposition) = 416°C. GPC ($CHCl_3$, RID): M_n = 9100 g · mol^{-1}, M_w =19200 g · mol^{-1}, PDI = 2.1.

P5 (PF95PFO5Ir0)

Yield 457 mg (64.5 %). ^{1}H-NMR (600 MHz, $CDCl_3$): δ [ppm] = 7.87, 7.71, 7.63, 7.52, 7.43, 2.16, 1.18, 0,85. UV/Vis: Abs ($CHCl_3$): λ_{max} [nm], ε [L · mol^{-1} · cm^{-1})] = 384, 508681. PL (exc. 380 nm, $CHCl_3$): λ_{max} [nm] = 418 nm. T_g = 73°C. T_d (5% decomposition) = 415°C. GPC ($CHCl_3$, RID): M_n = 14600 g · mol^{-1}, M_w = 29200 g · mol^{-1}, PDI = 2.0.

P6 (PF98PFO2Ir0)

Yield 377 mg (52.3 %). ^{1}H-NMR (600 MHz, $CDCl_3$): δ [ppm] = 7.87, 7.71, 7.63, 7.52, 7.43, 2.16, 1.18, 0,85. UV/Vis: Abs ($CHCl_3$): λ_{max} [nm], ε [L · mol^{-1} · cm^{-1})] = 386 nm, 527588. PL (exc. 380 nm, $CHCl_3$): λ_{max} [nm] = 416 nm. T_g = 66°C. T_d (5% decomposition) = 419°C. GPC ($CHCl_3$, RID): M_n = 17300 g · mol^{-1}, M_w = 33700 g · mol^{-1}, PDI = 1.9.

P7 (PF93PFO2Ir5)

Yield 439 mg (57.3 %). ^{1}H-NMR (600 MHz, $CDCl_3$): δ [ppm] = 7.87, 7.71, 7.63, 7.52, 7.43, 2.16, 1.18, 0,85. UV/Vis: Abs ($CHCl_3$): λ_{max} [nm], ε [L · mol^{-1} · cm^{-1})] = 379, 243898. PL (exc. 380 nm, $CHCl_3$): λ_{max} [nm] = 416 nm. T_g = 69°C. T_d (5% decomposition) = 395°C. GPC ($CHCl_3$, RID): M_n = 4000 g · mol^{-1}, M_w = 8000 g · mol^{-1}, PDI = 2.0.

P8 (PF95PFO0Ir5)

Yield 479 mg (54.2 %). ^{1}H-NMR (600 MHz, $CDCl_3$): δ [ppm] = 7.87, 7.71, 7.63, 7.52, 7.43, 2.16, 1.18, 0,85. UV/Vis: Abs ($CHCl_3$): λ_{max} [nm], ε [L · mol^{-1} · cm^{-1})] = 378 nm, 143310. PL (exc 380 nm, $CHCl_3$): λ_{max} [nm] = 416 nm. T_g = 69°C. T_d (5% decomposition) = 395°C. GPC ($CHCl_3$, RID): M_n = 4300 g · mol^{-1}, M_w = 8800 g · mol^{-1}, PDI = 2.0.

PW1

400 mg 9,9-dioctyl-9*H*-fluorene-2,7-diboronic acid bis(1,3-propandiol)ester (0.72 mmol), 385 mg 2,7-dibromo-9,9-dioctyl-9*H*-fluorene (**8**) (0.70 mmol), 3.32 mg [(Dicacac)Ir(piq)$_2$] (**6**) (0.002 mol), 3.87 mg 2,7-dibromo-9*H*-fluoren-9-one (0.01 mmol), and 49.7 mg Tetrakis(triphenylphosphine)palladium(0) (0.04 mmol) and two drops of Aliquat® 336 were placed in a 100 ml two-necked flask with reflux condenser and septum. The apparatus was flushed with argon three times and 30 ml degassed toluene and 10 ml of a degassed 2M Na_2CO_3 aqueous solution were added via syringe. The mixture was stirred at 85°C for 48h. The solution was cooled down a bit and 52.4 mg Phenylboronic acid (0.43 mmol) were added and the solution stirred for 24h at 85°C. Afterwards, the solution was again cooled down a bit and 164 mg iodobenzene (0.72 mmol) were added and the solution stirred again for 24h. After cooling down to rt, the mixture was diluted in 150 ml chloroform and the organic layer washed with 50 ml brine (1x) and 50 ml H_2O (2x). The organic layer was dried over $MgSO_4$ and the solvents removed in vacuum. After purification *via* short column chromatography (silica gel, tolunene/*n*-hexane 3:10 v/v), the product was dissolved in 10 ml chloroform and precipitated in methanol at -78°C. The solid was filtered off, dried, and extracted with acetone for 48h.

Yield 140 mg (22.0%). ^{1}H-NMR (600 MHz, $CDCl_3$): δ [ppm] = 8.00, 7.87, 7.71, 7.62, 7.52, 7.40, 2.15, 1.17, 0.85. UV/Vis: Abs (film): λ_{max} [nm] = 380. PL (exc. 380 nm, film): λ_{max}

[nm] = 534. T_g = 64.8°C. T_d (5% decomposition) = 421°C. GPC ($CHCl_3$, UV): M_n = 11300 g · mol^{-1}, M_w = 17500 g · mol^{-1}, PDI = 1.55.

5.5.2. General procedure for preparation of copolymers PW2-4

500 mg 9,9-dioctyl-9*H*-fluorene-2,7-diboronic acid bis(1,3-propandiol)ester (0.90 mmol), 2,7-dibromo-9,9-dioctyl-9*H*-fluorene (**8**), [(Dicacac)Ir(piq)$_2$] (**6**), 2,7-dibromo-9*H*-fluoren-9-one, and 49 mg Tetrakis(triphenylphosphine)palladium(0) (0.04 mmol), 4,4'-(2,7-dibromo-9*H*-fluorene-9,9-diyl)bis(*N*,*N*-diphenylaniline) (**7**) (145 mg, 0.18 mmol) and two drops of Aliquat® 336 were placed in a 100 ml two-necked flask with reflux condenser and septum. The apparatus was flushed with argon three times and 30 ml degassed toluene and 10 ml of a degassed 2M Na_2CO_3 aqueous solution were added via syringe. The mixture was stirred at 85°C for 48h. The solution was cooled down a bit and 52.4 mg Phenylboronic acid (0.43 mmol) were added and the solution stirred for 24h at 85°C. Afterwards, the solution was again cooled down a bit and 164 mg iodobenzene (0.72 mmol) were added and the solution stirred again for 24h at 85°C. Afterwards, the solution was again cooled down a bit and 460 mg Phenylboronic acid (3.76 mmol) were added and the solution stirred again for 24h. After cooling down to rt, the mixture was diluted in 150 ml chloroform and the organic layer washed with 50 ml brine (1x) and 50 ml H_2O (2x). The organic layer was dried over $MgSO_4$ and the solvents removed in vacuum. After purification *via* short column chromatography (silica gel, tolunene/*n*-hexane 3:10 v/v), the product was dissolved in 10 ml chloroform and precipitated in methanol at -78°C. The solid was filtered off, dried, and extracted with acetone for 48h.

PW2

Yield 201 mg (25.8%). ^{1}H-NMR (600 MHz, CDCl3): δ [ppm] = 7.87, 7.71, 7.63, 7.52, 7.41, 7.25, 7.12, 7.02, 2.14, 1.17, 0.84. UV/Vis: Abs (film): λ_{max} [nm] = 377. PL (exc. 380 nm, film): λ_{max} [nm] = 422. T_g = 70.7°C. T_d (5% decomposition) = 405°C. GPC ($CHCl_3$, UV): M_n = 7300 g · mol^{-1}, M_w = 11400 g · mol^{-1}, PDI = 1.56.

PW3

Yield: 91 mg (11%). ^{1}H-NMR (400 MHz, CDCl3): δ [ppm] = 7.85, 7.70, 7.62, 7.51, 7.39, 7.25, 7.13, 7.02, 2.13, 1.16, 0.84. UV/Vis: Abs (film): λ_{max} [nm] = 383. PL (exc. 380 nm, film): λ_{max} [nm] = 422. T_g = 80.7°C. T_d (5% decomposition) = 412°C. GPC ($CHCl_3$, UV): M_n = 11400 g · mol^{-1}, M_w = 15800 g · mol^{-1}, PDI = 1.39.

PW4

Yield: 305 mg (39.2%). ^{1}H-NMR (400 MHz, CDCl3): δ [ppm] = 7.85, 7.70, 7.61, 7.51, 7.40, 7.25, 7.11, 7.02, 2.13, 1.16, 0.84. UV/Vis: Abs (film): λ_{max} [nm] = 383. PL (exc. 380 nm, film): λ_{max} [nm] = 420. T_g = 68.3°C. T_d (5% decomposition) = 406°C. GPC ($CHCl_3$, UV): M_n = 8500 g · mol^{-1}, M_w = 14700 g · mol^{-1}, PDI = 1.73.

5.5.3. Copolymer PW5

500 mg 9,9-dioctyl-9*H*-fluorene-2,7-diboronic acid bis(1,3-propandiol)ester (0.90 mmol), 386 mg 2,7-dibromo-9,9-dioctyl-9*H*-fluorene (**8**) (0.70 mmol), 10.4 mg [(Dicacac)Ir(piq)$_2$] (**6**) (0.009 mmol), 1.21 mg 2,7-dibromo-9*H*-fluoren-9-one (0.004 mmol), and 49 mg Tetrakis(triphenylphosphine)palladium(0) (0.03 mmol), 78.3 mg 3,6-dibromo-9-(2-ethylhexyl)-9*H*-carbazole (**9**) (0.18 mmol) and two drops of Aliquat® 336 were placed in a 100 ml two-necked flask with reflux condenser and septum. The apparatus was flushed with argon three times and 30 ml degassed toluene and 10 ml of a degassed 2M Na_2CO_3 aqueous solution were added via syringe. The mixture was stirred at 85°C for 48h. The solution was cooled down a bit and 52.4 mg Phenylboronic acid (0.43 mmol) were added and the solution stirred for 24h at 85°C. Afterwards, the solution was again cooled down a bit and 164 mg iodobenzene (0.72 mmol) were added and the solution stirred again for 24h. After cooling down to rt, the mixture was diluted in 150 ml chloroform and the organic layer washed with 50 ml brine (1x) and 50 ml H_2O (2x). The organic layer was dried over $MgSO_4$ and the solvents removed in vacuum. After purification *via* short column chromatography (silica gel, tolunene/*n*-hexane 3:10 v/v), the product was dissolved in 10 ml chloroform and precipitated in methanol at -78°C. The solid was filtered off, dried, and extracted with acetone for 48h.

Yield 218 mg (30.7%). ^{1}H-NMR (600 MHz, $CDCl_3$) δ [ppm] = 7.87, 7.71, 7.63, 7.52, 7.40, 4.27, 2.15, 1.43, 1.17, 0.85. UV/Vis: Abs (film): λ_{max} [nm] = 383. PL (exc. 380 nm, film): λ_{max} [nm] = 422. T_g = 71.1°C. T_d (5% decomposition) = 413°C. GPC ($CHCl_3$, UV): M_n = 116300 g · mol^{-1}, M_w = 16200 g · mol^{-1}, PDI = 1.40.

6. List of Figures

7. List of Schemes

8. Appendix

8.A 2D ^{1}H-^{1}H COSY-NMR spectrum of PW5 (excerpt)

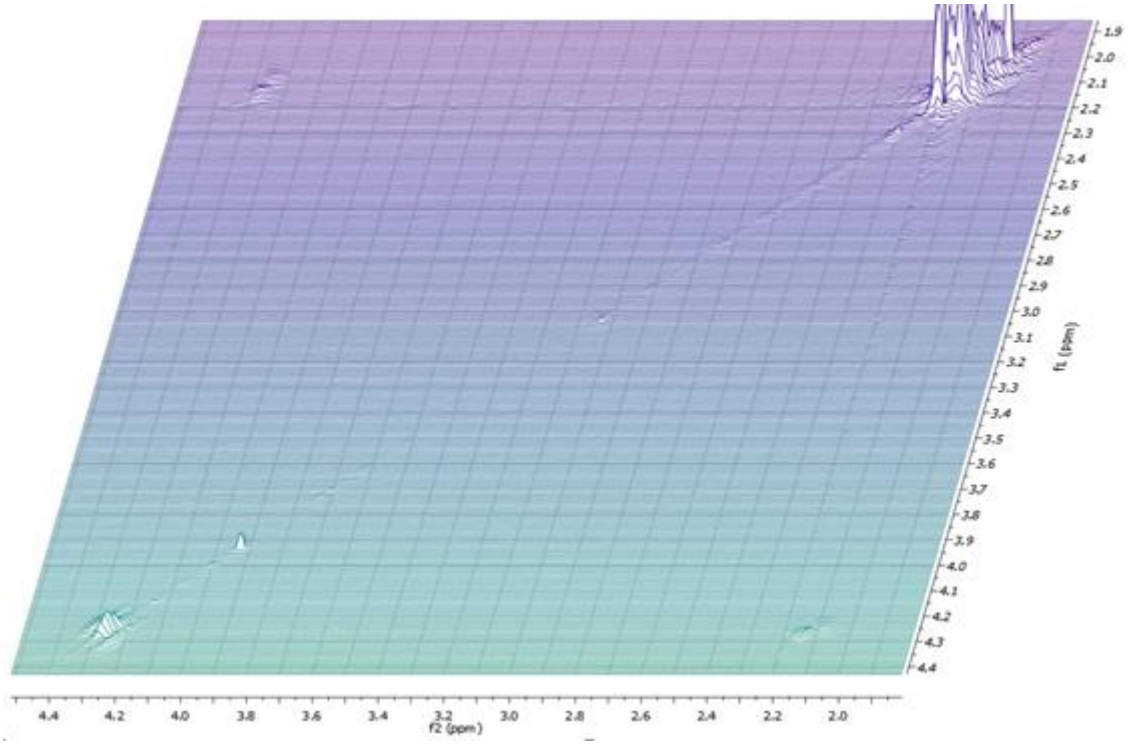

Appendix A. Excerpt of 2D ^{1}H-^{1}H COSY-NMR spectrum of PW5.

9. List of publications

Unveiling Photodeactivation Pathways for a New Iridium(III) Cyclometalated Complex, Daniel Escudero, Eike Heuser, Robert J. Meier, Michael Schäferling, Walter Thiel, Elisabeth Holder, Chemistry – A European Journal, **2013**, 15639 DOI: 10.1002/chem.201301291

10. Acknowledgement

At the end of my thesis, I would like to thank all the people that contributed to my studies and who supported me with their motivation, encouragement, knowledge and know-how and who made the working hours an unforgettable experience for me.

First of all, I would like to thank my supervisor, Jun.-Prof. Dr. Elisabeth Holder for the continuous support of my Ph.D. studies as well as her motivation, patience and sharing of knowledge.

I am very thankful to Prof. Dr. Ullrich Scherf and Prof. Dr. Michael Tausch for reviwing this thesis as referees.

Furthermore, I would like to thank the co-workers and staff of the functional polymers group and macromolecular chemistry for their endless support and all the fun we had. I will never forget you and the great times we had together.

My special thanks go to Anke Helfer, Dr. Michael Forster, Dr. Sibylle Allard and Kerstin Müller of the macromolecular chemistry group for their support and having an open ear for all sorts of problems.

Anke Helfer is furthermore acknowledged for countless APLI-MS, GPC, TGA and DSC measurements and for being there whenever needed.

Andreas Siebert of the organic chemistry department is acknowledged for performing all NMR measurements.

I would also like to thank all cooperation partners, especially M. Sc. D. Abbazadeh of the group of Prof. P. Bloom at the University of Eindhoven, Netherlands, for preparing the polymer OLEDs and investigating their properties, the group of Prof. Dr. H. Bolink at the University of Valencia, Spain, for preparing and investigating OLEDs with the orange emitter and last but not least, Dr. Anke Teichler of the group of Prof. Dr. U. S. Schubert at the University of Jena, Germany, for performing the inkjet printing experiments.

Furthermore, I thank the Dutch Polymer Institute (DPI) for funding and supporting my research activities.

Finally, I take this opportunity to express the profound gratitude to my beloved wife, my parents and my sister. Without their endless love and support I received, this thesis would not have been possible.

11. Literature

1. A. Bernanose, M. C., P. Vouaux, *J. Chim. Phys. Phys.- Chim. Biol.*, **1953**, *50*, 64.
2. Shirakawa, H.; Louis, E. J.; MacDiarmid, A. G.; Chiang, C. K.; Heeger, A. J., *J. Chem. Soc., Chem. Commun.*, **1977**, 578.
3. Yoo-chul, K., Galaxy S4 to hit market today http://www.koreatimes.co.kr/www/news/tech/2013/04/133_134603.html (accessed 05.02.2015).
4. LG Electronics, LG G Flex Product Page. http://www.lg.com/de/handy/lg-G-Flex (accessed 12.03.2014).
5. Adhikari, R. M.; Mondal, R.; Shah, B. K.; Neckers, D. C., *J. Org. Chem.*, **2007**, *72*, 4727.
6. Razeghi, M., *Fundamentals of Solid State Engineering*. Springer: **2009**.
7. Fischer, L. H.; Stich, M. I. J.; Wolfbeis, O. S.; Tian, N.; Holder, E.; Schäferling, M., *Chem. Eur. J.*, **2009**, *15*, 10857.
8. Kim, H.; Piqué, A.; Horwitz, J. S.; Mattoussi, H.; Murata, H.; Kafafi, Z. H.; Chrisey, D. B., *Appl. Phys. Lett.*, **1999**, *74*, 3444.
9. Kim, H.; Gilmore, C. M.; Piqué, A.; Horwitz, J. S.; Mattoussi, H.; Murata, H.; Kafafi, Z. H.; Chrisey, D. B., *J. Appl. Phys.*, **1999**, *86*, 6451.
10. Fortunato, E.; Ginley, D.; Hosono, H.; Paine, D. C., *MRS Bull.*, **2007**, *32*, 242.
11. Li, J.; Hu, L.; Wang, L.; Zhou, Y.; Grüner, G.; Marks, T. J., *Nano Lett.*, **2006**, *6*, 2472.
12. Bae, S.; Kim, H.; Lee, Y.; Xu, X.; Park, J.-S.; Zheng, Y.; Balakrishnan, J.; Lei, T.; Ri Kim, H.; Song, Y. I.; Kim, Y.-J.; Kim, K. S.; Ozyilmaz, B.; Ahn, J.-H.; Hong, B. H.; Iijima, S., *Nature Nanotech.*, **2010**, *5*, 574.
13. Wang, H.; Klubek, K. P.; Tang, C. W., *Appl. Phys. Lett.*, **2008**, *93*, 093306.
14. Staudigel, J.; Stößel, M.; Steuber, F.; Simmerer, J., *J. Appl. Phys.*, **1999**, *86*, 3895.
15. Hung, L. S.; Chen, C. H., *Mater. Sci. Eng., R*, **2002**, *39*, 143.
16. Tang, C. W.; VanSlyke, S. A., *Appl. Phys. Lett.*, **1987**, *51*, 913.
17. Abkowtz, M.; Pai, D. M., *Philos. Mag. B*, **1986**, *53*, 193.

18. Kalinowski, J., *International Journal of Electronics*, **1996**, *81*, 377.

19. Boris Minaev, H. A., He Tian, Zhijun Ning and Xin Li *Organic Light Emitting Diode - Material, Process and Devices*. InTech: 51000 Rijeka, Croatia, **2011**.

20. Perumal, S.; Minaev, B.; Ågren, H., *J. Phys. Chem. C*, **2013**, *117*, 3446.

21. Jiang, C.; Yang, W.; Peng, J.; Xiao, S.; Cao, Y., *Adv. Mater.*, **2004**, *16*, 537.

22. Costa, J. C. S.; Santos, L. M. N. B. F., *J. Phys. Chem. C*, **2013**, *117*, 10919.

23. Tokito, S.; Noda, K.; Shimada, K.; Inoue, S.-i.; Kimura, M.; Sawaki, Y.; Taga, Y., *Thin Solid Films*, **2000**, *363*, 290.

24. Shi, J.; Tang, C. W., *Appl. Phys. Lett.*, **1997**, *70*, 1665.

25. Murata, H.; Merritt, C. D.; Inada, H.; Shirota, Y.; Kafafi, Z. H., *Appl. Phys. Lett.*, **1999**, *75*, 3252.

26. Moon, C.-B.; Song, W.; Meng, M.; Kim, N. H.; Yoon, J.-A.; Kim, W. Y.; Wood, R.; Mascher, P., *J. Lumin.*, **2014**, *146*, 314.

27. Tao, S.; Niu, L.; Yu, J.; Jiang, Y.; Zhang, X., *J. Lumin.*, **2010**, *130*, 70.

28. Lee, K.-H. K., Sung-Min ; Kim, Jeong-Yeon ; Kim, Young-Kwan ; Yoon, Seung-Soo, *Bull. Korean Chem. Soc.*, **2010**, *31*, 2884.

29. Köhler, A.; Wilson, J. S.; Friend, R. H., *Adv. Eng. Mater.*, **2002**, *4*, 453.

30. Chaudhuri, D.; Sigmund, E.; Meyer, A.; Röck, L.; Klemm, P.; Lautenschlager, S.; Schmid, A.; Yost, S. R.; Van Voorhis, T.; Bange, S.; Höger, S.; Lupton, J. M., *Angew. Chem. Int. Ed.*, **2013**, *52*, 13449.

31. Baldo, M. A.; O'Brien, D. F.; You, Y.; Shoustikov, A.; Sibley, S.; Thompson, M. E.; Forrest, S. R., *Nature*, **1998**, *395*, 151.

32. Adachi, C.; Baldo, M. A.; Thompson, M. E.; Forrest, S. R., *J. Appl. Phys.*, **2001**, *90*, 5048.

33. Wang, Z. B.; Helander, M. G.; Hudson, Z. M.; Qiu, J.; Wang, S.; Lu, Z. H., *Appl. Phys. Lett.*, **2011**, *98*, 213301.

34. Tian, N.; Lenkeit, D.; Pelz, S.; Fischer, L. H.; Escudero, D.; Schiewek, R.; Klink, D.; Schmitz, O. J.; González, L.; Schäferling, M.; Holder, E., *Eur. J. Inorg. Chem.*, **2010**, 4875.

35. Kourkoulos, D.; Karakus, C.; Hertel, D.; Alle, R.; Schmeding, S.; Hummel, J.; Risch, N.; Holder, E.; Meerholz, K., *Dalton Trans.*, **2013**, *42*, 13612.

36. Du, B.; Wang, L.; Wu, H.; Yang, W.; Zhang, Y.; Liu, R.; Sun, M.; Peng, J.; Cao, Y., *Chem. Eur. J.*, **2007**, *13*, 7432.

37. Li, Z.; Li, Z. R.; Meng, H., *Organic Light-Emitting Materials and Devices*. CRC Press: **2006**.

38. Seo, J. H.; Namdas, E. B.; Gutacker, A.; Heeger, A. J.; Bazan, G. C., *Appl. Phys. Lett.*, **2010**, *97*, 043303.

39. Baldo, M. A.; Kozlov, V. G.; Burrows, P. E.; Forrest, S. R.; Ban, V. S.; Koene, B.; Thompson, M. E., *Appl. Phys. Lett.*, **1997**, *71*, 3033.

40. Zhou, T. X.; Ngo, T.; Brown, J. J.; Shtein, M.; Forrest, S. R., *Appl. Phys. Lett.*, **2005**, *86*, 021107.

41. Scriven, L. E., *MRS Online Proceedings Library*, **1988**, *121*, 717.

42. Schubert, D.; Dunkel, T., *Mater. Res. Innovations*, **2003**, *7*, 314.

43. Colella, S.; Mazzeo, M.; Melcarne, G.; Carallo, S.; Ciccarella, G.; Gigli, G., *Appl. Phys. Lett.*, **2013**, *102*, 203307.

44. Teichler, A.; Perelaer, J.; Schubert, U. S., *J. Mater. Chem. C*, **2013**, *1*, 1910.

45. Adhikari, R.; Postma, A.; Li, J.-H.; Hirai, T.; Bown, M.; Ueno, K., *Journal of the Society for Information Display*, **2013**, *21*, 151.

46. Cha, S. J.; Cho, S.-N.; Lee, W.-H.; Chung, H.-S.; Kang, I.-N.; Suh, M. C., *Macromol. Rapid Commun.*, **2014**, *35*, 807

47. Lee, J.; Han, H.; Lee, J.; Yoon, S. C.; Lee, C., *J. Mater. Chem. C*, **2014**, *2*, 1474.

48. Reineke, S.; Thomschke, M.; Lüssem, B.; Leo, K., *Rev. Mod. Phys.*, **2013**, *85*, 1245.

49. Tandon, K.; Ramasesha, S.; Mazumdar, S., *Phys. Rev. B: Condens. Matter*, **2003**, *67*, 045109.

50. Holder, E.; Langeveld, B. M. W.; Schubert, U. S., *Adv. Mater.*, **2005**, *17*, 1109.

51. Meng, L.-C.; Hou, Y.-B.; Lou, Z.-D.; Teng, F.; Yao, X.; Liu, X.-J.; Tang, A.-W.; Peng, J.-B., *Synth. Met.*, **2013**, *172*, 63.

52. Jeon, S. O.; Yook, K. S.; Joo, C. W.; Lee, J. Y., *Org. Electron.*, **2010**, *11*, 881.

53. Minaev, B.; Baryshnikov, G.; Agren, H., *Phys. Chem. Chem. Phys.*, **2014**, *16*, 1719.

54. Yang, X.; Neher, D., *Organic Light Emitting Devices: Synthesis, Properties and Applications*. 1st edition 2006 ed.; Wiley-VCH Verlag GmbH & Co KGaA, Weinheim, Germany: **2006**.

55. Escudero, D.; Heuser, E.; Meier, R. J.; Schäferling, M.; Thiel, W.; Holder, E., *Chem. Eur. J.*, **2013**, *19*, 15639.

56. Wang, Y.; Herron, N.; Grushin, V. V.; LeCloux, D.; Petrov, V., *Appl. Phys. Lett.*, **2001**, *79*, 449.

57. ChemWiki - The Dynamic Chemistry Textbook, Dexter Energy Transfer. http://chemwiki.ucdavis.edu/Core/Theoretical_Chemistry/Fundamentals/Dexter_Energy_Transfer (accessed 06.05.2014).

58. Förster, T., *Ann. Phys.*, **1948**, *437*, 55.

59. Dexter, D. L., *J. Chem. Phys.*, **1953**, *21*, 836.

60. Kappaun, S.; Slugovc, C.; List, E., *Int. J. Mol. Sci.*, **2008**, *9*, 1527.

61. Köhler, A.; Bässler, H., *Mater. Sci. Eng., R*, **2009**, *66*, 71.

62. Cleave, V.; Yahioglu, G.; Le Barny, P.; Hwang, D. H.; Holmes, A. B.; Friend, R. H.; Tessler, N., *Adv. Mater.*, **2001**, *13*, 44.

63. He, G.; Zheng, L., *Opt. Lett.*, **2010**, *35*, 2955.

64. Kido, J.; Kimura, M.; Nagai, K., *Science*, **1995**, *267*, 1332.

65. Kido, J.; Shionoya, H.; Nagai, K., *Appl. Phys. Lett.*, **1995**, *67*, 2281.

66. Burrows, P. E.; Forrest, S. R.; Sibley, S. P.; Thompson, M. E., *Appl. Phys. Lett.*, **1996**, *69*, 2959.

67. Williams, E. L.; Haavisto, K.; Li, J.; Jabbour, G. E., *Adv. Mater.*, **2007**, *19*, 197.

68. Kalinowski, J.; Cocchi, M.; Virgili, D.; Fattori, V.; Williams, J. A. G., *Adv. Mater.*, **2007**, *19*, 4000.

69. Kido, J.; Hongawa, K.; Okuyama, K.; Nagai, K., *Appl. Phys. Lett.*, **1994**, *64*, 815.

70. Huang, J.; Hou, W.-J.; Li, J.-H.; Li, G.; Yang, Y., *Appl. Phys. Lett.*, **2006**, *89*, 133509.

71. Kawamura, Y.; Yanagida, S.; Forrest, S. R., *J. Appl. Phys.*, **2002**, *92*, 87.

72. Wu, H. B.; Zou, J. H.; Liu, F.; Wang, L.; Mikhailovsky, A.; Bazan, G. C.; Yang, W.; Cao, Y., *Adv. Mater.*, **2008**, *20*, 696.

73. Huang, F.; Shih, P.-I.; Shu, C.-F.; Chi, Y.; Jen, A. K. Y., *Adv. Mater.*, **2009**, *21*, 361.

74. Cheng, G.; Fei, T.; Duan, Y.; Zhao, Y.; Ma, Y.; Liu, S., *Opt. Lett.*, **2010**, *35*, 2436.

75. Chao, C.-I.; Chen, S.-A., *Appl. Phys. Lett.*, **1998**, *73*, 426.

76. Thompson, J.; Blyth, R. I. R.; Mazzeo, M.; Anni, M.; Gigli, G.; Cingolani, R., *Appl. Phys. Lett.*, **2001**, *79*, 560.

77. Becker, H.; Spreitzer, H.; Kreuder, W.; Kluge, E.; Schenk, H.; Parker, I.; Cao, Y., *Adv. Mater.*, **2000**, *12*, 42.

78. Kohnen, A.; Irion, M.; Gather, M. C.; Rehmann, N.; Zacharias, P.; Meerholz, K., *J. Mater. Chem.*, **2010**, *20*, 3301.

79. Tasch, S.; List, E. J. W.; Ekström, O.; Graupner, W.; Leising, G.; Schlichting, P.; Rohr, U.; Geerts, Y.; Scherf, U.; Müllen, K., *Appl. Phys. Lett.*, **1997**, *71*, 2883.

80. Granström, M.; Inganäs, O., *Appl. Phys. Lett.*, **1996**, *68*, 147.

81. Hu, B.; Karasz, F. E., *J. Appl. Phys.*, **2003**, *93*, 1995.

82. Huang, J.; Li, G.; Wu, E.; Xu, Q.; Yang, Y., *Adv. Mater.*, **2006**, *18*, 114.

83. Liu, J.; Zhou, Q. G.; Cheng, Y. X.; Geng, Y. H.; Wang, L. X.; Ma, D. G.; Jing, X. B.; Wang, F. S., *Adv. Mater.*, **2005**, *17*, 2974.

84. Liu, J.; Shao, S. Y.; Chen, L.; Xie, Z. Y.; Cheng, Y. X.; Geng, Y. H.; Wang, L. X.; Jing, X. B.; Wang, F. S., *Adv. Mater.*, **2007**, *19*, 1859.

85. Liu, J.; Chen, L.; Shao, S. Y.; Xie, Z. Y.; Cheng, Y. X.; Geng, Y. H.; Wang, L. X.; Jing, X. B.; Wang, F. S., *Adv. Mater.*, **2007**, *19*, 4224.

86. Zhen, H.; Xu, W.; Yang, W.; Chen, Q.; Xu, Y.; Jiang, J.; Peng, J.; Cao, Y., *Macromol. Rapid Commun.*, **2006**, *27*, 2095.

87. Jiang, J. X.; Xu, Y. H.; Yang, W.; Guan, R.; Liu, Z. Q.; Zhen, H. Y.; Cao, Y., *Adv. Mater.*, **2006**, *18*, 1769.

88. Jiang, J.; Jiang, C.; Yang, W.; Zhen, H.; Huang, F.; Cao, Y., *Macromolecules*, **2005**, *38*, 4072.

89. Wu, H.; Ying, L.; Yang, W.; Cao, Y., *Chem. Soc. Rev.*, **2009**, *38*, 3391.

90. McNaught, A. D.; Wilkinson, A., *IUPAC. Compendium of Chemical Terminology, 2nd ed. (the "Gold Book")*. WileyBlackwell; 2nd Revised edition edition.

91. Karatsu, T.; Takahashi, M.; Yagai, S.; Kitamura, A., *Inorg. Chem.*, **2013**, *52*, 12338.

92. Tsuboyama, A.; Iwawaki, H.; Furugori, M.; Mukaide, T.; Kamatani, J.; Igawa, S.; Moriyama, T.; Miura, S.; Takiguchi, T.; Okada, S.; Hoshino, M.; Ueno, K., *J. Am. Chem. Soc.*, **2003**, *125*, 12971.

93. You, Y.; Park, S. Y., *J. Am. Chem. Soc.*, **2005**, *127*, 12438.

94. Kwon, T.-H.; Kim, M. K.; Kwon, J.; Shin, D.-Y.; Park, S. J.; Lee, C.-L.; Kim, J.-J.; Hong, J.-I., *Chem. Mater.*, **2007**, *19*, 3673.

95. Holmes, R. J.; Forrest, S. R.; Tung, Y.-J.; Kwong, R. C.; Brown, J. J.; Garon, S.; Thompson, M. E., *Appl. Phys. Lett.*, **2003**, *82*, 2422.

96. Adachi, C.; Kwong, R. C.; Djurovich, P.; Adamovich, V.; Baldo, M. A.; Thompson, M. E.; Forrest, S. R., *Appl. Phys. Lett.*, **2001**, *79*, 2082.

97. Nonoyama, M., *Bull. Chem. Soc. Jpn.*, **1974**, *47*, 767.

98. Dixon, I. M.; Collin, J.-P.; Sauvage, J.-P.; Flamigni, L.; Encinas, S.; Barigelletti, F., *Chem. Soc. Rev.*, **2000**, *29*, 385.

99. Sprouse, S.; King, K. A.; Spellane, P. J.; Watts, R. J., *J. Am. Chem. Soc.*, **1984**, *106*, 6647.

100. Ulbricht, C.; Beyer, B.; Friebe, C.; Winter, A.; Schubert, U. S., *Adv. Mater.*, **2009**, *21*, 4418.

101. Colombo, M. G.; Brunold, T. C.; Riedener, T.; Guedel, H. U.; Fortsch, M.; Buergi, H.-B., *Inorg. Chem.*, **1994**, *33*, 545.

102. Konno, H.; Sasaki, Y., *Chem. Lett.*, **2003**, *32*, 252.

103. Kaori, S.; Noriyuki, M.; Hiroshi, K.; Yuji, H.; Hisakazu, T.; Takeko, M., *Jpn. J. Appl. Phys.*, **2004**, *43*, 2733.

104. Leclerc, M., *J. Polym. Sci., Part A: Polym. Chem.*, **2001**, *39*, 2867.

105. Lin, Y.; Ye, T.-L.; Chen, Y.; Ma, D.-G.; Chen, Z.-K.; Dai, Y.-F.; Li, Y.-X., *J. Polym. Sci., Part A: Polym. Chem.*, **2010**, *48*, 5930.

106. Tian, N.; Thiessen, A.; Schiewek, R.; Schmitz, O. J.; Hertel, D.; Meerholz, K.; Holder, E., *J. Org. Chem.*, **2009**, *74*, 2718.

107. Chua, L.-L.; Zaumseil, J.; Chang, J.-F.; Ou, E. C. W.; Ho, P. K. H.; Sirringhaus, H.; Friend, R. H., *Nature*, **2005**, *434*, 194.

108. Uckert, F.; Setayesh, S.; Müllen, K., *Macromolecules*, **1999**, *32*, 4519.

109. Kanelidis, I.; Altintas, O.; Gasse, J.-C.; Frahm, R.; Eychmuller, A.; Holder, E., *Polym. Chem.*, **2011**, *2*, 2597.

110. Tian, N.; Aulin, Y. V.; Lenkeit, D.; Pelz, S.; Mikhnenko, O. V.; Blom, P. W. M.; Loi, M. A.; Holder, E., *Dalton Trans.*, **2010**, *39*, 8613.

111. Tian, N., PhD thesis, Bergische Universität Wuppertal, Wuppertal, **2012**.

112. Backes, J.; Brunner, E.; Eberbach, W.; Gossauer, A.; Jutz, C.; Kreher, R. P.; Rudorf, W. D.; Sauter, F.; Stütz, P., *Houben-Weyl Methods of Organic Chemistry Vol. E 6a, 4th Edition Supplement: Hetarenes I (Five-Membered Rings with One Heteroatom in the Ring System)*. Thieme: **2014**.

113. Crabtree, R. H., *The Organometallic Chemistry of the Transition Metals*. Wiley: **2014**.

114. Tucker, S. H., *J. Chem. Soc.*, **1926**, *129*, 546.

115. Podgoršek, A.; Zupan, M.; Iskra, J., *Angew. Chem.*, **2009**, *121*, 8576.

116. Bogdal, D.; Lukasiewicz, M.; Pielichowski, J., *Green Chem.*, **2004**, *6*, 110.

117. Conn, M. M.; Deslongchamps, G.; de Mendoza, J.; Rebek, J., *J. Am. Chem. Soc.*, **1993**, *115*, 3548.

118. Liu, S.-J.; Zhao, Q.; Fan, Q.-L.; Huang, W., *Eur. J. Inorg. Chem.*, **2008**, 2177.

119. Movassaghi, M.; Hill, M. D., *Org. Lett.*, **2008**, *10*, 3485.

120. Beyer, B.; Ulbricht, C.; Winter, A.; Hager, M. D.; Hoogenboom, R.; Herzer, N.; Baumann, S. O.; Kickelbick, G.; Gorls, H.; Schubert, U. S., *New J. Chem.*, **2010**, *34*, 2622.

121. Tian, N.; Lenkeit, D.; Pelz, S.; Kourkoulos, D.; Hertel, D.; Meerholz, K.; Holder, E., *Dalton Trans.*, **2011**, *40*, 11629.

122. Beyer, B.; Ulbricht, C.; Escudero, D.; Friebe, C.; Winter, A.; González, L.; Schubert, U. S., *Organometallics*, **2009**, *28*, 5478.

123. Zhuang, X.-D.; Chen, Y.; Li, B.-X.; Ma, D.-G.; Zhang, B.; Li, Y., *Chem. Mater.*, **2010**, *22*, 4455.

124. Lin, H.-Y.; Liou, G.-S.; Lee, W.-Y.; Chen, W.-C., *J. Polym. Sci., Part A: Polym. Chem.*, **2007**, *45*, 1727.

125. Prachumrak, N.; Thangthong, A. m.; Tarsang, R.; Keawin, T.; Jungsuttiwong, S.; Sudyoadsuk, T.; Promarak, V., *Tetrahedron Lett.*, **2012**, *53*, 5492.

126. Kanelidis, I.; Ren, Y.; Lesnyak, V.; Gasse, J.-C.; Frahm, R.; Eychmüller, A.; Holder, E., *J. Polym. Sci., Part A: Polym. Chem.*, **2011**, *49*, 392.

127. Ego, C.; Grimsdale, A. C.; Uckert, F.; Yu, G.; Srdanov, G.; Müllen, K., *Adv. Mater.*, **2002**, *14*, 809.

128. Scherf, U.; List, E. J. W., *Adv. Mater.*, **2002**, *14*, 477.

129. Kamtekar, K. T.; Vaughan, H. L.; Lyons, B. P.; Monkman, A. P.; Pandya, S. U.; Bryce, M. R., *Macromolecules*, **2010**, *43*, 4481.

130. Kim, G. Y.; Choi, M.-C.; Song, M.; Jin, S.-H.; Liaw, D.-J.; Wu, H.-Y.; Huang, Y.-C.; Ha, C.-S., *J. Nanosci. Nanotechnol.*, **2012**, *12*, 5735.

131. Pasini, M.; Giovanella, U.; Betti, P.; Bolognesi, A.; Botta, C.; Destri, S.; Porzio, W.; Vercelli, B.; Zotti, G., *ChemPhysChem*, **2009**, *10*, 2143.

132. Prins, P.; Grozema, F. C.; Nehls, B. S.; Farrell, T.; Scherf, U.; Siebbeles, L. D. A., *Phys. Rev. B: Condens. Matter*, **2006**, *74*, 113203.

133. Zhu, H.; Tong, H.; Gong, Y.; Shao, S.; Deng, C.; Yuan, W. Z.; Zhang, Y., *J. Polym. Sci., Part A: Polym. Chem.*, **2012**, *50*, 2172.

134. Wang, R.; Wang, W.-Z.; Yang, G.-Z.; Liu, T.; Yu, J.; Jiang, Y., *J. Polym. Sci., Part A: Polym. Chem.*, **2008**, *46*, 790.

135. Wang, H.; Ryu, J.-T.; Kwon, Y., *J. Appl. Polym. Sci.*, **2011**, *119*, 377.

136. Huang, J.; Niu, Y.; Yang, W.; Mo, Y.; Yuan, M.; Cao, Y., *Macromolecules*, **2002**, *35*, 6080.

137. Wang, R.; Liu, D.; Ren, H.; Zhang, T.; Yin, H.; Liu, G.; Li, J., *Adv. Mater.*, **2011**, *23*, 2823.

138. Singh, H.; Singh, A. K.; Sharma, S.; Iyer, R. N.; Srivastava, O. P., *J. Med. Chem.*, **1977**, *20*, 826.

139. Joule, J. A.; Mills, K., *Heterocyclic Chemistry*. Wiley: **2013**.

140. Crosby, G. A.; Demas, J. N., *J. Phys. Chem.*, **1971**, *75*, 991.

141. Song, S.; Kim, J. Y.; Suh, H.; Jin, Y., *Mol. Cryst. Liq. Cryst.*, **2012**, *567*, 171.

142. Kasama, D.; Takata, R.; Kajii, H.; Ohmori, Y., *Thin Solid Films*, **2009**, *518*, 559.

143. Dias, F. B.; Maçanita, A. L.; Seixas de Melo, J.; Burrows, H. D.; Güntner, R.; Scherf, U.; Monkman, A. P., *J. Chem. Phys.*, **2003**, *118*, 7119.

144. Knaapila, M.; Winokur, M., Structure and Morphology of Polyfluorenes in Solutions and the Solid State. In *Polyfluorenes*, Scherf, U.; Neher, D., Eds. Springer Berlin Heidelberg: 2008; Vol. 212, pp 227.

145. List, E. J. W.; Guentner, R.; Scanducci de Freitas, P.; Scherf, U., *Adv. Mater.*, **2002**, *14*, 374.

146. Montilla, F.; Ruseckas, A.; Samuel, I. D. W., *Chem. Phys. Lett.*, **2013**, *585*, 133.

147. Singh, M.; Haverinen, H. M.; Dhagat, P.; Jabbour, G. E., *Adv. Mater.*, **2010**, *22*, 673.

148. Scherf, U.; Neher, D., *Polyfluorenes*. Springer: Berlin, **2008**.

149. Zou, D.; Tsutsui, T., *J. Appl. Phys.*, **2000**, *87*, 1951.

150. Thangthong, A. m.; Prachumrak, N.; Namuangruk, S.; Jungsuttiwong, S.; Keawin, T.; Sudyoadsuk, T.; Promarak, V., *Eur. J. Org. Chem.*, **2012**, 5263.

151. Wetzelaer, G.-J. A. H.; Hartmann, D.; Santamaría, S. G.; Pérez-Morales, M.; Portillo, A. S.; Lenes, M.; Sarfert, W.; Bolink, H. J., *Org. Electron.*, **2011**, *12*, 1644.

152. Dong, M. W., Precision in HPLC. Mastering the art of HPLC. *Today's Chemist at Work*. **2000**, 28.